APPLICATION OF LASER BESSEL BEAMS IN VELOCITY MEASUREMENTS

By

Mahmud Sakah

Thesis submitted in partial fulfillment
of the requirements for the degree of
Doctor of Philosophy (PhD) in Engineering Science

The Office of Graduate Studies
Laurentian University
Sudbury, Ontario, Canada

THESIS DEFENCE COMMITTEE/COMITÉ DE SOUTENANCE DE THÈSE
Laurentian Université/Université Laurentienne
Office of Graduate Studies/Bureau des études supérieures

Title of Thesis
Titre de la thèse APPLICATION OF LASER BESSEL BEAMS IN VELOCITY MEASUREMENTS

Name of Candidate
Nom du candidat Sakah, Mahmud

Degree
Diplôme Doctor of Philosophy

Department/Program
Département/Programme Natural Resources Engineering

Date of Defence
Date de la soutenance June 24, 2022

APPROVED/APPROUVÉ

Thesis Examiners/Examinateurs de thèse:

Dr. brahim Chebbi
(Supervisor/Directeur(trice) de thèse)

Dr. Ubi Wichoski
(Committee member/Membre du comité)

Dr. Meysar Zeinali
(Committee member/Membre du comité)

Dr. Ramesh Subramanian
(Committee member/Membre du comité)

Dr. Martin Agelin-Chaab
(External Examiner/Examinateur externe)

Dr. Robert Leclair
(Internal Examiner/Examinateur interne)

Approved for the Office of Graduate Studies
Approuvé pour le Bureau des études supérieures
Tammy Eger, PhD
Vice-President Research (Office of Graduate Studies)
Vice-rectrice à la recherche (Bureau des études supérieures)
Laurentian University / Université Laurentienne

ACCESSIBILITY CLAUSE AND PERMISSION TO USE

Abstract

In this thesis we explore the use of Laser Bessel beams in solid surface and fluid velocity measurements. We present a novel simple technique to measure two velocity components of a solid surface, using a Bessel beam Laser Doppler Velocimetry (LDV) system. The experiments examined the intersection of similar two Bessel beams to generate interference fringes at the intersection region. These fringes, along with the Bessel beam fringes can be used in a simple LDV system to measure two velocity components. We also explored the use of single Bessel beams for measurement of fluid flow velocity in a horizontal transparent smooth straight circular pipe using forward scattering Laser Bessel velocimetry (LBV). The measurements were validated using a commercial LDV system. In order to produce an acceptable spatial resolution for fluid flow measurements, we investigated experimentally and numerically the use of Durnin rings (annular slits) with finite width to produce nearly Bessel beams with limited transverse profile extent and depth of field (DOF). One purpose of the work was to develop the suitability of laser Bessel Velocimetry for flow conditions where velocity measurements by alternative instrumentation were not feasible or were subject to optical access limitation. We also demonstrated, a significant advantage in using a single Bessel beam to measure the total velocity of two-dimensional flows.

Keywords: Bessel beams, laser Bessel velocimetry, laser Doppler velocimetry, axicons, Durnin's rings, depth of field, fluid flow velocity measurement.

Co-Authorship Statement

I hereby declare that this thesis incorporates material that is result of my research, as follows:

This thesis consists of seven chapters and was written by the candidate as the primary author, and overall direction by my supervisor Dr Chebbi.

Dr Chebbi developed the diffraction theory, equations and wrote the programs used for numerical simulations; the candidate ran the programs. The candidate planned experimental design, built the apparatus and performed laboratory experiments, data analysis, and primary writing with assistance and overall direction by supervisor Dr Chebbi.

Chapter four has been published in manuscript (Optical Society of America) was written by the candidate and Dr Chebbi. The experimental work was completed by the candidate and the numerical simulations were written by Dr Chebbi and performed by the candidate.

Chapter five is intended for submission to an optical journal. All slits design, experimental work, CMOS photos, in this chapter was completed by the candidate and overall direction by Dr Chebbi. The numerical simulations program was written by Dr Chebbi performed by the candidate.

Chapter six incorporates unpublished material under the supervision of professor Chebbi. The experimental work, data analysis, interpretation, graphing results, and writing were performed by the candidate with the supervision of Dr Chebbi. The research topic and key ideas were suggested by Dr. Chebbi and explored by the candidate.

Acknowledgements

In the first place, I would like to express my sincere gratitude to my research supervisor, Professor Brahim Chebbi since I started my M.A.Sc. thesis in 2013 until the end of my Ph.D. thesis in 2022. Professor Brahim Chebbi, I sincerely thank you for your continuous support, encouragement, constructive feedback, patience, technical advice and knowledge and valuable discussions we had both in science and in life as well. The successful completion of this thesis would not have been possible without your continuous support, advice and the guidance given throughout the research work. I appreciate your valuable advice, highest professionalism and for all the precious ideas throughout this work. I appreciate your human qualities that have set a precious example which I follow, and I seek to attain someday. Throughout my years of graduate studies, you have helped me develop my research skills and scientific writing.

I am also grateful for the support in the experiment and discussions to make this thesis work in Optics and Experimental Fluid Mechanics Laboratory and the input throughout this effort.

I would like to thank the Faculty of Engineering of Laurentian University for giving me the opportunity to perform this research. The construction of the water channel could not have been completed without the support of the Laurentian University engineering machine shop and the technicians. I would like to express my sincere thanks and appreciation to my thesis committee for their time and effort to help me through this journey and their feedback and input to the search thesis.

Last, but in no way least important, I extend my thanks to my family and my friends always behind me and so supportive during this project, I thank them all for the care, concern, and support.

Table of Contents

List of Tables

List of Figures

Nomenclature

c	Speed of light
C	Capacitance
d	Diameter of central spot of Bessel beam
d_b	Diameter of laser beam before expansion defined to $1/e^2$ of maximum intensity
da	Diameter of an annulus used for Bessel beam generation
d_{eff}	Effective diameter of Bessel beam fringes
d_f	Fringe spacing
d_p	Particle diameter
dR	Lens diameter uncertainty
dF	Lens focal length uncertainty
D	Pipe inside diameter
D_b	Expanded laser beam diameter
g	Acceleration of gravity
E	Electric field vector
f	frequency
$f_{B,}$	Bessel frequency
f_c	Cut-off frequency
f_D	Doppler Frequency
f_{max}	Maximum frequency
F	Focal length of a lens
f_s	Sampling frequency
h	Height of Fluid
H	Height
I	Light intensity
I_{max}	maximum intensity
I_0	The incident on- axis intensity
J_0	Bessel function of order *0*

k	Wavenumber
k_r	radial component of the wave vector
k_l	longitudinal component of the wave vector
Le	Effective length
n_{lens}	Index of refractive of a lens
n	Axicon index of refraction
n_f	Index of refraction of fluid
n_x	Index of refraction
n_w	Index of refraction of cylinder wall
P	Pressure
Q	Flow rate
r	Radius in cylindrical coordinates
ra	Radius of virtual position of laser beam without refraction
r_f	True position of the lase beam inside pipe with refraction
r_o	Bessel beam spot radius
R	Transmitting lens radius
R_{avg}	Annular Slit average radius
r_1	Annular Slit inside radius
r_2	Annular Slit outer radius
R_f	Feedback resistance
R_i	Tube inner diameter
R_{in}	Input resistance
R_{lens}	Radius of a lens
Re	Reynolds number
R_0	Tube outer diameter
Δf_B	Uncertainty in Bessel frequency
Δr	Annular slit ring width
ΔR	Thickness (R_0-R_i)
T	Time (sec)

t	Thickness
t_p	Particle time
u	Velocity component in x direction
u_d	Uncertainty in fringe spacing
u_f	Uncertainty in measured frequency
u_v	Uncertainty in measured velocity
u_β	Total uncertainty in lens design
u_λ	Uncertainty in laser wavelength
$u(r)$	Fluid flow velocity
u_p	Particle velocity
U	Velocity of LDV
U_{avg}	Average flow velocity
U_{max}	Maximum flow velocity
v	Velocity component in y direction
v	Velocity from Bessel fringes
v_t	Tangential velocity
V	Velocity of Bessel beam
V	Voltage
V_{in}	Input voltage
V_{out}	Output voltage
W_0	Beam waist at focus
z	longitudinal distance in cylindrical coordinates
z_{max}	Maximum diffraction-free propagation distance of Bessel beam
z_{min}	Bessel beam propagation distance after obstruction

Greek symbols

α	Base angle of an axicon
α_w	Angle of beam with respect to cylinder wall
β	Laser Beam Axicon refraction angle
θ	Half the angle of intersection between two laser beams
θa	Angle of unrefracted laser beams
θ_f	Angle of refracted laser beams
ϕ_f	Angle between r_a and r_f
λ	Wavelength
ρ	Fluid density
ρ_p	Particle density
ω	Angular speed
μ_f	Dynamic viscosity of fluid
τ	Angle of the location of the measurement position on the rotating disk
τ_p	Seeding particle time constant

Abbreviations

BS	Beam Splitter
DOF	Depth of Field
FFT	Fast Fourier Transform
LBV	Laser Bessel Velocimetry
LDV	Laser Doppler Velocimetry
LPF	Low Pass Filter
SNR	Signal to Noise Ratio

Chapter 1

INTRODUCTION

Significant advances in experimental fluid mechanics were observed in the past few decades in part thanks to the adoption of optical flow measurement techniques. Contrary to the traditional techniques using mechanical probes, optical techniques have the significant advantage that the measurements can be done noninvasively, that is without causing any disturbance to the measurement area. Another advantage of these techniques is that they cause no damage to the surface of the sensor especially in harsh environments such as in combustion chambers and corrosive media. They are recognized to be accurate and usually have a fast time response. Most of these optical techniques use laser light which has properties such as coherence, monochromatic, low divergence and high intensity, which makes it ideal for measurements. Because of these properties, optical measurement techniques have been regularly used in flow measurements for many years, for example to measure velocities of small particles seeded in the flow. The most common used technique in flow measurements is the laser Doppler velocimetry (LDV) used to measure single point velocities, and the particle image velocimetry (PIV) which is appropriate to quantitatively image the flow distribution. The LDV, is a well-proven technique for fluid flow measurement with high spatial resolution; high accuracy and the ability to measure the three velocity components [1]. It is widely used and commercially available. The commonly available Gaussian laser beams are usually used in LDV systems.

In this research, nearly non diffraction beams, specifically Bessel beams [2], are used for velocity measurement using the fringes they generate. A technique using Bessel beams for solid velocity measurement called laser Bessel velocimetry (LBV), was developed during my M.A.Sc. research,

[3] [4], is experimentally extended to measure fluid flow velocity with defined spatial resolution. The system has very simple components setup and has some similarities to the LDV. It uses light scattered from moving particles crossing the circular fringes of a single nearly non-diffracting beam. The idea of non-diffraction beams was first demonstrated by J. Durnin in 1987 [2]. Bessel beams generated using axicons have large depth of field and were proved useful for many applications including imaging [5] and optical sorting [6].

1.1 Motivation

The idea of producing non-diffracting beams such as Bessel beams that can overcome propagation losses has always been an interesting one. These beams are also characterized by a narrow long DOF and of the presence of concentric circular fringes. The main drive in the present research, is to explore the use of Bessel beams in velocity measurements. The fringes of the Bessel beams have a well defined spacing and as such can be used for measurements. As mentioned earlier, the development of the optical velocimetry technique using Bessel beams has been proposed in my M.A.Sc., where axicons were used to generate the beams. One of the main obstacles in using this system in fluid flow measurement is the long DOF obtained using these devices which translated into a large measurement volume leading to very poor spatial resolution. In this thesis we explore producing a reduced measurement volume and better spatial resolution by generating nearly Bessel beams using Durnin's slits with finite width. This system is expected to be simple and will have less expensive focusing capability compared to other optical measuring systems. Researchers continue looking for a simple system of flow measurement, which, suitably applied, will give results similar to costlier and vibration-sensitive interferometers. Since Durnin produced Bessel beams using annular slits in 1987 [7], they have been extensively researched. They offer non diffracting over certain propagating distance and thus can be used inside an absorbing media where

other beams would typically suffer from an intensity decay. This is particularly suitable in applications where light matter interaction occurs in turbid fluid. It is known that Bessel beams have the unique property of self healing and an ability to reconstruct after obstructions compared to Gaussian beams. Theses properties also very beneficial for applications such as material processing [8] and imaging [9]. Using Bessel beam fringes to measure flow velocities is a simple concept and has not been demonstrated before this work. Being indeed an interesting topic, it was decided to investigate this technique further in fluid flow measurements. Therefore, this work is to continue the development of the LBV technique and implement new tools to the LBV system to measure flow velocity in a fluid flow channel. The basis for the work of this thesis is to contribute to the continuous advancing knowledge and research on new or more advanced tools, devices, or components in optical technology. The technique was a relatively new addition to those available to the fluid measurements and had been applied only to a variety of solid surfaces. Since the LBV technique has a simple and compact configuration, it can provide additional advantages in some applications with limited space and optical access where measurements by other techniques may be limited. In addition**,** this technique has potential advantages over alternative methods of fluid velocity measurement.

Finally, the circular fringes of the Bessel beams present some opportunities in resolving velocity components when used in an LDV system instead of gaussian beams. They also have potential of measuring total velocities in two dimensional flows in a single setup.

1.2 Objectives

The overall objective of this thesis is to use Bessel beams for velocity measurements. We explore using their fringes in an LDV system in addition to the intersection fringes to resolve velocity components. The LBV technique previously developed [3] [4] , measures only solid surface velocities and has a very long DOF and large transverse extent making it non-suitable for fluid velocity measurement. The primary objective of this thesis is to adapt this technique so that it can be used for fluid flow velocity measurement with acceptable longitudinal and transverse spatial resolutions. In order to develop the technique, it is intended to use it to measure velocity in the test section of a pipe water flow channel. The technique will be validated by comparison of its measurements to those made using a commercial LDV system. The research work involves the development, construction and testing of the system with Bessel beams generated with axicons and annular slits. In order to produce a limited measurement volume and acceptable spatial resolution, we will explore using Durnin's annular slits with finite width to produce nearly Bessel beams and control the DOF and transverse intensity variation by varying the parameters of the slits.

We intend to measure the total velocity using Bessel beam fringes, as the tank drains, and compare the results to the prediction of Bernoulli's equation. When the water is allowed to flow from the drain hole, the water level in the tank will eventually reach the desired height where measurement is taken. In the upcoming pages of the present work, this interesting and yet challenging measuring technique will be described in detail.

1.3 Thesis Structure

This section focuses on the contributions of this thesis. Most of this thesis is a description of the experiments carried out including their design and the results obtained, and a discussion of the advantages and disadvantages in using Bessel beams to measure fluid flow velocity. We introduce new applications and perform analysis to interpret the results and provide information that may assist in further developing the technique.

The thesis is divided into 7 chapters.

Chapter 1, the introduction, outlines the objectives, motivation, and context of this research.

Chapter 2 provides the theoretical background and literature review of relevant work applicable to this thesis and information necessary to understand the established fundamental concepts presented in this thesis. It presents insights into laser, Bessel beams generation and applications, and the theoretical background for the development of the LBV technique. This chapter contains some basic background on Optics and Optical Metrology, the concepts that made the LBV and data processing.

Chapter 3 introduces and defines the instrumentations and apparatuses used in this research, and the rationale for experimental methodology and measurement tools development.

Chapter 4 presents the results and the system developed for a novel Bessel beam LDV technique to measure two velocity components of solid surfaces. This chapter is published in [10].

Chapter 5 discusses the development of spatial resolution for the measurement technique, the generation of nearly Bessel beams using annular slits with finite width by applying Durnin's setup. Experimental and numerical simulation of the beams obtained from several annular slits are presented.

Chapter 6 provides the measurements of laminar and turbulent flows using the LBV technique within the water channel and comparison to LDV measurements. It also presents measurement of the total velocity of a two-dimensional flow exiting from a water tank.

Chapter 7 summarizes the conclusion and outlines the contributions of this thesis with recommendations provided for future work. The significance of this research to the optical engineering development are discussed and outlining some future work with recommendations that naturally expands on the work already completed.

1.4 Thesis Contributions

The following are the major contributions of this thesis have been made over the course of this research:

1) Development of a new LDV-LBV system and present for the first-time detailed images and description of the intersection of two similar Bessel beams. We use the resulting fringe systems to develop a simple Bessel beam LDV system to measure two velocity components using a simple configuration. This technique is considerably cheaper and simpler to implement than the existing two velocity components LDV systems. This has been attempted by using an axicon to generate the Bessel beams.
2) The research extended the experimental work using Durnin's circular slits of finite width with different parameters. We produced many nearly Bessel beams with limited DOF and transverse extent. The ability to freely shape the longitudinal and transverse intensity profile of the beam, controlling the propagation distance and number of fringes, is important for the development of LBV measurement volume. The present work provides an extensive experimental and numerical set of produced nearly Bessel beams corresponding to different parameters of Durnin's slits compared to related work in the literature [11] .

3) Experimental measurements of laminar and turbulent fluid flow velocities in a water channel were made using Bessel beams. These measurements constitute a proof of concept and could be an important addition to optical sensors applications.
4) We demonstrated a significant advantage of using Bessel beams in fluid flow measurements compared to the widely used LDV technique. With the Bessel beam fringe configuration, the total velocity for a two-dimensional flow can be made in a single measurement using a very simple and cost-effective system compared to using the LDV technique which measures each component separately using two sets of parallel fringes and at least two laser systems with different wave lengths. This was demonstrated by measuring the total velocity exiting a water tank.

Chapter 2

THEORY AND LITERATURE REVIEW

This chapter discusses the background and theory and devices used for the optical systems developed in this thesis. Since the LBV is based in optics and interferometric techniques, there is a need to describe some basics of Optics and Optical Metrology. It is intended to give the reader a brief understanding of the LBV technique development and its application with a brief overview of light source that the LBV system uses. Followed by general description of Bessel beam, which is one class of quasi propagation invariant beams.

2.1 Basics of Optics

Light can be described as an electromagnetic wave which is specified by its amplitude, the polarization and the wavelength λ. The electromagnetic spectrum waves are characterized by their frequency f, wavelength λ which are related by, $c = f\lambda$, where c is the speed of light. A plane light wave having and electric field of an amplitude E_0 propagating in the positive x-direction, at time t, can be expressed by

$$E = E_0 \cos(\omega t - kx) \qquad (2.1)$$

Where

$\omega = \frac{2\pi}{T}$ represent the circular frequency ($2\pi f$), $T = \frac{1}{f}$, is the time period and $k = \frac{2\pi}{\lambda}$ represent the wavenumber of the light wave.

2.1.1 Reflection and Refraction

The transmission of light from one medium to another can be related to the change in the direction of its propagation. The phenomena of reflection and refraction can be understood in terms of plane electromagnetic waves, but usually geometrical optics is sufficient to explain these phenomena. Reflection of light involves a change in direction of light rays when they are reflected off a surface. When light is reflected from a surface of different refractive index, the angle of incidence is always equal to the angle of reflection, as shown in Figure 2.1. Refraction of light waves involves a change in the direction of waves or bending of the path of the waves as they pass from one medium to another with different refractive indices. The refractive index is defined as the ratio of the speed of light in vacuum to the speed of light in of a material.

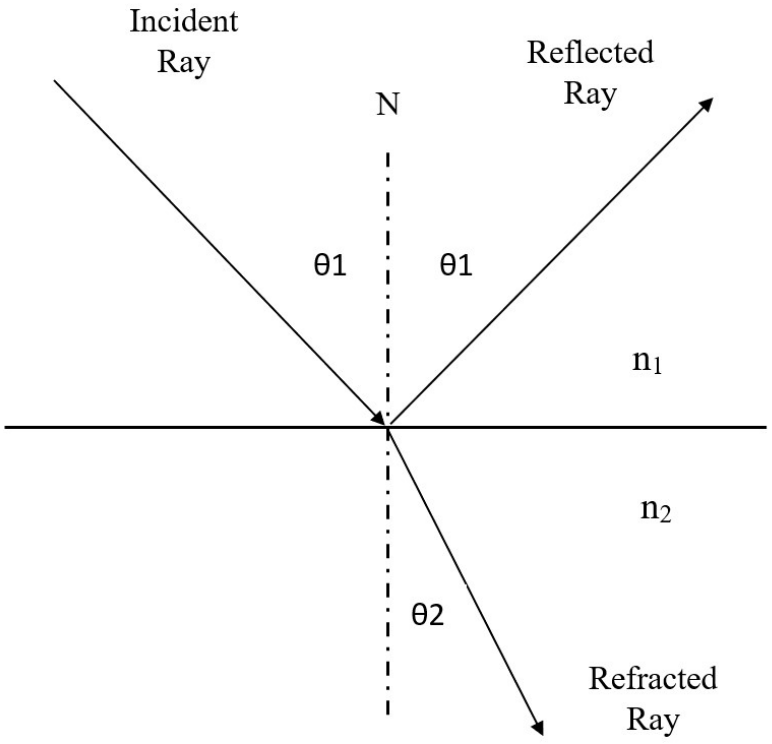

Figure 2.1 Reflection and refraction of a light ray

The angle of refraction θ2 is related to the angle of incidence θ1 by Snell's law, also called the law of refraction.

$$n1 \sin \theta 1 = n2 \sin \theta 2 \qquad (2.\ 2)$$

where n1 and n2 represent the indices of refraction of the first and second medias respectively. Snell's law is applied in the measurements to correct the refraction of the laser beam as it passes from air, through the walls, to the measurement medium.

2.2 Optical Components

Some of the most common optical components used the experiments of this work are briefly described in what follows.

2.2.1 Lasers

Since its invention, Laser became widely popular in many engineering applications and has many uses in different fields which depend on that effective invention. Lasers have become essential parts of today's technological society, such as in the infrastructure to provide the internet, and the backbone of the global network telecommunication through fiber-optics technology. They are widely used in many applications in engineering, physics and chemistry that they can be viewed as the experimentalist's most important type of optical source [12]. For example, they have been become widely used in 3D scanning for reverse engineering with accurate and high-resolution 3D scans while remaining simple to use. It is a perfect tool for inspection. Laser emits electromagnetic waves in the form of a special type of narrow, monochromatic, coherent light beam. In contrast, regular white light is polychromatic, composed of many different wavelengths. LASER stands for Light Amplification by the Stimulated Emission of Radiation. Lasers are also characterized by the

duration of laser emission and can be made to operate into two categories: pulsed and continuous wave (CW). Pulsed lasers emit light in the form of optical pulses. The energy output per pulse varies from low (< 10 mJ) to very high (> 100 J). Depending on the pulse duration, pulse energy, pulse repetition rate and wavelength required, very different methods for pulse generation and very different types of pulsed lasers are used for different applications. Continuous wave lasers (CW) have constant output over a set interval. This means that laser beam parameters output power, intensity, etc. remain constant throughout the beam's duration. In particular, it provides power outputs at many different wavelengths, and the available power varies from line to line. The expression continuous wave refers to the coherent beam of monochromatic light emitted by the gain medium which determines the laser wavelength. Generally, a laser source must be well-collimated, highly coherent meaning its electromagnetic wave fronts are all in phase, and it is nearly monochromatic meaning it is composed of very narrow range of wavelengths of one color. In measurement applications lasers operating with a stable average beam power are recommended. Lasers with wavelengths in the visible spectrum (400–750 nm) are commonly used.

2.2.2 Axicons

An axicon is a special type of lens that has a conical surface which creates long and narrow focal lines along the optical axis. It can be made of any optical material. Axicons can be used to convert a Gaussian beam into a zero-order Bessel-type beam which preserves its transverse distribution along the axis. The Bessel beam, which will be discussed in section 2.5, is ideal for many applications in measurements, instrumentation and medical research [13].

2.2.3 Beam splitters

A beamsplitter is an optical component, which can come in different shapes, but the most common is made in the shape of a cubic piece of glass used to split an incident light beam into two beams by reflecting and transmitting the incident beam at the same time. Cube beamsplitter is made from a pair of identical precision right angle prisms carefully cemented or optically contacted together on their hypotenuse faces. Before cementing, the hypotenuse of one of the prisms is coated with a metal or dielectric semi reflecting layer to minimize surface reflection losses. Antireflection-coated cube prisms have virtually no ghost image difficulties and are more rigid than plate type beamsplitters. The beamsplitter ratio of reflectance to transmittance depends on the polarization state of the light.

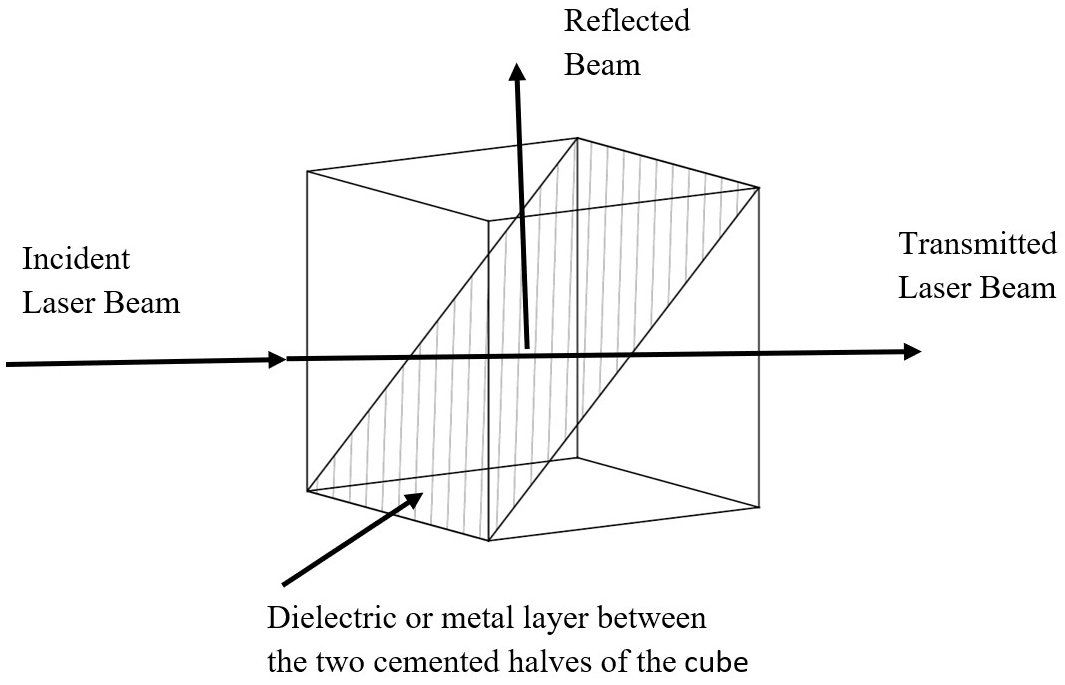

Figure 2.2 Cube Beamsplitter

2.2.4 Lenses

A lens is used to bring light to a fixed focal point by focusing rays of light and forms images of objects situated in front of it. It is specified by the transparent material of which it is made, the two faces curvature radius1 and radius2, the thickness of the lens at its midpoint, and its aperture diameter, which determines its thickness at the edge. It is generally circular in shape, with two polished precisely regular opposite surfaces, either or both are curved and may be either convex or concave. Due to the curvature of the lens surfaces, the rays of an incident light beam are refracted through different angles, so all parallel rays of the beam will converge, or diverge from, a single point. This point is called the focal point of the lens. The lens has an effective focal length F measured from its principal planes, and front and back focal lengths, which specify the distances of the focal points from the front and back surfaces of the lens. All lenses used in this thesis are spherical type and 1 inch in diameter.

2.3 Laser Doppler Velocimetry

A laser Doppler velocimeter is a non-intrusive optical instrument designed to measure flow velocities. The LDV principle is based on measuring velocities of particle passing through the probe measuring volume. The Laser Doppler Velocimetry (LDV) is a well-proven technique for fluid flow measurement with high spatial resolution; high velocity accuracy and can measure all the three velocity components [1]. LDV uses the Doppler shift of a laser beam to measure the velocity of solids or fluid flows. The two main LDV configurations are the dual beam [14] and reference beam modes [1]. In the dual beam mode, which is the most frequent, the laser beam is split into two beams which are made to intersect each other forming a region called the measurement volume [15]. The crossing region forms an interference pattern of light and dark

parallel fringes and constitutes the measurement volume in Figure 2.3. As a particle passes through the measurement volume, it scatters light from the fringes. The particles must be appropriately small enough to follow the flow and must have surface to reflect light which are neutral buoyancy to avoid gravitational effects. Usually seeding particles have densities comparable to fluid flow density to avoid gravitational effects. Additional discussion on flow seeding particles is in section 2.10. Typically, the probe measuring volume must be as small as possible for good spatial resolution and to achieve measurement of high signal-to-noise ratio (SNR). A lens focuses the beams on the measuring volume with an angle 2θ. At the focal point of the lens the beams cross each other, forming interference fringes in the measuring volume. The measuring volume has ellipsoid shape. A schematic diagram showing two focused laser beams forming the measuring volume shown in Figure 2.3. A particle traveling at velocity U is shown entering the probe volume in the diagram and crosses the fringes it scatters light when it passes a bright fringe, and scatters no light as it passes a dark fringe. The scattered light is collected by a photodetector and converted to time varying signals (voltage). The measured signal is extracted from the measured voltage is called a "Doppler burst signal" and has its frequency directly proportional to the particle velocity. Hence the particle velocity [16]. The fringe spacing d_f depends simply on the laser light wavelength λ and half the intersection angle of the two beams, θ.

$$d_f = \frac{\lambda}{2\sin\theta} \qquad (2.3)$$

Therefore, the frequency f_D measured and U, the speed component perpendicular to the fringes are related by the following equation:

$$f_D = \frac{U}{d_f} = \frac{2U \sin}{\lambda} \qquad (2.4)$$

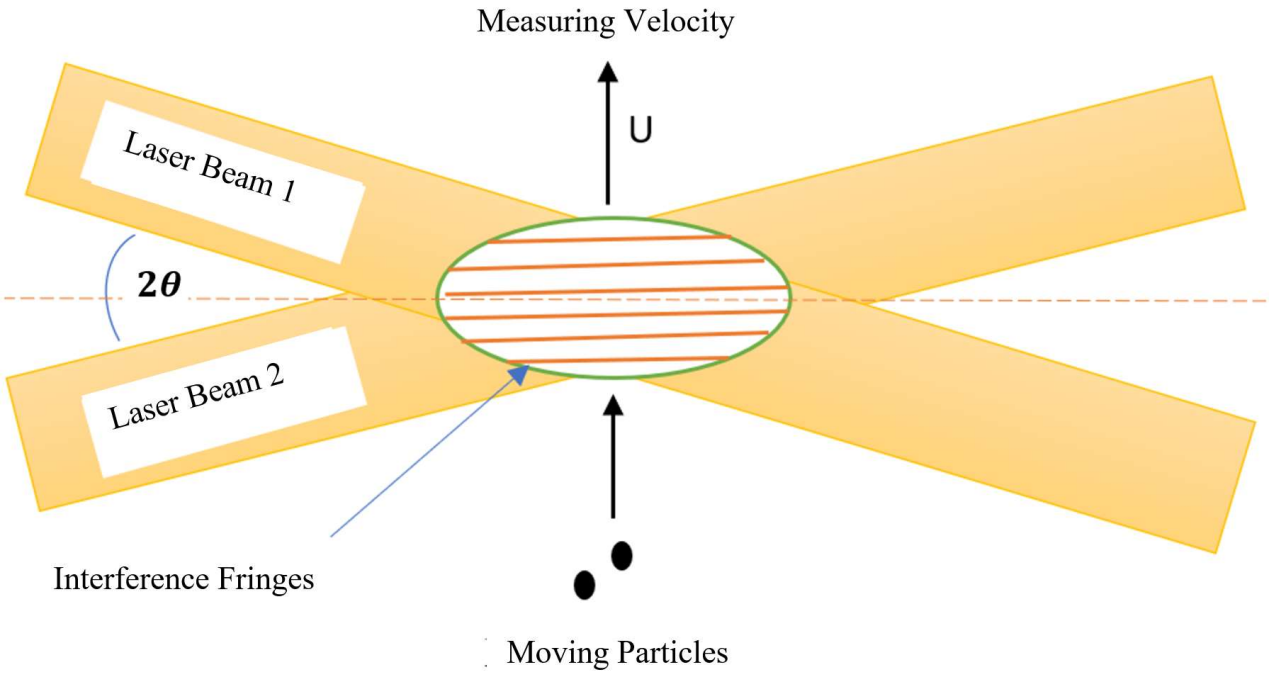

Figure 2.3 LDV Measurement Volume

2.4 Bessel Beams

The idea of the Bessel beam first arose in 1987 when Durnin [2] showed that a Bessel beam distribution is a solution to the wave equation [2]. Soon after, the first experimental realization of the equivalent Bessel beam was reported [17]. Since then, Bessel beams have been theoretically investigated by many researchers [2] [18] [19] [20]. Bessel beam with zero order has a transverse intensity profile with a bright central spot (lobe) surrounded by concentric rings as shown in Figure 2.5. Also, higher order Bessel beams have a transverse intensity profile of centered rings without the central bright spot. By referring to Figure 2.4, the size of the central spot is given by its diameter:

$$2ro = \frac{2.4048\lambda}{\pi \sin\beta} \qquad (2.5)$$

Where β is the axicon angle of refraction as shown in figure 2.4, r0 is Bessel beam spot radius and λ is the laser wavelength. The electric field of a Bessel beam can be defined by a zeroth-order Bessel function of the first kind (J_0) [21] [22]

$$E(r, \phi, z, t) = E_0 \exp(i(-\omega t + k_z z)) J_0(k_r r) \qquad (2.6)$$

Where E_0 is the field amplitude, r and φ are transverse and polar coordinates, z is the coordinate in the propagation direction, k_z and k_r are the longitudinal and radial wave vectors. The wavenumber can be found

$$k = \sqrt{{k_z}^2 + {k_r}^2} = \frac{2\pi}{\lambda} \qquad (2.7)$$

From the Fresnel approximation, a more realistic distribution can be obtained by considering an incoming Gaussian beam (Friberg, 1996). If an axicon is illuminated by a collimated Gaussian beam, the beam generated is called Bessel-Gaussian beam. The following variation of intensity distribution [23] is obtained:

$$I(r, z) = I_0 \left(4\pi^2\beta^2 \frac{z}{\lambda}\right) * \exp\left[\frac{2(\beta z)^2}{w_0}\right] * {J_0}^2(k\beta r) \qquad (2.8)$$

Where J_0 is first kind Bessel function of zero order, (r,z) are radial and longitudinal coordinates, I_0 is incident on-axis intensity, k is the wavenumber in free space and w_0 is the beam waist. Equation (2.9) gives the variation of the intensity in a cylindrical coordinate system (r,ϕ,z), but since the lenses considered are symmetric about the z axis there is no variation with ϕ. The on-axis intensity is obtained by setting r = 0:

$$I(0,z) = I_0 \left(4\,\pi^2\beta^2\,\frac{z}{\lambda}\right) * \exp\left[\frac{2(\beta z)^2}{w_0}\right] \qquad (2.9)$$

The radial/transverse distribution can also be obtained by setting **z** to a constant value along the axis. The Bessel beam has the advantage over Gaussian beam in many applications is that the Gaussian beam focuses to a small spot and immediately expands, whereas the Bessel beam retains a small central spot size over its diffraction free propagation distance. In this thesis, we are only using zero order Bessel beams (J_0). In theory, the intensity profile of the ideal Bessel beam propagates for an infinite distance and it can contain an infinite number of rings but it requires an infinite energy. Since this is impossible, however, a finite approximation to the ideal Bessel type beam, which has a finite diffraction-free propagation distance and finite energy, can be produced experimentally in the lab [24]. In practice, the generated beams do not change the laws of diffraction, so that the diffraction free properties are valid only of a limited length, but nonetheless these beams were very useful for example in alignment [25], due to the long and narrow line of light.

2.4.1 Generating a Bessel Beam

Experimentally, several methods for generating Bessel-type beams have been suggested such as narrow annular slit (Durnin rings) [26] [27]**,** axicons [28]**,** diffractive phase elements [29], computer-generated holograms [30], optical refracting systems [31], and Fabry-Perot cavity [32]**.** As first demonstrated by Durnin et al., a Bessel beam can be generated by illuminating an annular slit located at the back focal plane of a lens, each point source along the ring is transformed by the lens to a plane wave [17]**.** The basic idea of Bessel beam generation using annular slit (Durnin ring) is explained in chapter 5 with the aid of Figure 5-1**.** Using the Durnin ring technique has the advantage of simplicity and ease of alignment. The Ring can be easily fabricated in mass

production with cost effective compared to axicons. Hence, the generation of Bessel beams by the Durnin ring is thus an ideal solution. However, the main limitation in this generation technique is the low amount of power passing through the ring and carried by the beam because the majority of light from the Gaussian beam is blocked at the annulus. Diffraction-free Bessel-type beams were also generated by axicons, reflective axicons [33] and holographic axicons [30] [34]. However, a more efficient method of generating Bessel beam has been proposed using axicons**.** When passing a collimated laser beam through the axicon center, the traverse intensity along the focal line can be approximated by a zero-order Bessel-type beam as shown in Figure 2.4 and Figure 2.5. The beam propagates without diffraction and maintains its transverse distribution along the axis [2]. The Bessel beam has its energy evenly distributed between its rings [35] [36], so the more rings the beam has the lower the energy in the central core or spot intensity.

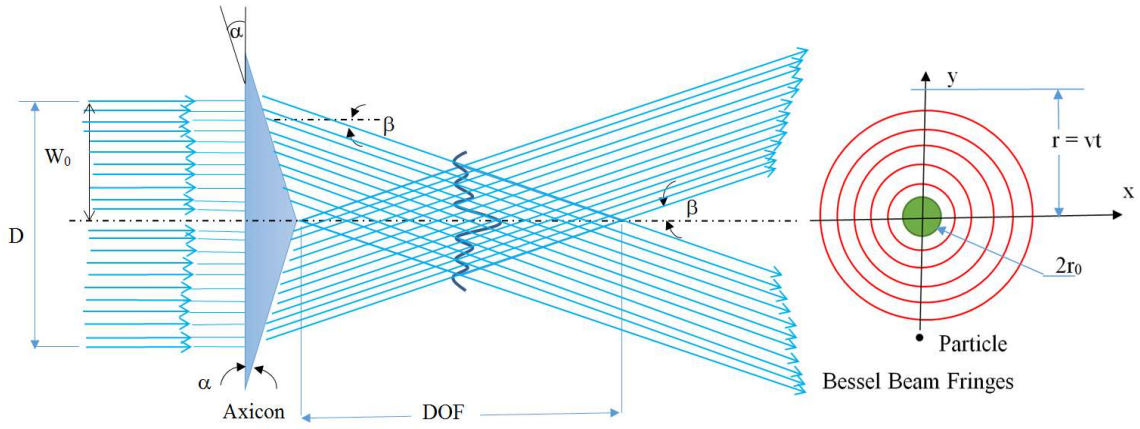

Figure 2.4 Bessel beam and axicon depth of field

The refraction angle β is related to the angle of the axicon, α which is the axicon base angle, and n is the axicon index of refraction:

$$\beta = (n - 1)\alpha \qquad (2.10)$$

Since sinβ≈β from the small angle approximation $\mathrm{ro} = \frac{2.4048\lambda}{2\pi\beta}$

The propagation distance of the Bessel beam is denoted as the depth of field (DOF) which can be found from the geometry of the axicon in Figure 2-4 by

$$\mathrm{DOF} = \frac{\mathrm{W0}}{\tan} \qquad (2.11)$$

From equation 2.8, it is clear that a larger beam waist or a smaller value of α result in a larger maximum diffraction-free propagation distance (DOF). A larger number of rings come with an increased propagation distance [22]. Combining an axicon with spherical lenses generates a varying ring pattern along its optical axis and extends the depth of field (DOF) [37]. An extended DOF is one of the main properties of axicons. This property specifically differentiates the axicons from typical spherical lenses.

$$k_z = (\frac{2\pi}{\lambda})cos\beta \qquad (2.12)$$

$$k_r = (\frac{2\pi}{\lambda})sin\beta \qquad (2.13)$$

By multiplying the electric field by its conjugate (assuming k is real) the transverse intensity $I=ExE^*$ is proportional to: $J_0^2(k\beta r)$.

Jaroszewicz [38] [39] presented a comprehensive review on the different types of axicons, their design, construction and properties. Chebbi and co-investigators [40] showed experimentally an optical system that produces a variable position and extends focal depth utilizing axicons. The proposed system consisted of three axicons. The first two axicons are identical and they create an annular beam propagating in free space or in a fiber bundle. This beam was focused by a third

axicon generating a controllable DOF. By adjusting the distance first between the two axicons the focal distance can be controlled which depends on the diameter of annular beam. This system setup allows a simple and adjustable focus capability. This system has applications in laser Doppler velocimetry, endoscopy and tomography [40]**.** Zhai et al. [41] used an axicon with a common lens to extend its depth of field (DOF).

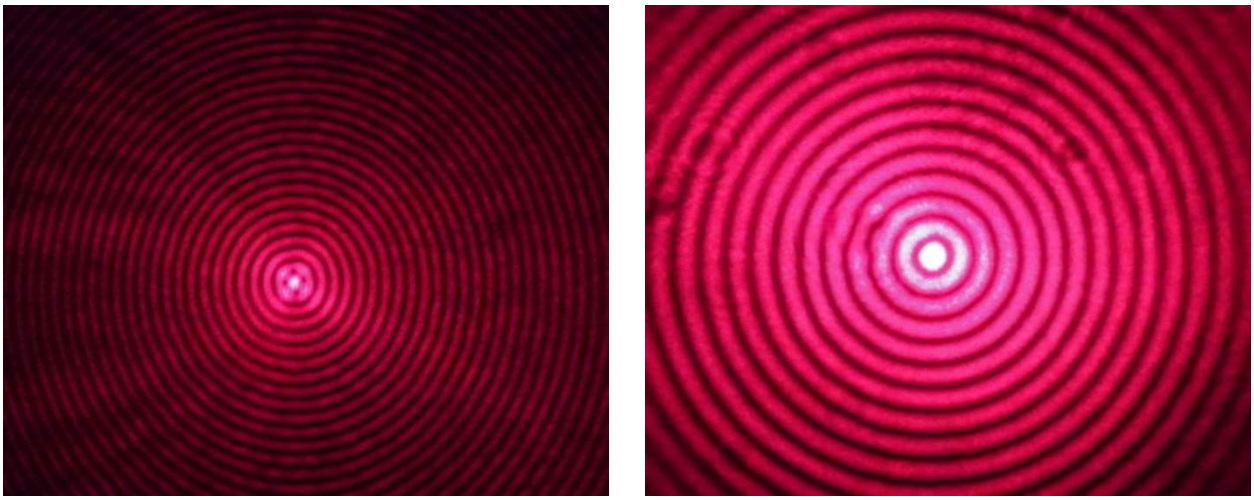

Figure 2.5 Bessel Beam Generated by 5° Axicon Bessel Beam Generated by 0.5° Axicon

2.4.2 Self-Healing Property of Bessel Beams

Now that Bessel beam generation has been described, another remarkable feature of a Bessel beam's self-healing property can be explained. The Bessel beam can be explained as an interference pattern generated by waves propagating on a conical wavefront. When an obstruction is placed in the path of the Bessel beam, the beam will reform itself at a distance after the obstruction. Figure 2.6 shows how the beam is generated using an axicon and able to reform after an obstruction. The obstruction blocks some of the incoming waves, while the waves that pass the obstruction interfere and reconstruct the beam. The optical rays illuminating the axicon reconstruct

the Bessel beam after the obstruction. The minimum distance for the Bessel beam to reconstruct after an obstruction, Z_{min}, is related to the wavevectors k and k_r by

$$Z_{min} \approx \frac{r_{obs}k}{k_r} \qquad (2.14)$$

where r_{obs} is the radius of the obstruction measured from the beam centre.

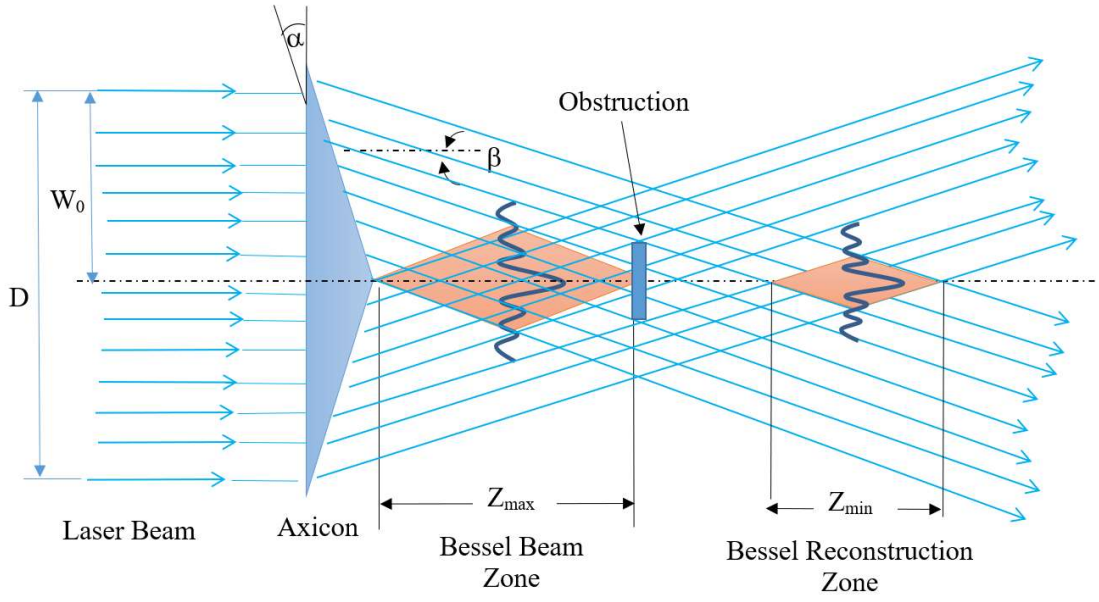

Figure 2.6 Bessel beam reconstruction after an obstruction

2.4.3 Applications of Bessel Beams

The Bessel beam proved useful for many applications including optical sorting, [42] [43] , cellular transfection [44] and optical atom guiding [45]. Because Bessel beams have the property of propagation invariance and extremely narrow intensity profile. Recently, Bessel beams were used to manipulate micrometer-sized particles [46]. Using the self-regeneration property of Bessel beam, it is possible to manipulate tiny particles (of micron-sized) simultaneously in multiple planes. Aruga and Li [47] argued that a diffraction-free Bessel beam is applicable in imaging providing a longer focal depth compared with Gaussian beams and improving the resolution of

imaging system [9]. Since Bessel beams can stand the atmospheric turbulence more than other beams they were used for large-scale measurement and straightness [48], Bessel beams were used to accelerate the particles of the electron beam when radially polarized [49]. The Bessel beams distinctive properties for particle trapping, gathered a lot of interest. Recently, Bessel beams have generated lots of interest due to their distinctive properties for particle trapping [50] [51] [52] [53]. It is used in applications of particle handling and rotation [54] and acoustic radiation force strategies in liquids [55]. Bessel beam have also been used in photopolymerization [56] and in material processing [8]. However, they have not been investigated in high-throughput 3D printing. Li et al applied Bessel beams to optical interconnection and promotion of free electron laser gain [57]. Tewari et al. [58] proposed the use of Bessel beam in nonlinear optics to generate third harmonic which is usually only observed at very high intensities of light such as those provided by lasers. The increase of scan sensitivity in measurement using Bessel beams was demonstrated in [59]. Bessel beams have been widely used in applications related to acoustics. In acoustics, generally Bessel beams are used in applications such as ultrasound imaging systems [60] [61] [62]. Yala et al. used focused Bessel beams to study optical traps which offer highly superior capabilities for manipulation of individual glass beads in the three spatial directions compared with standard optical tweezers based on focused Gaussian beams [63]. Over the last few years, a research group at the department of Technical Cybernetic, Samara National Research University, Russia [64] has published several research papers exploring different applications utilizing Bessel beams, such as free-space long-distance self-healing [65] [66] material processing [67] [68], optical trapping [69], astigmatic transformed Bessel beams [70] [71], encryption in optical communication [72] [73] and sharp focusing [74] [75]. Because Bessel beam have a distinct property of self healing after being

disturbed and their ability to control their longitudinal intensity distribution, they are particularly advantageous for use in measurement of fluid flow velocity in turbid media.

2.5 Basic Theory of Laser Bessel Velocimetry (LBV)

The technique of Laser Bessel Velocimetry (LBV) [3] [4], as the name stands for, is a technique of using laser light and the interference for velocity measurements which was developed in my M.A. Sc [76]. It is an optical technique and hence strongly related to both the physical and geometrical optics. It is based on the scattered light of tracer particles which scatter laser light as they flow through a liquid medium. LBV resembles Laser Doppler Velocimetry. It is simple, compact, and easy to set up. In [76] we have performed experiments, theoretical analysis and simulations to proof the concept of measuring velocity with Bessel beam fringes. It was found that by calculating the spectrum of the corresponding signal, its frequency is directly related to the velocity of the particles. In order to analyze the system theoretically, we consider particle crossing Bessel beam fringes with a constant velocity normal to the longitudinal axis and passing through the center of the beam. This particle scatters light with intensity given by: $I = I_0 {J_0}^2(k\beta r)$, where I_0 is a reference intensity, r is the radius from the center of the beam, k is the wave number given by $\mathrm{k} = \frac{2\pi}{\lambda}$, and λ is wavelength of the laser beam. The scattered light from the particle passing through Bessel beam fringes is collected by the photodetector producing a proportional current, which is converted to a voltage. The signal from the photodetector is passed through an amplifier and filtering circuit then digitized and stored for processing. The frequency content of the voltage signal is analyzed by Fourier transform, which will give the spectrum of the signal. In our case we need the Fourier transform of the function $[\mathrm{J}_0(\mathrm{k}\beta\mathrm{r})]^2$, which can be written as $[\mathrm{J}_0(\mathrm{k}\beta\mathrm{vt})]^2$, by

substituting the radius r as a function of the velocity of the particle (r=vt). The spectrum F(*f*) as a function of the frequency f, of the signal is found by calculating its Fourier transform:

$$F(f) = F[J_0(k\beta vt)]^2 \qquad (2.15)$$

F(f) was theoretically and numerically calculated in [76]. It is shown in Figure 2.7. This distribution is characterized by the Bessel frequency f_b which can be related to the velocity by

$$f_B = \frac{k\beta v}{\pi} = \frac{2\beta v}{\lambda}(Hz) \qquad (2.16)$$

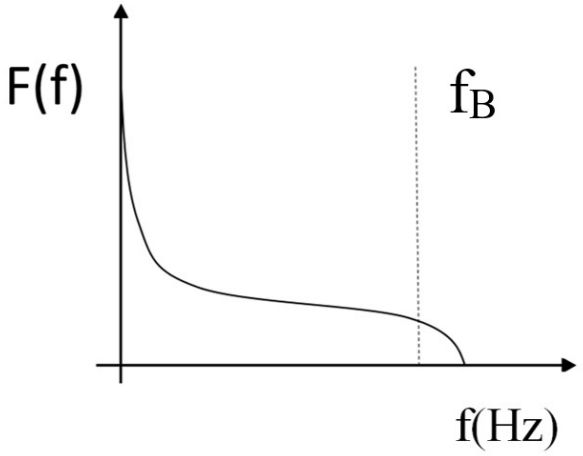

Figure 2.7 Spectra and Bessel Frequency of $F[J_0(k\beta vt)]^2$

It has a half hut shape, and it has higher value at low frequencies and decreases until f_b becomes zero. The expression f_b denotes the Bessel frequency, which is similar to the expression of the Doppler frequency f_D for the LDV dual beam mode. Measurements performed in [76] confirmed the distribution. Using this measured frequency of the particle f_b the velocity as a function of the frequency and other parameters of the optical setup can be found from the relationship:

$$v = \frac{\lambda f_B}{2\beta} \qquad (2.17)$$

Where β is the refraction angle of the axicon. The difference is that in the case of LDV the spectrum represented by a peak at f_D, while in the case of Bessel frequency f_B marks the edge of the hut shaped frequency distribution. The technique for measuring velocity with Bessel beam has many similarities with laser Doppler velocimetry. In both cases, the frequency of the signal produced by the photodetector is proportional to the velocity of the particles. The equations of velocity are derivable from first principles, so calibration is not necessary in both cases. The difference is in the way the fringe patterns are produced and on their geometry. The laser Doppler velocimetry has the advantage that small measuring volume with uniform fringe spacing. The Bessel beam technique, however, is simple but with larger depth of field and axisymmetric non-uniform fringe spacing. In this work, we explore the use of the fringes of one Bessel beam to measure one component of fluid flow velocity in the flow horizontal direction. We measure the light scattered intensity from particles moving in the flow channel crossing the Bessel beam fringes generated using axicon.

2.6 Light Scattering Particles in Flow

Rather than relying on naturally existing particles in the flow, it is common to add seeding particles to the flow to have control over their size, surface reflection, density and concentration. The scattering particles are important for suitable signal detection in LDV, PIV and for the present investigation. Generally, these seeding particles should be small enough to follow flow, and large enough to scatter sufficient light that can be collected. It must follow the flow speed being measured and to reflect a strong signal. Some seeding particle materials available are listed in table 2.1 [77]. The particle shape, size density, and concentrations are important parameters for selecting the seeding particles. A better index of refraction and large geometric particle size can increase the signal quality and signal strength. The seeding particles follow the flow according to a time constant τ_p [77]. Based

on Mie theory, particles with small diameters scatter a larger percentage of their light at wider angles than larger particles [78] . For these reasons, the signal is affected by the seeding particles. Many series instruments have become popular in a diverse field of particle studies. Results are relatively sensitive to the shape, composition, and size distribution of the particles in suspension. The intensity of the scattered light increases with particle surface size and relative index of refraction (Fingerson et.al. 1990). The scattering light from a particle may depend on some parameters such as: wavelength λ of incident light, size of the seeding particle and the particle index of refraction.

Table 2.1 Common Seeding materials and their refractive indices given by Tavoularis [77]

Seed Material	Index of refraction n	ρ_p (kg/m^3)	Fluid
Al_2O_3	1.76	$3.96x10^3$	Gas-liquid
Polyamid	1.5	$1.03x10^3$	Gas-liquid
Polystyrene	1.59	$1.05x10^3$	Gas-liquid
SiC	2.6	$3.2x10^3$	Gas-liquid
Hollow glass beads	1.52	$1.1x10^3$	Liquid

The seeding particles follow the flow according to a time constant τ_p given by Tavoularis [77]

$$\tau_p = \frac{\rho_p d_p^2}{18\mu_f} \qquad (2.18)$$

Where ρ_p density of particle, d_p diameter of particle and μ_f is viscosity of fluid, and the system behaves as a first order one

$$\frac{du_p}{dt}\tau_p = u(r) - u_p \qquad (2.19)$$

Where u(r) is fluid velocity, u_p is the particle velocity, so that if a particle is injected with zero initial velocity at time t_p=0, its velocity becomes

$$u_p = u(r)\left(1 - e^{-\frac{t_p}{\tau_p}}\right) \qquad (2.20)$$

Chapter 3

INSTRUMENTATION AND EXPERIMENTAL APPARATUS

This Chapter describes the experimental apparatuses and the instrumentation designed, developed and built-in order to conduct the experiments. The apparatuses include a rotating disk attached to a direct current (DC) motor to measure the solid surface *u* and *v* velocity components, a water tank to measure the total plane velocity in any direction and a water channel to measure laminar and turbulent pipe flows. The optical instrumentation to generate the Bessel beams, the traversing, alignment and refraction of the laser beams are also discussed. Finally, the photodetector used to measure the scattered light, the signal conditioning and data acquisition are described.

3.1 Experimental Apparatuses

Different apparatuses were designed and built to provide the measurement media for the techniques developed in this thesis. In order to test the two-component LDV system a rotating disk with a sandpaper was used. This setup is described in detail in Chapter 5 and will not be further described here. To generate the fluid flows to be measured a water tank and a closed loop water channel were used.

3.1.1 Water Tank

The experimental model was a plastic cylindrical tank with a constant circular cross section. The tank is open to the atmosphere at the top so that water can be poured into the tank easily. The tank was held fixed on the bench and placed vertically such that the open end faced up. It has an inside diameter of 28.5 cm and a height of 35 cm with cross sectional area of 2552 cm^2 and volume of

90587 cm^3. A drain was placed 5cm above the base through which liquid can drain as shown in the sketch, Figure 3-1. The exit hole was drilled into the tank using a drill bit as a discharge drainage of 6mm in diameter located 30.5 cm from the top as shown in Figure 3.1. The drain was closed using a removable plug. A graduated scale was glued vertically along the length of the tank and it was used to track the position of the water level in the tank during filling and draining process.

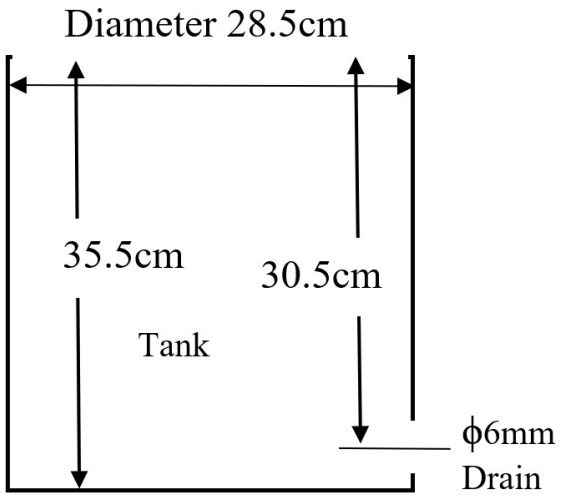

Figure 3.1 Water Tank (not to scale)

3.1.2 Closed Loop Water Channel

The water channel is mounted horizontally in the laboratory and a general sketch is shown in Figure 3.2**.** This allowed the water channel components to remain stationary while the flow was measured and optical system moved to map out velocity profiles. The working fluid is domestic tap water at an average room temperature 22ºC whose physical properties can be easily obtained from literature, and experiments were performed with the addition of seeding particles. The water channel operates as a continuous flow channel. The flow loop consists of tank, pump, settling

chamber (contraction), pipes, test section and flow meter. The PVC pipes are 1.5 inch in diameter fixed horizontally of 3-meter-long. A 1/4 Hp motor pump continuously draws water from the reservoir and delivers it to the test section providing a maximum volumetric flow rate Q=15 GPM. After the pump and before entering the pipe, a contraction was placed in the start of the loop. The flow was conditioned in the upstream region of the pipe after the contraction using flow straightener. Then through the settling chamber and it is connected to the pipe by a smooth contraction. The pipe section is made long enough to make the flow fully developed before the measurement section. A glass test section is connected to the PVC pipe after 3.5 m length. The test section is 1.5 m long by 38mm inside diameter and 4mm wall thickness made of a transparent glass to permit optical access and flow observation. It was interchangeable and was connected horizontally to the loop by flexible rubber flanges. The inner surface of the two flanges connecting the test section and the flow loop were mounted flush to ensure minimum disturbance to the flow. A square glass box was built around the test section, where the measurements can be made. The flow channel pipes and apparatus are aligned, leveled and fixed on a rigid bench surface to prevent movement and vibration. The water channel, the test section and pump were mounted to ensure vibration of the system was minimum. Control valve A regulates the flow rate measured by a gravitational type flow meter which is based on the suspension of a steel truncated conical cylinder due to the resultant from the gravity, buoyancy and hydrodynamic forces. Valve A is closed slightly to increase the system operating pressure as needed and reduce the flow rate, which will allow removing air which entered the system. Closing the exit valve A too much could cause an over pressure and damage the system pipes and components. Valve B is used to drain the water back into the reservoir without pumping it through the system. Valve C was added before the flow meter to control system pressure and readjust the flow rate if needed without allowing water to

flow and spill over the bench. It is used to remove air bubbles caused by the pump suction if required. At system start up, valve C is fully open to reduce the flow rate and prevent sudden pressure surge which might damage the system. It is used to return the flow back to the reservoir and to control the flow in the system.

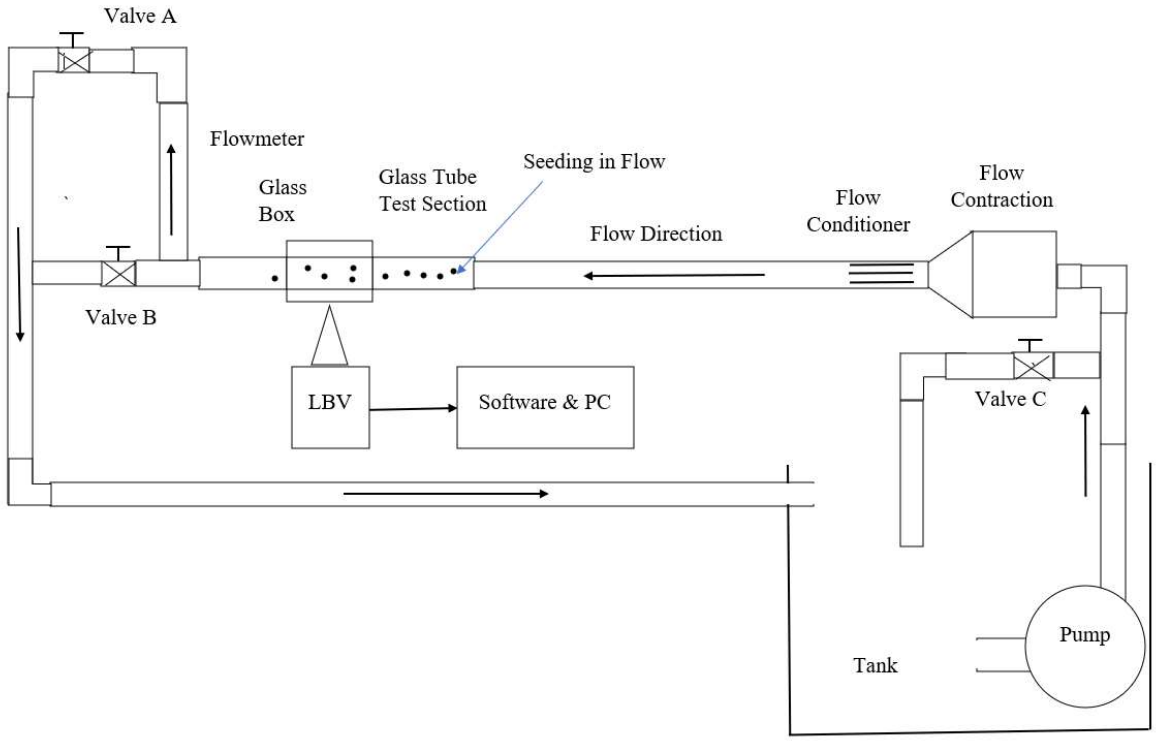

Figure 3.2 Fluid Flow Channel Experimental Apparatus Set-up

3.2 Instrumentation

This section describes the instrumentation developed which constitutes a major contribution of this thesis.

3.2.1 Bessel Beam LDV System

This system was developed in order to conceive a simple LDV system to measure two velocity components. It is described in detail in Chapter 4.

3.2.2 LBV System Using Axicon

For the tank in Figure 3.1 and velocity measurements using LBV technique, a red laser beam (λ =658 nm) was expanded to a diameter of ≈6 mm and passed through an axicon with base angle 0.5° to generate a nearly Bessel beam with an average fringe spacing of 70 μm. The optical components were mounted and aligned to focus on the tank drain. Measurements were made on the velocity exiting the tank at seven different height levels using the described optical technique. The data acquisition and data processing used are the same for all measurements as stated for the water channel measurements. An axicon with base angle 5° was used to compare images of the beams obtained from slits presented in chapter 5. Table 3-1 shows the axicons parameters. The general optical set up using axicon is shown in Figure 3.3.

Table 3.1 Axicons Experimental Parameters

Parameter	β°	DOF cm	Spot size $2r_0$ (μm)	Average Fringe Spacing d_f (μm)
0.5° axicon	0.265	86.2	109.90	70.5
5° axicon	2.66	8.60	10.853	7

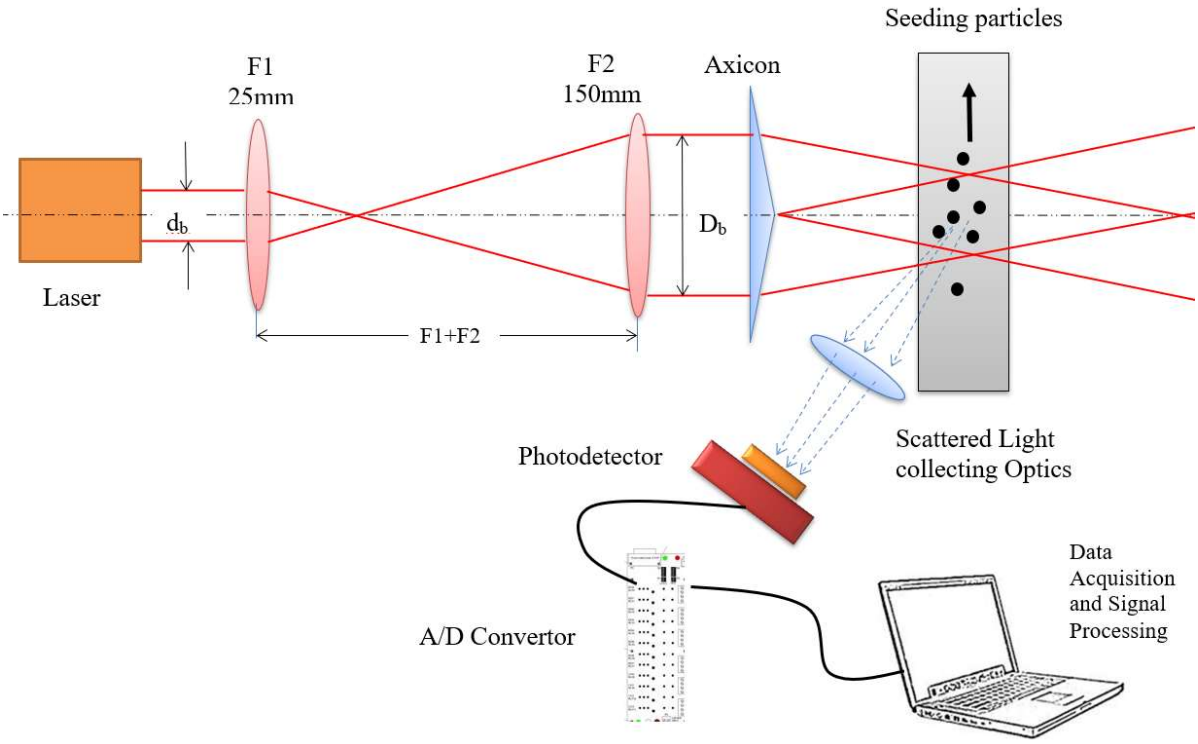

Figure 3.3 LBV Optical Arrangement Set up using Axicon

3.2.3 LBV System Using Durnin's Slits

In order to provide good spatial resolution, Durnin's slits were used to generate the nearly Bessel beams. The manufacturing of the slits and the characterization of the generated beams are described in detail in Chapter 5. A general sketch of the LBV system is shown in Figure 3.4. The optical setup consists of red laser with continuous output power of 107 mW with a wavelength of 658 nm mounted horizontally on the lab bench. The laser beam is expanded using a telescope consisting two lenses 25 mm focal length and 75 mm focal length to get a beam size of approximately $D_b \approx 3$ mm diameter focused on the slit. Using the relationship $D_b = d_b \left(\frac{F2}{F1}\right)$ as shown more clearly in Figure 3.4. The expanded laser beam was aligned and centered on the annular slit. All lenses used in this thesis have a diameter of 25.4 mm.

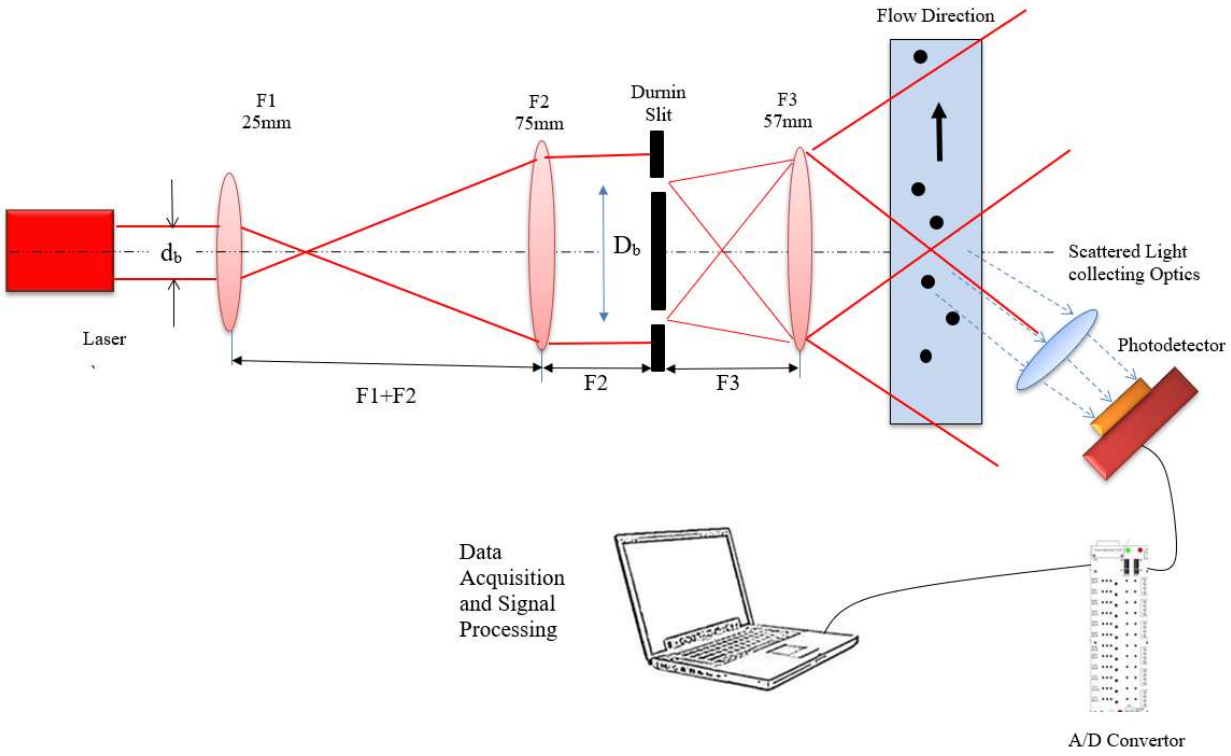

Figure 3.4 LBV Optical Arrangement Set up using Durnin Ring (Slit)

A 57mm focal length lens was positioned after the annular slit to generate Bessel type beam approximately at the lens's focal length. The annular slit was placed in the focal plane of the 57mm focal length lens as shown in Figure 3.4. Several slits were made and used in the measurements. A Thorlabs photodetector (PDA36A2) was used to detect and measure the scattered light from the moving particles once they cross the fringes of the Bessel beam inside the flow. Lens 4 has 25mm focal length was used to collect the scattered light from the measuring volume and focuses it on the photodetector aperture. The photodetector converts this signal into a measurable voltage. The signal from the photodetector was filtered and amplified. This signal was then digitized with an (A/D) converter connected to a personal computer and the obtained data files were stored in data files for processing. All the optical components: the laser, the lenses, the slits and the photodetector were mounted on posts and holders and secured into an optical breadboard bench fixed on a traversing stage. Proper adjustment and alignment procedures of each component were followed.

Translating each component on the optical bench can be done without losing alignment. The assembly could be moved along the bench to accurately match the position of the measurement location. A power supply voltage (BK Precision 1671) used to supply a 12-Volt DC to the amplifier and filtering circuit. The choice of the transmitting lens was based on the dimension of the measurement volume for optimal resolution. Smaller focal length provides a smaller depth of field, however, due to the size of the square glass box around the test section poses a limitation if one want to perform measurements at the middle of the test section tube. Following this, in order to obtain good spatial resolution, lens 3 with focal length of F=57mm was used. The measurement volume dimensions depend on the slit used with lens 3 (details are shown in table 5.1). Collection of the scattered light using lens 4 (F=25mm) to improve the sensitivity and increase the signal strength. The geometrical information and the dimensions of the measurement volume are listed in chapter 5 (Table 5-1).

3.3 Traversing LBV System

The traversing system consists of adjustable stage (jack) set on supporting table. The supporting table is leveled and fixed on the floor. The breadboard optical bench is fixed on the adjustable stage which can be moved for alignment without difficulty. The jack ensures vertical displacement of the optical breadboard bench holding the LBV components. The optical assembly could be moved along this stage to accurately match the position of the measurement location. A digital indicator type Pro Point was used to measure the vertical distance and specify the location of measurements as the stage being traversed. The digital indicator is 6.2 x 4 x 2.2 in and used with a clamping device to accurately measure small linear distances (detailed specifications are shown

in table 3.2). It has manual power ON/OFF, ZERO setting at any position and mm/in conversion at any position.

Table 3.2 Digital Dial Indicator Specifications

SPECIFICATIONS	
Spindle Diameter	3/8 in.
Resolution	0.01 mm/0.0005 in.
Accuracy	±0.03 mm
Spindle Size	4-48 UNF Thread
Operating Temperature	0° to 40°C

3.4 Seeding

Seeding is one of the most critical issues in making LBV measurements. The seeding particles must have a uniform size, small enough to accurately follow the flow and able to scatter light sufficiently for detection. The seeding particles chosen for the present experiment was aluminum oxide with a uniform size of 5μm as shown in table 2.1. For all measurements, the fluid was allowed to flow for few minutes in the water channel before taking measurements. which is more than the required time for the particle to reach fluid velocity.

3.5 Data Acquisition

An Omega-DAQ Board-3000 is used for data acquisition in connection with NI LabVIEW. A Graphic User Interface (GUI) was developed using NI LabVIEW and used for the experimental measurements. The GUI allowed selection of the sampling frequency, the number of samples and

the files to store the data. The sampling rate was set according to fringe spacing within the measuring volume and depending on expected magnitude of the velocity based on the flow rate. The average of 10 measurement records were performed for each point. Some knowledge of the flow was known prior to measurements, for instance the expected range of velocities and direction.

3.6 Photodetector

The photodetector (PD) used in all measurements was Thorlabs model PDA36A2 switchable gain silicon photodiode. It has spectral range of 350-1100 nm and a spectral responsivity of 0.65 A/W. The active area of the photodetector is approximately 13mm^2. It has a bandwidth of 150 MHz at the minimum gain setting but, the bandwidth decreases as the gain setting is increased. It has a fixed gain of 1.51 kV/A -4.75 MV/A with high-Z load and a maximum output current of 100mA. It converts the scattered light into an electric current. A load resistor of 50 kΩ was used and connected to the photodetector to convert the generated current to an output voltage signal.

3.6.1 Photodetector Limitations

The scattered light from a moving particle in the measurement volume must be focused on the aperture of the photodetector. The aperture size has large effect on the signal quality. Because of the small aperture of the photodetector, only particle velocities at a specific region along the length of the measurement volume will be measured each time. Extra receiving optics might be used to focus scattered light to enhance the optical measurement performance and improve the signal to noise ratio (SNR). Because LBV operates with seeding particles in the flow, the accuracy with which the seeding particles essentially follow the flow is important. The particles have to be in the

micron size but large enough to scatter sufficient light adequately to obtain a good signal-to-noise ratio SNR at the photodetector output.

Table 3.3 Photodetector specifications

Detector	Si PIN
Active Area	13 mm^2 (3.6 mm x 3.6 mm)
Wavelength Range	350-1100 nm
Peak Wavelength	970 nm
Peak Response	0.65 A/W
Amplifier GBP	600 MHz
Output Impedance	50 Ohm
Max Output Current	100 mA
Gain Adjustment Range	0 dB to 70 dB
Gain Steps	8 x 10 dB Steps
Load Impedance	50 Ohm to Hi-Z
Transimpedance Gain	1 x 10^4 V/A 5 x 10^3 V/A
Output Voltage	0 to 5 V (50 Ω) 0 to 10 V (Hi-Z)
Operating Temperature	10 to 40 ºC
Storage Temperature	-20 to 70 °C
AC Power Supply	AC – DC Converter
Input Power	6 W 100 V / 120 V / 230 V (50 – 60 Hz)

3.6.2 Photodetector Signal Detection

For a single particle passing through the measurement volume. Scattered light signals are generated as particles pass through the Bessel beam which is the laser beam in the fluid stream. The scattered light signals are converted to electronic signals (voltages) by the photodetectors. The signals are amplified and digitized for a stronger signal. A voltage pulse is created when a particle crosses the Bessel beam and starts to scatter light. When the scattered light signals (photons), strike one side of the photodetector aperture, they are converted into a proportional number of electrons that are multiplied, generating a greater electrical current. The electrical current travels to the amplifier and passes through 5KΩ resistor and is converted to a voltage. The highest peak of the pulse occurs when the particle crosses the spot which is the center of the Bessel beam and the maximum amount of scatter is achieved. As the particle leaves the center of the beam, the signal starts to decrease back down. The intensity of the voltage signal depends on the number of photons detected and the photodetector voltage pre-amplifier gain All signals are continuously digitized during measurement operation.

3.7 Signal Conditioning

The signal conditioning circuit has two components: one for signal amplification and the second for signal filtering. The amplification circuit, shown in Figure 3.5, is built using an operational amplifier. The two resistors, R_f =10kΩ and R_i=1kΩ, give gain:

$$\text{Gain} = \frac{\text{Rf}}{\text{Ri}} + 1 = 11 \qquad (3.1)$$

The filtering circuit is a low pass filter (LPF) and is shown in Figure 3.6. The LPF allows only frequencies below the cut-off frequency f_c to pass and above f_c are attenuated. It reduces high frequency noise but also eliminates aliasing. Based on the Nyquist criteria the sampling frequency has to be larger than two times the maximum frequency of the signal ($f_s > 2f_{max}$), but for better reconstruction of the signal, a much larger sampling frequency is used.

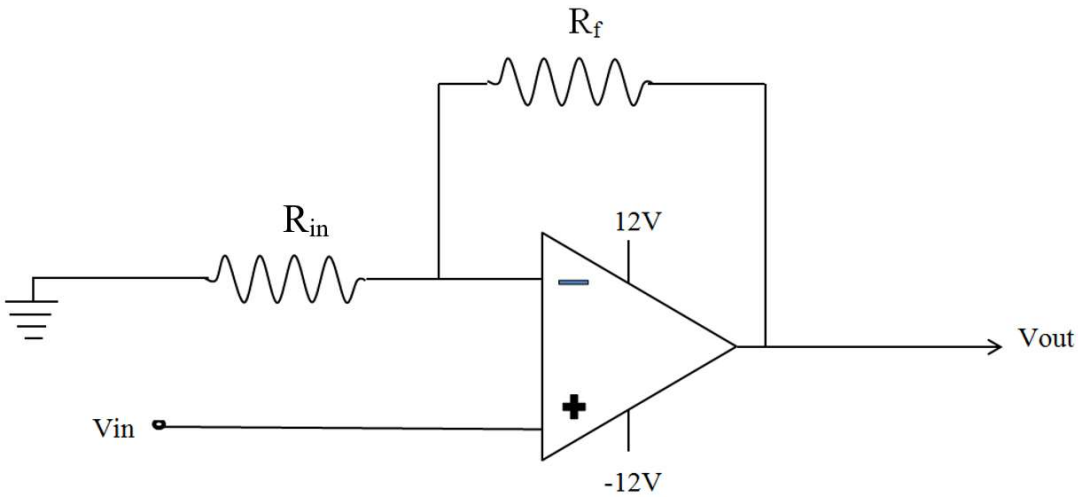

Figure 3.5 Non-Inverting Amplifier Circuit

The cut-off frequency $f_c = \frac{1}{2\pi RC}$ (3.2)

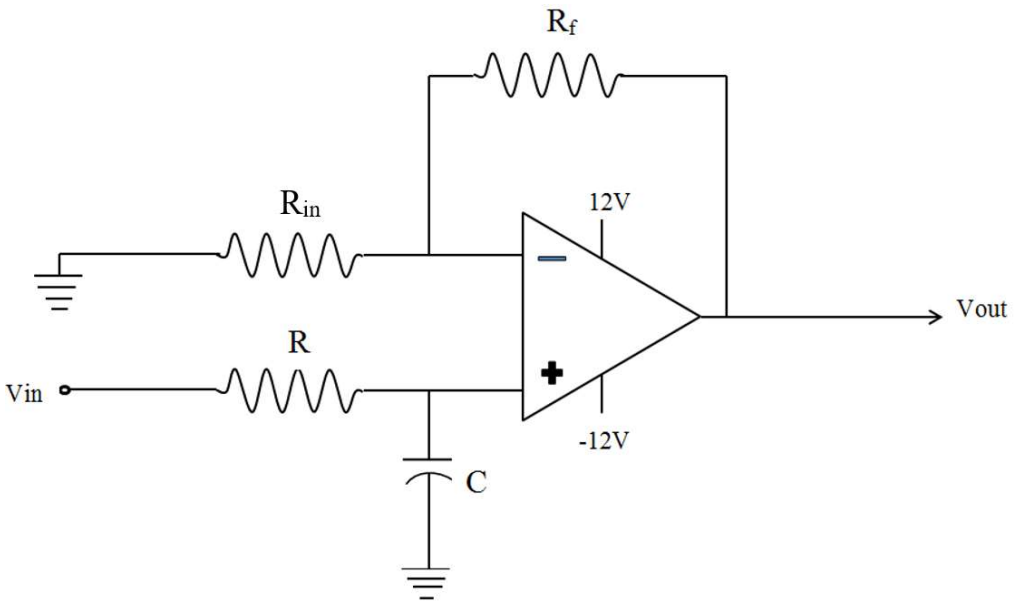

Figure 3.6 Low Pass Filter Circuit

The capacitor and resistor values of the circuit shown in Figure 3.6 were chosen to yield appropriate values for the cut-off frequency, f_c, depending on the expected value of the Bessel frequency.

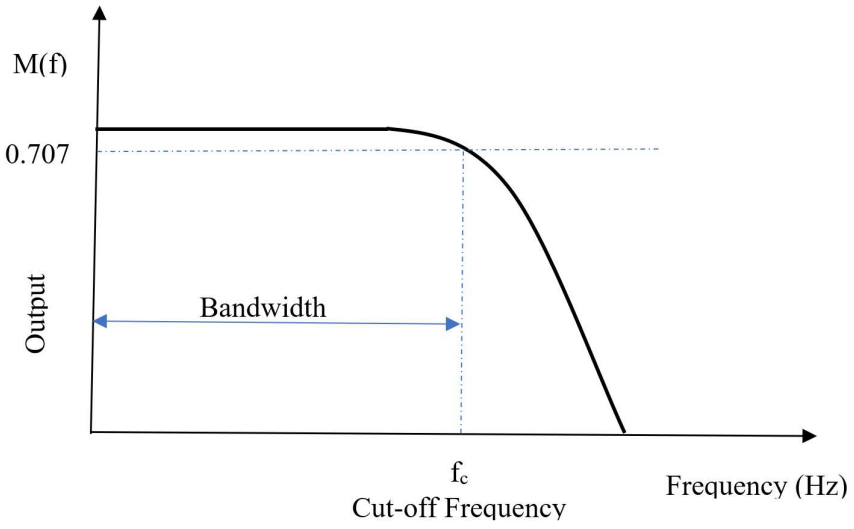

Figure 3.7 Low Pass Filter

3.8 Laser Doppler Velocimetry System

The laser Doppler technique is the reference measuring system selected to assess the measurement technique developed in this work. The MiniLDV (MSE) system manufactured by Measurement Science Enterprise, Inc. is used. The probe is fixed on the adjustable stage to allow obtaining 1D velocity profiles at various locations of the transparent tube. The system operates with red laser of wavelength λ=658nm and power of 107 mW and requires no calibration. The probe volume was factory set at a distance of 255 mm from the transmitter and receiver unit. The MiniLDV is capable of measuring flows in the low and high ranges [79] . The measurement volume size is 150x300μm with a fringe spacing of 9.15μm. The full specifications of the system are shown in Table 3.4.

Table 3.4 MiniLDV specifications

Laser Characterization Sheet	
Fringe separation	9.14 μm
Frequency shifting slope	284.25 Hz/RPM
Frequency shifting @3000 rpm	852.8 KHz
Frequency shifting @4000rpm	1137.0KHz
Frequency shifting @5000rpm	1421.3KHz
Driver used for Frequency shifting	FSA
Probe volume distance	255mm
Power in the probe volume	107mW
Transmission efficiency	76%
Wavelength	658 nm
Probe volume size at FWHM	150x300 μm
Probe volume length at FWHM	2.5mm
Colour	Red

3.9 Signal Processing

Velocities were measured using a single LBV beam system in the forward scatter mode with laser beam along the horizontal midplane of the pipe. The single line laser (Red 658nm wavelength) was operated at a laser power of 107mW which was the highest attainable power. The sampling frequency range selected for the experiment was according to the velocity of the flow and fringe spacing. The flow is artificially seeded using aluminum oxide particles (Table 2.1). The measurement signal is amplified for a better detection then acquired by an analog-to-digital converter for processing and processed for noise reduction. The output files from the acquisition module and LabView are saved in TXT format, that contain voltage and time values referred to the observed measurement. A MATLAB code is used to open the TXT files and generate a graphic from those values V(t) then calculate the spectrum of the signal using FFT to show the frequency that occur in the captured signal.

3.10 Refraction of Laser Beams

When flows in curved pipes are to be measured, the curvature of the pipe walls and diffraction effects can make accurate positioning of the laser beam difficult. The glass test section presented in the water channel measurements is 38 mm in internal diameter and 4mm in thickness. In our measurements, the laser beam will pass through air-glass-water, having different indices of refraction leading to change in the position of the laser beam. The purpose of the LBV measurements is to measure flow velocities along the vertical diameter of the pipe centre. To accomplish this, the problems involving refraction of the laser beam can be minimized by matching the index of refraction of each material. It is to improve the optical measurement conditions. It is a method that involves the selection of fluids and substances, matching the pipe material, that have

nearly equal or nearly equal refractive indices so that effects of refraction are quite small. In order to minimize refraction of the measuring volume path, a square glass box was built outside the circular tube, Figure 3.8 displays the principle of the system. The space between the wall of the box and the tube was filled with water which is the same kind of fluid as that inside the test section. The two side walls perpendicular to the incoming laser beam were made of thin glass, and the other four sides of the square box was made of rubber and metal. This way the beam will pass through air-glass-water-glass-water-glass, which will have similar refraction indices. The box glass surface installed parallel to the transmitting lens, that the refraction will be constant along the vertical diameter of the pipe. Then, the laser beam through the circular geometry of the pipe wall will travel without refraction as well as through the fluid inside the pipe. When the refractive index matching procedure is perfect, the laser beam will only be refracted when it travels from open air and through the glass surface of the box. The slope of the beam path traced out by the measuring volume is small after using the square box. The refractive index matching procedure is a well-established method used by several investigators. It was found that refraction effects could be reduced to a minimal level over the glass tube diameter with a simple glass box fixed around the tube. Durst et al. [80] performed LDV measurements using rectangular box built around a glass circular pipe. The aim was to measure turbulent statistics in the near-wall region of the pipe. The circular pipe was made from Duran-50 glass. Two diesel oils one with lower refractive index than Duran-50 and one with higher were used inside the glass box and the circular pipe. When they properly mixed the two diesel oils, they were able to get a mixture with the exact refractive index as the solid material. Toonder and Nieuwstadt et al. [81] suggested a procedure to measure turbulent water flow in a pipe with refraction index matching by constructing a special test section. To obtain good measurements near the pipe wall, the wall was made from Perspex (n=1.49). They

used foil in combination with the square Perspex (n=1.49) box filled with water around the cylindrical foil minimises the refraction of the laser beams. The pipe wall was replaced by a thin foil made of Teflon FEP (fluorised ethylene propylene) with a refractive index of n=1.334. Lei, U and Lin et al [82] build a square glass box outside the circular glass tube to reduce the slope of the path of the measuring volume to perform LDV measurements. The space between the glass tube and the box walls was filled with similar fluid as in the tube. This way measurements were performed with beam refraction correction. This way the beam will pass through air-glass-water-glass-water-glass-water-glass-air, which will have similar refraction indices.

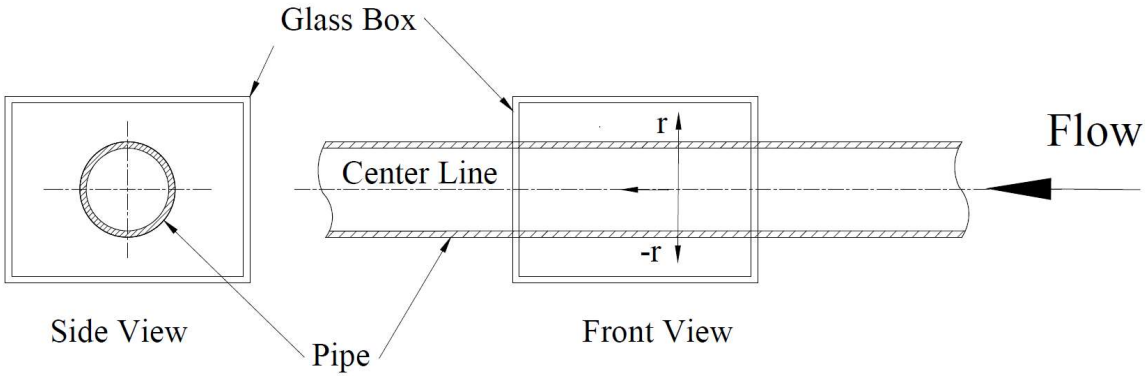

Figure 3.8 Square Glass Box around Pipe

3.10.1 Position Change of The Laser Beam

Initially measurements without the square glass box were performed. Correction for the position change of the laser beam was necessary. This is explained in this section.

Refraction of a laser beam occurs in the majority of optical applications. The refractive index of a material n_x is defined as the ratio of the speed of light in a medium relative to its speed in a vacuum.

$$n_x = \frac{c}{v} = \frac{speed\ of\ light\ in\ vacuu}{speed\ of\ light\ in\ the\ medium} \qquad (3.3)$$

Where c is speed of light $3x10^8$ m/sec in vacuum and ν is the speed of light in the material. In every media except vacuum, light travels with a speed that is less than c. This means that n is equal to unity in vacuum which is assigned a value of 1, and has greater value in all other materials. Snell's law used to calculate the refractive index of a medium. Using Snell's law, the refraction of a laser beam passing from a medium with refractive index n1 into a medium with index n2 can be calculated:

$$n_1 \sin \Theta_1 = n_2 \sin \Theta_2 \qquad (3.4)$$

Where θ1 is the angle of incidence and θ2 is the angle of refraction, measured from the normal to the interface between the two materials mediums. The wavelength of the laser beam as it passes from a medium into another will be also taken into consideration according to:

$$n_1 \lambda_1 = n_2 \lambda_2 \qquad (3.5)$$

The indices of refraction used are: $n_{air} = 1$, $n_{glass} = 1.52$ and $n_{water} = 1.33$.

Adjustment was performed to remedy any distortion of the laser beam configuration of the measurement volume in the optical measurement section.

Figure 3.9 shows the beam refraction inside the tube. The procedure and equations from reference [83] were used.

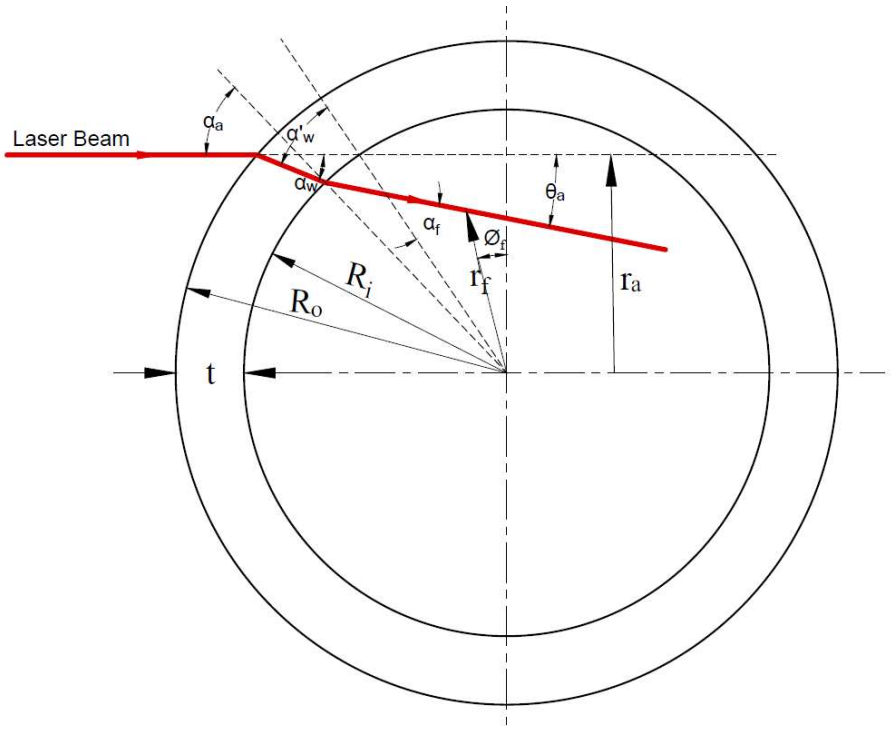

Figure 3.9 Beam Refraction [83]

Chapter 4

INTERFERENCE OF TWO INTERSECTING BESSEL BEAMS AND APPLICATION TO LASER DOPPLER VELOCIMETRY

We studied the interference of two intersecting similar Bessel beams. The front waves of the two beams interfere to form a distinct pattern of parallel fringes superimposed on the circular concentric fringes of the Bessel beams. We show that the two sets of fringes at the intersection region can be used in a simple laser Doppler velocimetry system to measure two velocity components. Simulations and measurements are presented to characterize the fringes and prove the concept of two-component measurement.

4.1 INTRODUCTION

The interference of two or more traveling aligned coaxial Bessel beams has been studied analytically, numerically, and experimentally and was shown to result in a smaller spot size and periodic longitudinal variation [84] [85] [86] [87]. It was suggested for applications such as particle manipulation [88] and characterization of optical components' surfaces [89]**.** In this work, we study the interference of two Bessel beams intersecting at symmetric angles on the longitudinal axis. Needless to say, interference of light beams is a vast area in optics and has extensive applications in many areas, including metrology, instrumentation, microscopy, and imaging. The interference of two Gaussian beams is widely used, for example, for laser Doppler velocimetry (LDV), a well-established technique to measure fluid flow velocity and solid surface velocity. The fringe configuration, where two or more beams intersect to form the measuring volume, is the most common due to its reliability and practicality. We limit the following discussion to systems

implementing this configuration. Commercial one-dimensional (1D), 2D, and 3D velocity component measurement systems are available, and upgrading from one system to the next is associated with significant complexity and cost. For example, while a 1D system needs one pattern of parallel fringes, usually obtained from a single laser beam split into two components intersecting at the measurement volume, a typical 2D fringe configuration system to measure velocities in the lateral plane has to meet two requirements [90] : the creation of two orthogonal fringe patterns to detect the two components, and the ability to distinguish between the signals coming from these two fringe patterns to resolve the two velocity components. The most common configuration uses two different wavelengths [91], but other methods reported in the literature use only one wavelength to generate the two orthogonal fringe patterns and adopt different techniques to differentiate between the signals coming from the two fringe systems. For example, in [92] optical multiplexing was used, where the beams corresponding to the two fringe systems are shifted at different frequencies using Bragg cells. Another reported technique uses a high-frequency single pulsed laser source to generate two train pulses, each for one fringe pattern, and demultiplexing the obtained pulsed electrical signal to resolve the two velocity components [93]. In the present investigation, we propose a 2D LDV system using a single monochromatic source and a configuration similar to that of 1D systems, but we use a Bessel beam instead of a Gaussian beam. By referring to the two requirements mentioned above for a system to measure two components in the lateral plane, our system uses a simple configuration to meet these requirements. Using Bessel beams, two fringe patterns are created: the parallel fringes generated by the interference of the plane waves of the beams and the circular fringes of the Bessel beam. The obtained electrical signal from the scattered light has two frequencies that can be easily processed to resolve the two velocity components. The main advantage of the system we propose is its simplicity: Only one laser source

with a single wavelength is used and no additional optical or electronic components, usually associated with 2D systems, are needed. The use of Bessel beams in LDV has already been reported by [94] to improve the spatial resolution and accuracy of the measurements. However, in that study, Voight et al. focused on improving the performance of the presented one-component system. They used the near nondiffracting property of the Bessel beam to reduce the variation of the fringe spacing and its small central core to improve the spatial resolution. A fringe type LDV system using the intersection of two beams usually measures the one velocity component perpendicular to the parallel fringes in the plane perpendicular to the longitudinal direction. Our study demonstrates, for the first time to our knowledge, that by using Bessel beams in this kind of System we can measure the second velocity component in this plane. It should also be mentioned that in [3] [4] single Bessel beams were used to measure solid-surface velocities.

4.2 Interference of Intersecting Bessel Beams

the propagation of a Bessel beam in a coaxial cylindrical coordinate system (z_b, r_b, φ_b) is described by its electric field as [95]

$$E(z_{b,} r_b, \varphi_b) = E_0 \exp(i k_l z_b) J_0(k_r r_b), \qquad (4.1)$$

where E_0 corresponds to the amplitude of the beam, and k_r and k_l correspond, respectively, to the radial and longitudinal components of the wave vector with magnitude $k = \frac{2\pi}{\lambda}$, and λ being the wavelength. By referring to Figure 4.1, we investigate the interference at any point in the (x, y, z) coordinate system of two Bessel beams traveling at angles θ and −θ, respectively, relative to the z axis. We consider first the interference at any plane parallel to the (x, y) plane, such that the distance between the centers of the two beams is $2y_0$ [Figure 4.1(a)]. By making the proper

transformations between the cylindrical coordinate systems of each beam and the (x, y, z) coordinate system, equation. (1) is written for beams 1 and 2, respectively, as

$$E_1(x,y,z) = E_{01}\exp\left(ik_{l1}\left(\frac{z}{cos} + (y_0 - y)sin\theta\right)\right)\mathrm{x}J_0(k_{r1}\sqrt{\mathrm{x}^2 + (y_0 - y)cos\theta))^2} \quad (4.2)$$

$$E_2(x,y,z) = E_{02}\exp\left(ik_{l2}\left(\frac{z}{cos\theta} + (y_0 + y)sin\theta\right)\right)\mathrm{x}J_0(k_{r2}\sqrt{\mathrm{x}^2 + (y_0 + y)cos\theta))^2} \quad (4.3)$$

$$E_1(x,y,z) = E_{01}\exp\left(ik_{l1}\left(\frac{z}{cos\theta} - ysin\theta\right)\right)\mathrm{x}J_0\left(k_{r1}\sqrt{\mathrm{x}^2 - (ycos\theta)^2}\right) \quad (4.4)$$

$$E_2(x,y,z) = E_{02}\exp\left(ik_{l2}\left(\frac{z}{cos\theta} + ysin\theta\right)\right)\mathrm{x}J_0\left(k_{r2}\sqrt{\mathrm{x}^2 + (ycos\theta)^2}\right) \quad (4.5)$$

We numerically simulate the variation of the intensity $I \propto |E|^2$ at any point in the (x, y, z) coordinate system of the interference field by taking the summation of the electric fields $E = E_1 + E_2$. The values of E_1 and E_2 were calculated by substituting the different parameters and the coordinates at small step sizes in equations 4.4 and 4.5 respectively. A CMOS sensor is used to measure the intensity at different locations parallel to the (x,y) plane. For a small angle θ, the measured and simulated interference intensity contour images are shown in Figures 4.2 and 4.3, for the plane of intersection of the central axes of the beams and a plane prior to that, respectively. For the present investigation, we used an axicon with a base angle α=0.5° to generate the Bessel beams. The parameter $\beta = \tan^{-1}\left(\frac{\mathrm{kr}}{\mathrm{kl}}\right)$ is then approximated by β ≈ (n − 1)α ≈ 0.26◦, where n is the index of refraction of the axicon. By looking at Figure 4.2, as the plane waves of the two beams interfere, they form fringes at the central spot and also at the rings of the Bessel beams. For a plane prior to the intersection plane, we can see from Figure 4.3 the fringes due to interference of the outer rings and also the fringes at the central spots due to interference of the outer rings of the other beam. Distinct pattern of fringe islets due to the

interference of the outer rings is formed and clearly seen in the measured and simulated results. Similar patterns were observed at other planes (not shown here) at different distances from the intersection plane. An analytical relationship can be derived for the intensity at the plane of intersection [Figure 4.1(b)] for two similar beams with, $E_{01} = E_{02} = E_0$, $k_{r1} = k_{r2} = k_r$, and $k_{l1} = k_{l2} = k_l$, so

$$I(x,y,z) \propto E_0^2[\cos(k_l y sin\theta\,]^2\, J_0^2\big(k_r \sqrt{x^2 + (ycos\theta\,)^2}\,\big) \qquad (4.6)$$

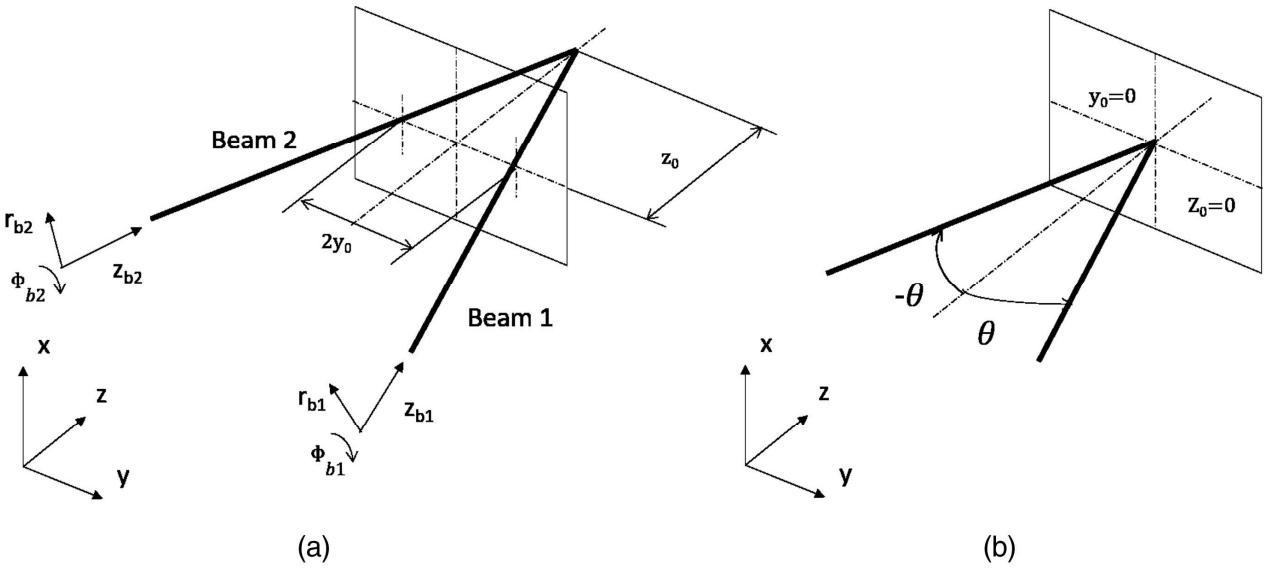

Figure 4.1 Geometry and coordinate systems of intersecting beams. (a) Plane away from intersection point. (b) Plane at intersection point

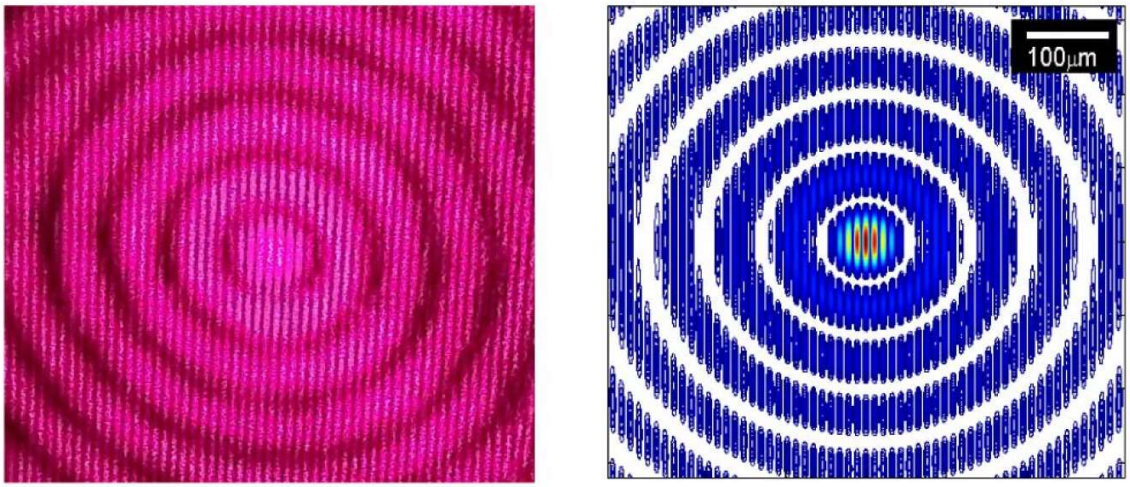

Figure 4.2 Intensity fringes at intersection plane $z_0 = 0$ mm for a Bessel beam with $\beta = \tan^{-1}\left(\frac{kr}{kl}\right) = 0.26°$ and an angle of inter- section $\theta = 1.75°$. Horizontal axis (y axis). Vertical axis (x axis). (a) Measurement with CMOS sensor. (b) Numerical and analytical simulations.

The term $[\cos(k_l y \sin\theta)]^2$ corresponds to the interference of the plane waves of the two beams. It is the term that gives the parallel fringes and, for $k_l \approx k = \frac{2\pi}{\lambda}$ it can be easily shown that the fringe spacing is $d_f = \frac{\lambda}{2\sin\theta}$ as is known for LDV systems. The term $J_0^2\left(k_r \sqrt{x^2 + (y\cos\theta)^2}\right)$ corresponds to the Bessel term. equation. (4-6) illustrates the effect of the intersection angle θ on the fringes. Increasing θ makes d_f smaller and results in a larger number of parallel fringes [Figure 4.1(b)]. For small angles θ, the Bessel term in Eqn. (4-6) can be approximated by with $J_0^2(k_r\, r)$ and $r = \sqrt{x^2 + y^2}$ which represents the intensity of the individual Bessel beams. For these angles, the Bessel fringe spacing does not change significantly, even with a threefold increase for the angle θ [Figures. 4.1(a) and 4.1(b)]. For larger values of θ, such as in Figure 4.5, this term results in an elliptic geometry for the intensity distribution with a larger Bessel fringe spacing in the *y* direction, while the Bessel fringe spacing in the *x* direction does not change. For an LDV system

using intersecting Gaussian beams, the measurement volume is usually defined by an ellipsoid characterized by

$$a = d, \quad b = d/\cos\theta, \quad c = d/\sin\theta, \qquad (4.7)$$

in the x, y, and z coordinates, respectively, where the coordinate system and the angle θ have a configuration similar to those defined in Figure 4.1(b), and (d) is the diameter of the beams at intersection [91]**.** By analogy to this, and since the cross section of a Bessel beam has a central spot surrounded by concentric rings, one can tentatively define the measurement volume resulting from the intersection of the two Bessel beams by a central ellipsoid surrounded by hollow concentric ellipsoids. The dimensions of the central ellipsoid are given by equation. (4-7), but with *d* corresponding to the diameter of the central spot, approximated by $\frac{2.405}{\pi \sin(\beta)}$, and the dimensions of the hollow ellipsoids are also given by the same expressions with d corresponding to a diameter characterizing the specific circular fringe. Since the circular fringes for a Bessel beam extend large distances from its axis, the measurement volume of the present system is not as well defined as for a Gaussian beam LDV. However, distant outer rings have a significantly diminishing intensity and would not contribute to the signal. A quantitative analysis, based on experiments and/or numerical simulations to better specify the extent of the measurement volume and spatial resolution, is needed. It is especially important when performing measurements in a fluid flow where scattering particles are present everywhere in the flow, as opposed to the solid-surface velocity measurements performed in the present investigation, where a rotating disk is placed in the middle of the intersection region. This kind of analysis is out of the scope of the present study, but we will discuss the spatial resolution in the lateral plane in Section 5. Next, we examine the variation of the dimensions of the central ellipsoid resulting from the intersections of the cores of the Bessel beams with the angle of intersection θ using equation. (4-7). These dimensions are plotted in Figure

4.6. The variations of the dimensions in the central lateral plane, shown as a and b in Figure 4.5, can also be deduced from equation. (4-6) and were confirmed by numerical simulation. The base angle α=0.5° of the axicon used to generate the Bessel beams and an angle θ=1.75° generate a central ellipsoid with dimensions a ≈ b ≈ 110 µm and c ≈ 3.7 mm. The selected angle θ resulted in a relatively long central ellipsoid, but since one of the main objectives of the present investigation is to study the interference of Bessel beams, this angle resulted in a parallel fringe spacing $d_f \approx 11$ µm, which can be easily visualized in the CMOS images of Figures. 4.2 and 4.3 along with the Bessel beam fringes. For a fluid flow measurement application, an axicon with a larger base angle θ and a larger intersection angle θ should be selected and would result in a smaller measurement volume. For example, Voigt *et al.* [94] used an axicon with base angle α=1° to generate the Bessel beams. Then, from the value of the fringe spacing $d_f \approx 4.58$ µm that they reported for one of the configurations used, we can estimate the angle θ ≈ 4.1°. From this estimate, we can then approximate a central ellipsoid with dimensions, a ≈ b ≈ 55 µm and c ≈ 0.77 mm. It should be noted that, for simplicity, we did not adjust the above dimensions to $1/e^2$ of the maximum intensity.

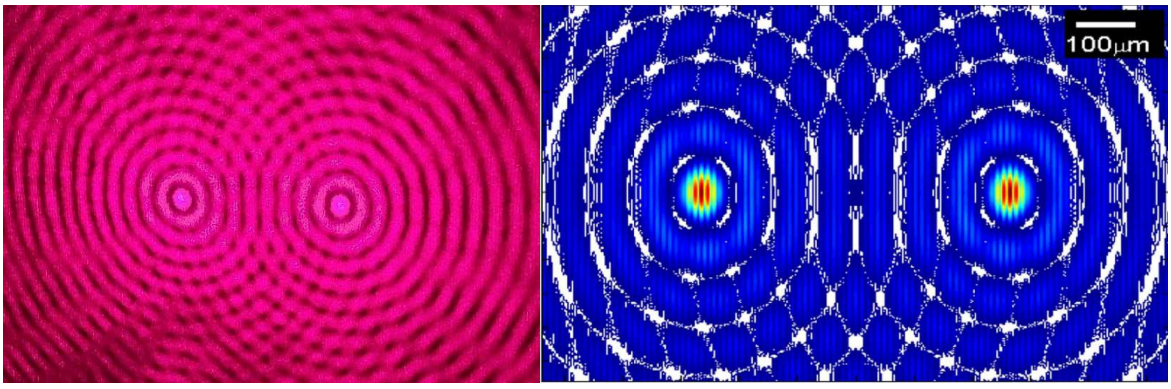

(a) (b)

Figure 4.3 Intensity fringes at a distance from intersection plane z0 = 8.67 mm for a Bessel beam with $\beta = \tan^{-1}\left(\frac{kr}{kl}\right)$ =26° section θ = 1.75°. Horizontal axis (y axis). Vertical axis (x axis). (a) Measurement with CMOS sensor. (b) Numerical simulations.

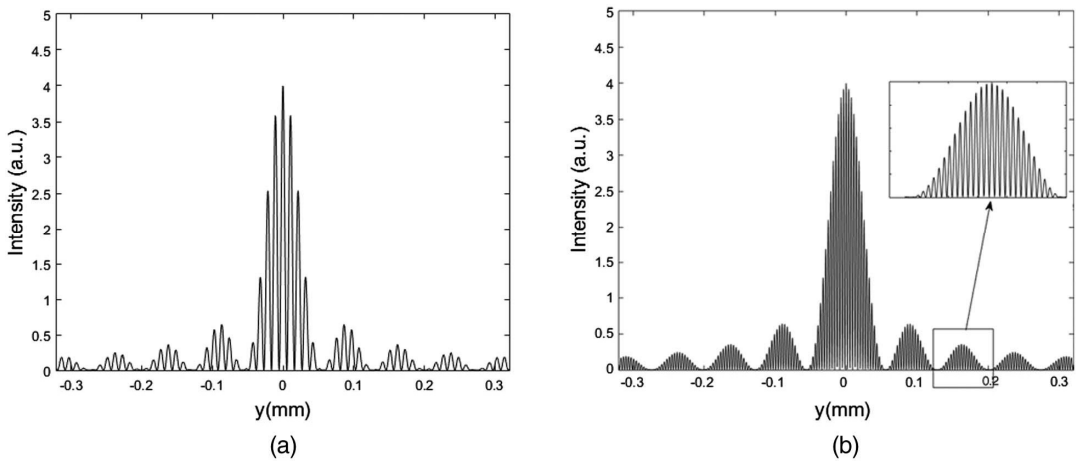

Figure 4.4 Effect of the angle of intersection on fringe spacing for a Bessel beam with $\beta = \tan^{-1}\left(\frac{kr}{kl}\right)$ =26°. (a) θ = 1.75◦. (b) θ = 5.25°

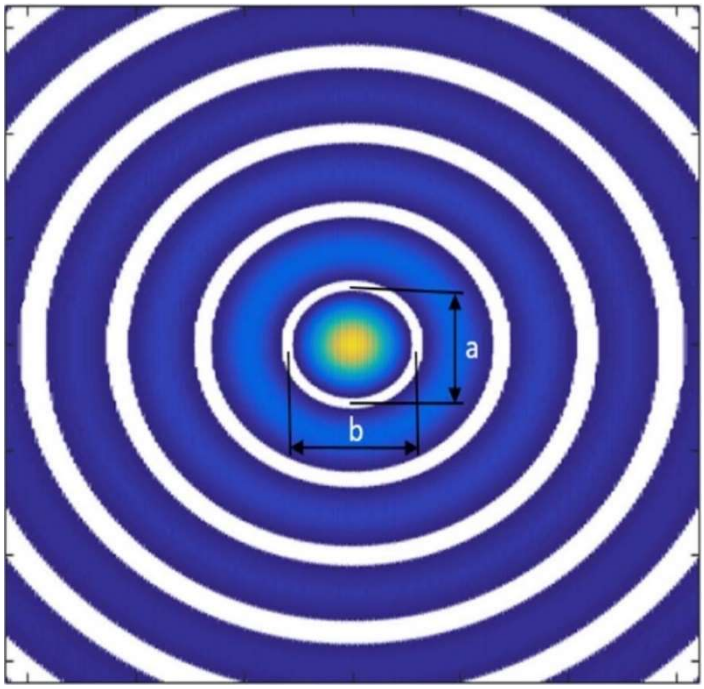

Figure 4.5 Fringes at plane of intersection for θ=22.5° for a Bessel beam with $\beta = \tan^{-1}\left(\frac{kr}{kl}\right)$ =26°

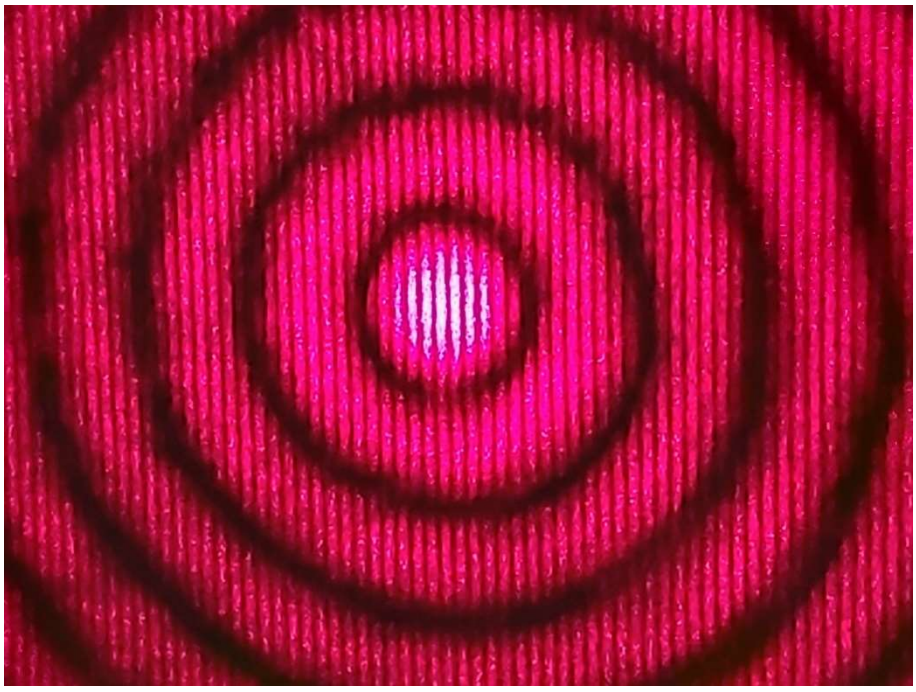

Figure 4.5a The circular are Bessel beam fringes, and the longitudinal fringes are LDV fringes

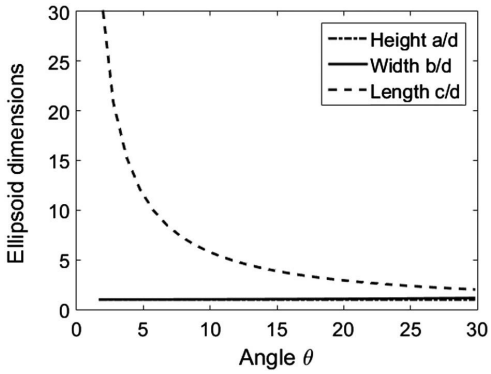

Figure 4.6 Variation of dimensions of an ellipsoid resulting from the intersection of the cores of Bessel beams with the angle of intersection θ.

4.3 Application to Laser Doppler Velocimetry

We propose to use the interference pattern, generated at the plane of the intersection of two similar Bessel beams from a single coherent monochromatic source, as the basis of a simple LDV system to measure two velocity components. The main idea is that while the front plane waves of the two

intersecting beams would generate parallel fringes that cause light scattered from particles crossing these fringes to have an intensity variation at the Doppler frequency, the Bessel beams themselves have concentric fringes that would cause light scattered from crossing particles to be characterized by a different frequency, the Bessel frequency. A frequently used signal processing technique for LDV is based on calculating the spectrum of the signal representing the intensity of the scattered light. A particle crossing the parallel fringes at a velocity v perpendicular to the fringes would have a peak frequency, the Doppler frequency, given by $f_D = v\frac{2sin\theta}{\lambda}$. On the other hand, a particle crossing the Bessel fringes at velocity v in a plane perpendicular to its longitudinal axis would scatter light at an intensity proportional $J_0{}^2(k\beta Vt)$ where for small angles $\beta \approx \frac{k_r}{k}$. The spectrum of this intensity is given by its Fourier transform [3]

$$\mathrm{F}(f) = F\left(\left(J_0(k\beta Vt)\right)^2\right) = \begin{cases} \frac{2}{f_B \pi^3} K\left(1 - \frac{f^2}{f_B}\right), & f < f_B \\ 0 \quad otherwise \end{cases} \tag{4.8}$$

In this case, F() is the Fourier transform, K () is the complete elliptic integral of the first kind, and $f_B = V\frac{2\beta}{\lambda}$. This variation has a half-hut shape distribution (Figure 4.7), with a maximum at a frequency of 0 and extending up to a limiting frequency value of f_B. We previously showed that Bessel beams can be used to measure the velocity of solid surfaces [4].

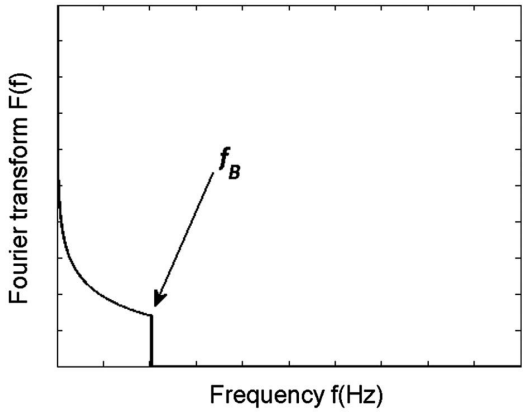

Figure 4.7 Fourier transform of scattered light intensity from particles crossing an ideal Bessel beam fringes.

The parallel fringes detect particles moving with velocities perpendicular to them and the Bessel beams' concentric fringes would detect particles moving at any velocity in a plane perpendicular to the axis of propagation. For small angles θ, and by taking the velocity components u and v in the x and y directions, respectively, as shown in Figure 4.8, it is expressed as

$$\mathrm{v} = \frac{\lambda}{2si} f_D \qquad (4.9)$$

$$|V| = \sqrt{u^2 + \mathrm{v}^2} = \frac{\lambda}{2\beta} f_B \qquad (4.10)$$

$$u = \lambda \sqrt{(\frac{f_B}{2\beta})^2 + (\frac{f_D}{2sin\theta})^2} \qquad (4.11)$$

Similar to a conventional LDV system, no calibration is needed for small angles θ, and the two velocity components can be determined directly from equationns. (4.8) and (4.10). However, to overcome errors due angle misalignments and uncertainties in the different parameters, calibration is recommended.

4.4 Experimental Setup and Procedures

The experimental setup is shown in Figure 4.8. A coordinate system similar to the one in Figure 4.1 is used. A laser beam with a maximum power of 60mW and wavelength of 660 nm (CUBE, Coherent Inc., Santa Clara, CA, USA) is expanded through a two-lens telescope system and passes through an axicon with a base angle α=0.5°. The generated Bessel beam is split into two beams by a beam splitter and mirror system, each making an angle θ with the longitudinal axis, and the intersection of the two beams constitutes the measuring volume. The angle θ is kept at constant value of θ =1.75° for the velocity measurements. A disk, with an extra-fine grain sandpaper attached to its surface is mounted on a motor rotating at different angular speeds ω. The measurement points are marked on this disk on a circumference with radius r at different angles θ with respect to a reference axis. The total velocity v, which is the tangential velocity of the points on the circumference was fixed to 173 mm/s. To perform a measurement at a specific point, the reference axis of the disk was adjusted with respect to the optical system and the motor-disk assembly, placed on a stage, was moved so that the measurement point coincided with the center of the intersection of the beams. Using the backscattering mode, a lens with a focal length of 25 mm was used to collect the light scattered from the extra-fine grain particles of the sandpaper and focus it on the photodetector (PDA10A, Thorlabs, Inc., Newton, NJ, USA). The sandpaper was chosen to scatter light since it provided a better representation of the tracer particles in a real flow measurement application [96]. Fine adjustments in the z direction were made by monitoring the spectra of the signal. The generated signal was conditioned, and its spectrum was calculated. The average of 10 measurement records were taken for each point. The tangential velocity $v_t = r\,\omega$ is constant, but as we change the angular position τ, different velocity components u and v are obtained. The parallel fringes obtained from the interference of the front waves of the two beams

would detect the velocity component v, while the concentric fringes of the Bessel beams would detect the total velocity V as in figure 4.8. By using equations. (4.9) – (4.11), we can resolve the two velocity components. It should be mentioned that the experimental setup used in the Bessel beam LDV system proposed by [94] is similar, except it uses a diffraction grating instead of the beam splitter/mirror of the present system

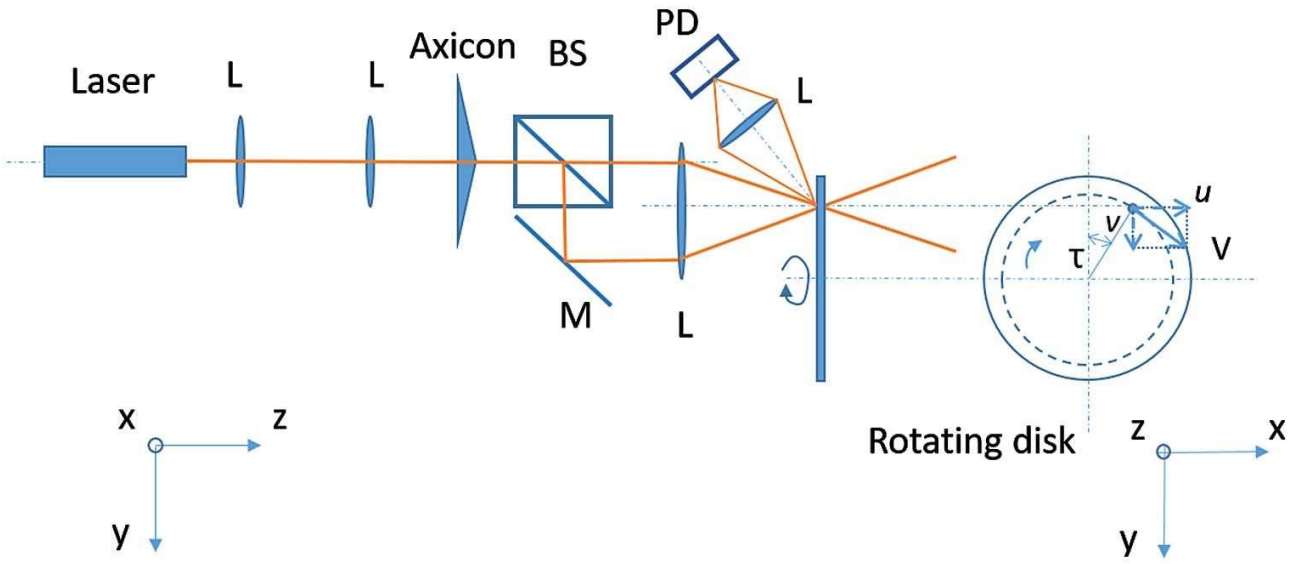

Figure 4.8 Experimental setup. Components: L, lens; M, mirror; BS, beam splitter; PD, photodetector.

4.5 Results and Discussion

The intensity of the scattered light is measured, and its spectra is calculated. Figure 4.9 shows sample spectra for different angular positions. The Bessel frequency is associated with a much higher energy than the Doppler frequency, but they can be both clearly distinguished from these figures. These frequencies are used to calculate the two velocity components according to equations. (4.9**),** and (4.11). While the Bessel frequency remains the same since the total velocity magnitude does not change, the Doppler frequency changes as the v component changes. Figure

4.10 shows the two velocity components as a function of the angle τ of the location of the measurement position (Figure 4.8). These measurements show that the two velocity components can be measured with reasonable accuracy using this system. Note that the simple signal processing technique currently adopted, namely using the spectrum of the signal, is associated with velocity component determination ambiguity when the Doppler frequency is equal to or lower than the Bessel frequency.

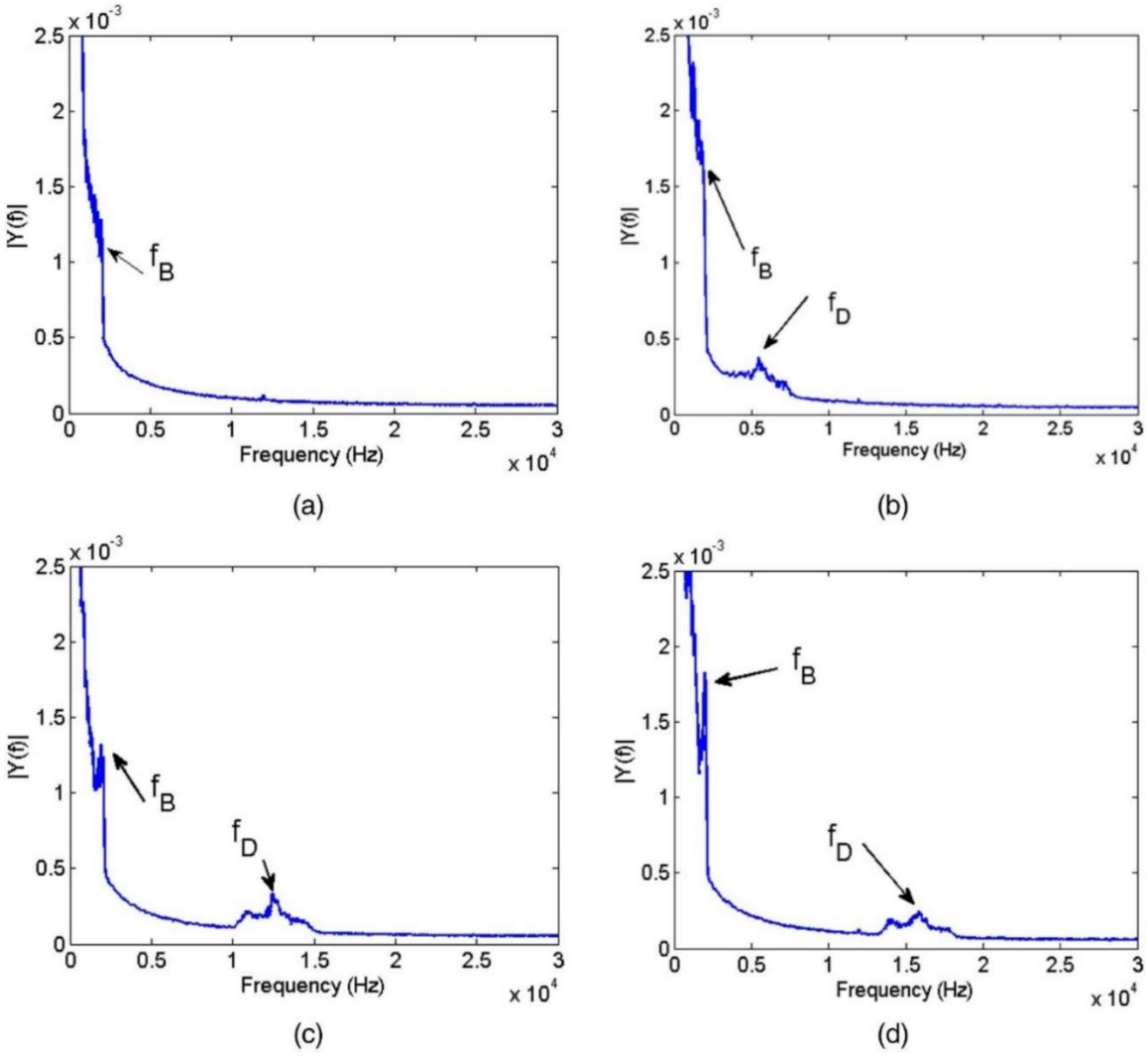

Figure 4.9 Spectra of scattered light intensity showing f_D and f_B at different angles τ. (a) τ = 0°. (b) τ = 20°. (c) τ = 50°. (d) τ = 80°.

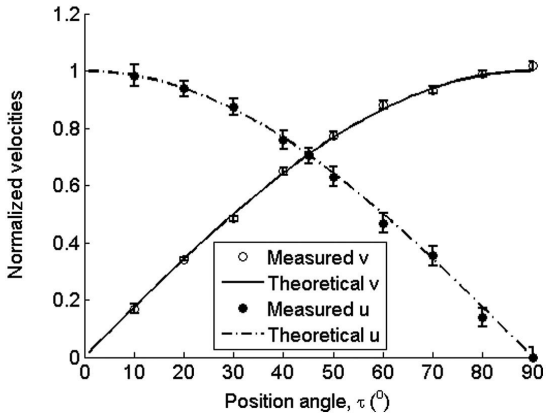

Figure 4.10 Velocity component measurements.

In other words, for a given configuration of the system, small values of v with respect to u cannot be measured and only the total velocity can be determined from f_B since f_D cannot be easily determined from the signal spectra. For example, in the limiting case when v = 0 and u = 0, we get $f_D = 0$ and f_B will have a finite value. Setting the condition of unambiguity, $f_D > f_B$ translates to

$$vsin\theta > \lambda\sqrt{u^2 + v^2} = \frac{\lambda}{2\beta} f_B \qquad (4.12)$$

By setting v = ku, we can determine the limiting value of the magnitude of v with respect to u as a function of the angle θ, by

$$k = \sqrt{\frac{1}{\left(\frac{sin\theta}{\beta}\right)^2 - 1}} \qquad (4.13)$$

Equation (4.13) shows that by increasing the angle θ, smaller values of v can be measured. This can also be seen in Figures. 4.4(a) and 4.4(b), where larger θ values reduce the Doppler fringe spacing (increasing f_D), while the Bessel envelope does not significantly change. However, a large increase of the angle θ affects the validity of the Bessel beam assumption in determining f_B in equation. (4.10). In these cases, it would be necessary to use calibration to find a relationship

between the frequency and velocity rather than using $f_B = v\frac{2\beta}{\lambda}$. In addition, the unambiguity may be resolved by using another signal processing technique such as time domain analysis. As mentioned earlier, the use of Bessel beams in LDV systems has been proposed in the past to improve the performance of these systems by taking advantage of the low diffraction properties of these beams and their small central spot size [94]. Since we are using the outer fringes of the Bessel beam, the proposed method comes with a trade-off in terms of the spatial resolution compared to the study by Voigt et al. [94], where only the central spot of the Bessel beam is used for measurements. However, it should be mentioned that the outer rings have a diminishing intensity. For example, the fifth ring of the ideal Bessel beam, which corresponds to a diameter about 7.5 times larger than that of the central lobe, has a maximum intensity less than 4% of the maximum intensity of the beam. For a more realistic Bessel–Gaussian beam, the outer rings have an even smaller intensity [97]. Even though the proposed system exhibits a significant decrease of the spatial resolution compared to the system reported by Voigt et al. [94], it can still mark an improvement compared to a similar system using only Gaussian beams. The spatial resolution of the Bessel beam LDV system can be further improved by selecting an axicon with a larger base angle α (smaller central spot and fringe spacing).

4.6 CONCLUSIONS

Similar to the case of intersecting Gaussian beams, the interference of the wavefronts of intersecting Bessel beams generates parallel intensity fringes of constant thickness. However, in the case of Bessel beams, these interference fringes are superimposed on the concentric circular fringes characteristic to these beams. It results in an intensity profile at the intersection transverse

plane having constant frequency oscillations with a Bessel-like variation envelope. In the present investigation, we showed that the existence of the two types of fringes resulting from the interference of two intersecting Bessel beams can be used to resolve two velocity components in a configuration usually used for measurement of one velocity component. The main advantage of the system we propose is its simplicity. We used what is known as a one-component system to measure two velocity components, without the need for additional devices or complex multiple wavelength laser systems. The main shortcomings of the system in its current form are the measurement volume, which is not well defined, and the ambiguity in velocity determination when $f_D < f_B$. Another limitation of the system in its current state is that it does not include direction discrimination. These issues must be addressed to make this system a viable alternative 2D fluid flow measurement system.

Chapter 5

GENERATION OF NEARLY BESSEL BEAMS WITH REDUCED DEPTH OF FIELD AND LIMITED SPATIAL TRANSVERSE PROPAGATION

5.1 Introduction

The spatial resolution of a measurement technique is defined by the volume in physical space used to obtain a sample measurement. Similarly, the temporal resolution is defined as the duration of time averaged to obtain a specific measurement. For Laser Doppler Velocimetry and similar techniques, the spatial resolution cannot be smaller than the seeding particle size used to make an accurate measurement in the flow. With this in mind, in order to achieve an accurate measurement, the seeding particles should be selected smaller than the fringe spacing and large enough to give a strong signal. Using the above criteria for defining spatial resolution, many authors have performed studies and estimated the spatial resolution of several velocimetry techniques. For fringe based LDV systems, the spatial resolution is defined by the 3D measurement volume formed by the intersection of the two Gaussian beams. This results in an ellipsoid shape illustrated in Figure 5.1 and characterized by the following dimensions [98] [99]: $\delta y = \frac{4\,F\lambda}{\pi D}$, $\delta x = \frac{de}{\cos\beta}$ and $\delta z = \frac{de}{\sin\beta}$, where F is the focal length of the focusing lens, D is the laser beam diameter, de is the focused laser beam diameter, β is the half angle of intersection and λ is its wavelength. The measuring volume is given by: $\frac{\pi\, de^3}{6\,(cos^2\beta\, sin\beta)}$.

In general, reducing the measurement volume translates into more accurate measurements and there were some attempts in the literature to this end. For example, Compton et al. [100] used

optics of short focal length to obtain a measurement volume of 35μm x 66μm. In many cases, the authors do not specify estimates of spatial resolution due to the difficulty of obtaining an accurate value. However, small measurement volume introduces significant constraints on the optical system that can limit its performance. The chance of a scattering particle entering the measurement volume during a given time interval decreases with the small measurement volume.

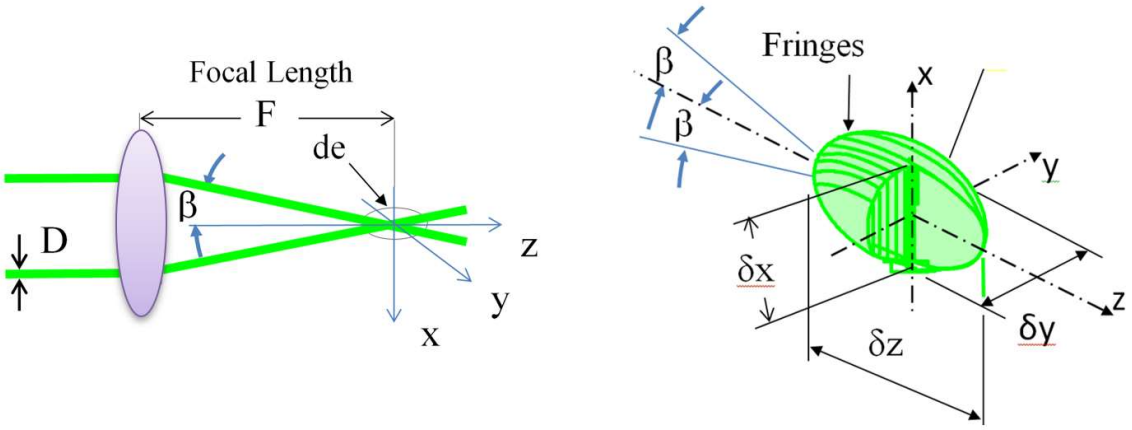

Figure 5.1 LDV Measurement Volume

5.2 Spatial Resolution of Laser Bessel Velocimetry for Fluid Flow Measurement

As described above, an LDV system has a spatial resolution formed by the 3D measurement volume from the intersection of the two laser beams. For LBV measurements in fluid flow, the spatial resolution is defined by the extent of the Bessel beam fringes in the transverse plane and by the DOF in the longitudinal direction. For the transverse resolution, unlike the LDV, which has a bounded measuring volume, the LBV uses the fringes of the Bessel beam which in theory extend indefinitely in the transverse direction. The Bessel beam fringes are axisymmetric and have equal energy distribution but the intensity is different, higher at the center and decreases as the radius

increases. But even though theoretically the fringes extend indefinitely, practically only particles within a certain distance to the center, scatter measurable intensity by the photodetector. The light scattered by a particle crossing Bessel beam fringes is higher at the center and low in the outer fringes collected by the photodetector. When using axicons, the Bessel beam is more efficiently produced, but the transverse intensity extent cannot be controlled. The longitudinal intensity depends on the axicon angle and the diameter of the incoming laser beam Figure 2.4. Thus, using axicons results in larger DOF and transverse intensity extending to large distances. There were attempts, to produce limited DOF Bessel beams. Rao and Samanta [101] demonstrated experimentally segmented zero order Bessel beams with tunable range, by placing a slit after the axicon and illuminating the axicon with gaussian beams, Bessel type beam was generated of varying range at different positions away from the axicon. They showed the control of the zero-order Bessel beam along the propagation distance and the Bessel beams appear at a distance away from the axicon. Recently, Müller et al. [102] investigated Bessel beams by placing annular slits after an axicon illuminated with laser beam. By using the combination of axicons and variable annular slits they produced segmented zero-order Bessel beam with controlled range at different distances along the depth of field. Another alternative to generate a Bessel beam is to use Durnin's slits configuration shown in Figure 5.3. As will be shown next, this configuration allows both longitudinal and transverse resolutions to be reduced and controlled compared to using axicons.

5.3 Generation of Nearly Bessel Beams Using Annular Slits with Finite Width

The Durnin's setup [7] shown in Figure 5.2, is used to produce the nearly Bessel beams used in the experiments. A 107mW laser beam with wavelength $\lambda = 658\,nm$, was expanded using a

telescope to produce nearly plane waves for illumination of circular slits Figure 5.2. The slit is placed in the back focal plane of a focussing lens of focal length F. When the slit ring is illuminated by a laser beam the points along the slit behave as a coherent point source emitting circular waves which the lens transforms into plane waves Figure 5.4. The plane waves travel on a cone with an angle θ, given by

$$tan\,\theta = \frac{R}{F} \qquad (5.1)$$

Where R is the transmitting lens radius and F is its focal length. Generating Bessel type beam [7], with an electric field given by:

$$E = J_0(k_r r) \qquad (5.2)$$

where $k_r = k\,sin\,\theta$, k being the wave vector with magnitude $\frac{2\pi}{\lambda}$. The spot radius of the Bessel beam is given by

$$r_{spot} = \frac{2.408}{k_r} \qquad (5.3)$$

and the average fringe spacing is [10]

$$d_f = \frac{\lambda}{2\theta} \qquad (5.4)$$

The maximum distance of travel of the Bessel beam is given by:

$$Z_{max} = \frac{R}{\tan\theta} \qquad (5.5)$$

Where R is the radius of the lens. Recognizing that in practical situations, the lens area might be larger than the illuminated region, Lin et al. [103] recommended using the smaller of the radius of the lens and the effective radius given by

$$R_{eff} = r + \lambda \frac{F}{\Delta r} \qquad (5.6)$$

To produce the Bessel beam, Durnin [7] recommended that $\Delta r \ll \lambda \frac{F}{R}$. Using a larger slit width Δr results in a reduced longitudinal and transverse profiles [104] [11]. It was determined that the DOF will be centered at the focal distance of the focusing lens and estimated by the following expression

$$DOF = \frac{2.8F^2}{R\mathrm{k}\,\Delta\mathrm{r}} \qquad (5.7)$$

Table 5.1 Characterization of beams generated by different circular slits and a lens with focal length F=50mm. All dimensions are in (mm) except spot size and fringe spacing in (μm)

r_1 (mm)	r_2 (mm)	Δr (mm)	r_{avg} (mm)	DOF (mm)	d_{eff} Transverse Diameter[1] (mm)	Number of Fringes	Spot Size (μm)	d_f Average fringe spacing (μm)
0.5	0.7	0.2	0.6	6.1	0.3	4	24	27.5
0.6	0.8	0.2	0.7	5.3	0.2	5	41	23.6
0.7	0.9	0.2	0.8	5	0.22	5	18	21
0.8	1	0.2	0.9	4	0.2	7	32	18.3
1.2	1.4	0.2	1.3	3	0.18	10	22	12.7
2	2.2	0.2	2.1	1.8	0.16	13	12	8

[1] Based on apparent number of fringes.

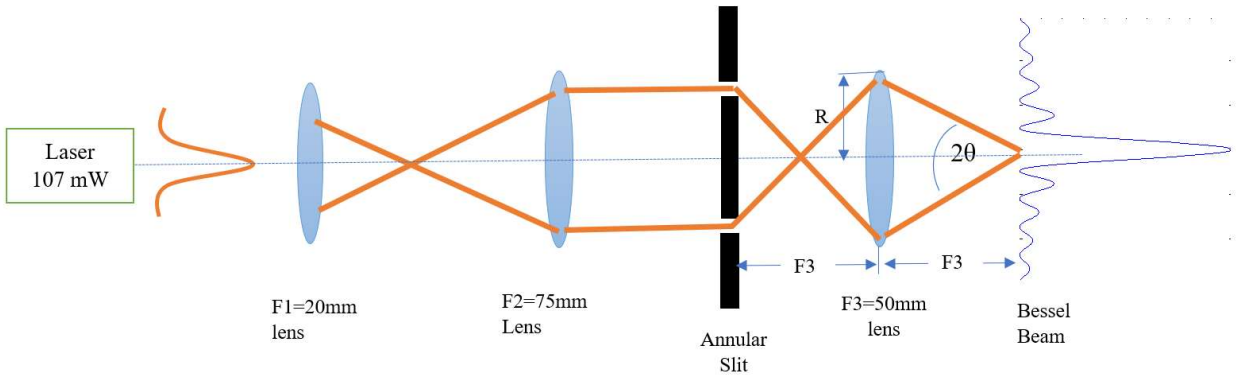

Figure 5.2 Experimental Setup

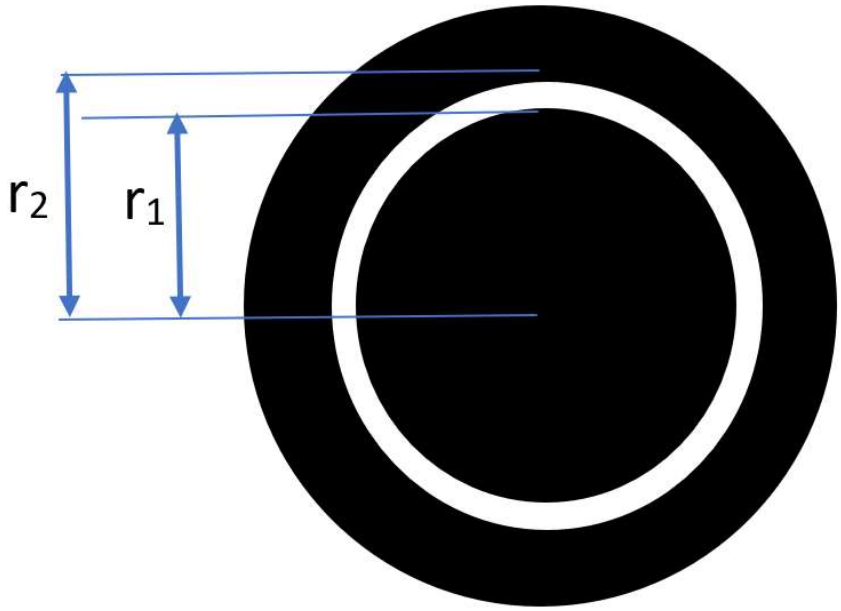

Figure 5.3 Durnin Ring (Annular Slit)

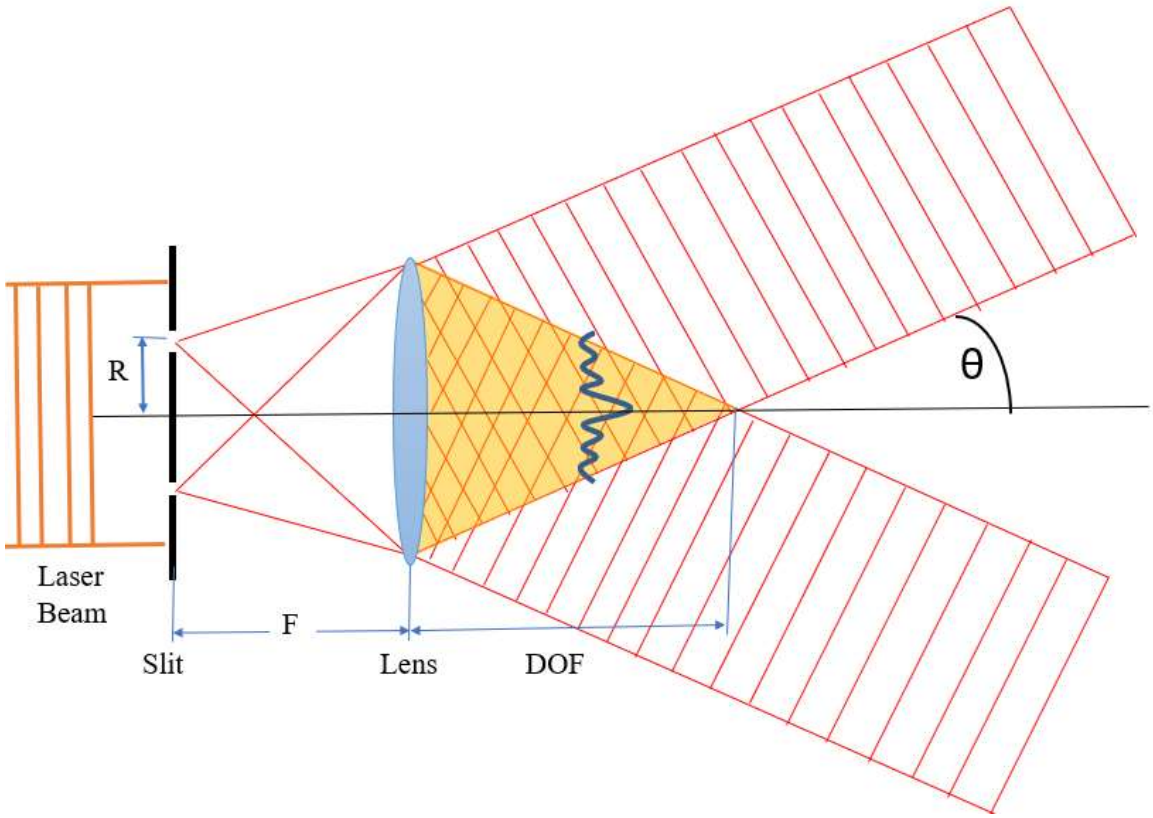

Figure 5.4 Formation of Bessel Beam from Durnin's Setup Using Annular Slit.

While the generation of Bessel beam using slits, ring has limitations in the amount of power passing through the ring and carried by the beam, it is a simple and economical method. Most importantly, for the present work it also allows to have a limited DOF and reduced transverse spread, which is needed to get a good spatial resolution for velocity measurements. Several annular slits and focusing lenses were explored to generate zero order nearly Bessel beams and to control the longitudinal and transverse resolutions limiting the fringes' extent in transverse direction and controlling the depth of field. We examined the effect of the ring dimensions on the quality of the generated nearly Bessel beam as well as its depth of field and its transvers number of rings (transverse intensity). Additionally, by adjusting the ratio of the spherical lens focal length, Bessel like beams can be generated with controlled DOF. A first set of annular slits with different ring

dimensions designed on CAD and printed on transparent paper using a standard laser printer of 1200 dpi. A second set was manufactured at Simon Fraser University wafer fab (4D LABS), by metallic deposition on glass plates. While both sets allowed the generation of nearly Bessel beams, the first suffered degradation after extended use due to overheating from laser exposure. The measurements presented in this thesis were obtained from the second set. In [11] the authors did not study in detail the variation the profiles and the transverse extent of the beams. In the following section, we perform a numerical study using scalar diffraction theory on the effect of the slit width on the quality of the generated beams, their closeness to Bessel beam distribution and their transverse variation. This will be followed by presentation of experimental results of CMOS pictures of the cross sections of beams generated by different combination of slit radii and width.

5.4 Numerical simulation

We use the Fresnel-Kirchhoff diffraction integral [105] to compute the transverse and longitudinal intensity distribution resulting from the Durnin set-up with finite slit width. The electric field in Cartesian coordinates is

$$E(x,y,z) = \frac{1}{j\lambda}\iint_A E(x',y',0)\frac{exp[jkR(x,x',y,y',z)]}{R(x,x',y,y',z)}\cos(\vec{n},\vec{R}(x,x',y,y',z))dx'dy' \qquad (5.8)$$

where integration is performed over the area A of the aperture, (x,y,z) and $(x',y',0)$ refer to coordinates of points on the image plane and the aperture planes, respectively, $E(x',y',0)$ is the electric field at the aperture plane, $R(x,x',y,y',z)$ is the distance between the two points, $\vec{n}$ is the normal vector at the aperture, λ is the wavelength and k the wave number. In equation (5.8) it is assumed that $R(x,x',y,y',z) \gg \lambda$. This integral is applied twice. First the aperture is the entrance to the circular slit and the image plane is computed at entrance to the lens. Then, the

aperture is the entrance to the spherical lens and the image is computed at the focal plane of the lens and also on the longitudinal axis to determine the depth of field DOF. When the spherical lens is used as the aperture plane, it introduces a phase transmission given by a term, $exp(ik\varphi(x', y'))$, where $\varphi(x', y')$ is the phase function of the lens.

5.5 Results and discussion

Shown in Figure 5.5 are the CMOS images and the images obtained from numerical simulation for a cross section of the beams obtained at the focal region of the lens and corresponding to a wavelength $\lambda=660nm$, a lens with focal length $F=50mm$, and slits with different radii and slit width Δr combinations. These images correspond to a square region (0.3 mm x 0.3 mm). The CMOS images obtained from an axicon with an angle $\alpha=5^{o}$ (Figure 5.6) were used to calibrate these images since its spot size and fringe spacing were measured to be accurate and correspond to the theoretical values [106] . In general, the images obtained experimentally and those from numerical simulation agree reasonably well. They show that the intensity distribution resembles that of a Bessel beam with limited extend in the transverse direction. In Figure 5.7, the intensity profiles at the focal plane of the lens corresponding to the different configurations of Figure 5.6 are displayed. For comparison plots of Bessel beam profiles corresponding to the angle θ given by equation (5.1) are also shown in Figure 5.7. For the values shown, the central spot and the neighboring fringes also generally match, in terms of their radii, those of an ideal Bessel beam corresponding to the angle θ. The produced beams have cross sections resembling those of a Bessel Gaussian beam, which is characterized by similar central core and circular fringes to those of an ideal Bessel beam, with limited extent of the secondary fringes in the transverse direction [107]. These plots also show that for a fixed focal length f and fixed slit width ΔR, as the radius of the slit increases, the angle θ increases resulting in a smaller spot size and fringe spacing. The intensity profile obtained

from an axicon with an angle $\alpha=5^{o}$ is shown in Figure 5.8 for comparison. In table 5.1, the DOF is estimated based on equation. (5.7) and the effective diameter of the generated beam is determined from the apparent fringes of the beams. These two dimensions define in practical terms the spatial resolutions in the longitudinal and transverse directions respectively, when using these beams for velocity measurements. Selecting the required slits and the optimum combination of the types of lenses can thus produce the required measurement volume. It should also be mentioned that, using different wavelengths result in considerable fringe spacing and DOF changes.

5.6 Conclusions

In this work, the spatial resolution requirements for measurements of fluid flow velocity using Bessel beams are investigated. We examined the effect of the ring dimensions on the quality of the generated Bessel beam as well as its depth of field and its transvers number of rings (transverse intensity). The focal length of the transmitting lens defines the position of the measurement volume. However, the generation of Bessel beam using slits ring has limitation in the amount of power passing through the ring and carried by the beam. The beam may lose some of its quality due to the absence of power when the ring is very thin. In comparison to the beam generated by axicons, the extent of the beam in transverse intensity can be controlled, and the length of beam propagation can be adjusted based on the spherical lens focal length, but the Bessel beam generated using axicons has higher power and more efficient. When the number of fringes is kept low, the intensity increases in the Bessel beam since the light distribution is kept at a smaller region. From these results, we can assume the limitation of the measurement volume is defined by the extent of the fringes in longitudinal and transverse direction of the Bessel beam.

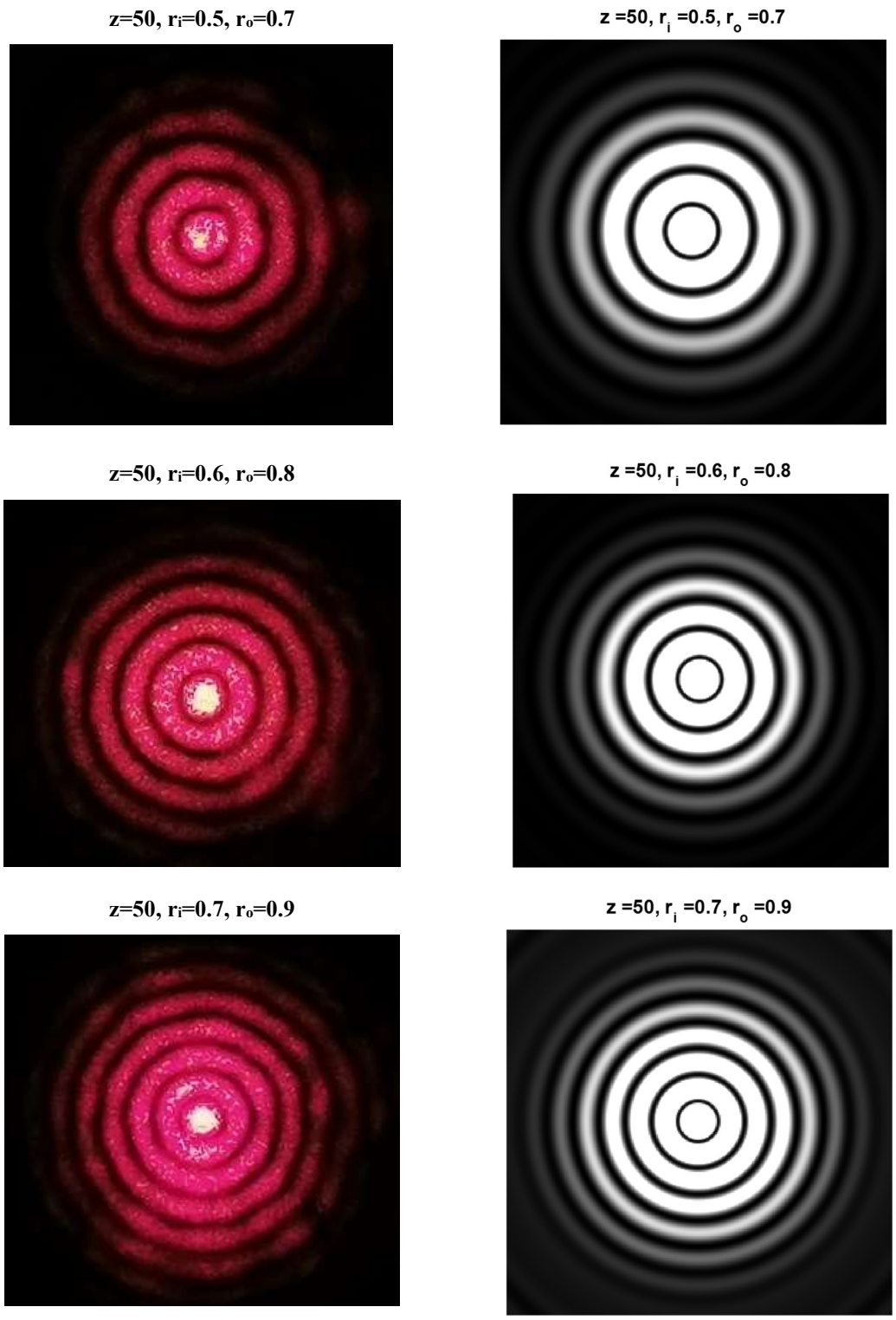

Figure 5.5 Transverse distribution obtained from Durnin's configuration with a lens of *F=50mm.* Left: CMOS image. Right: Numerical simulation. (Continued on next page).

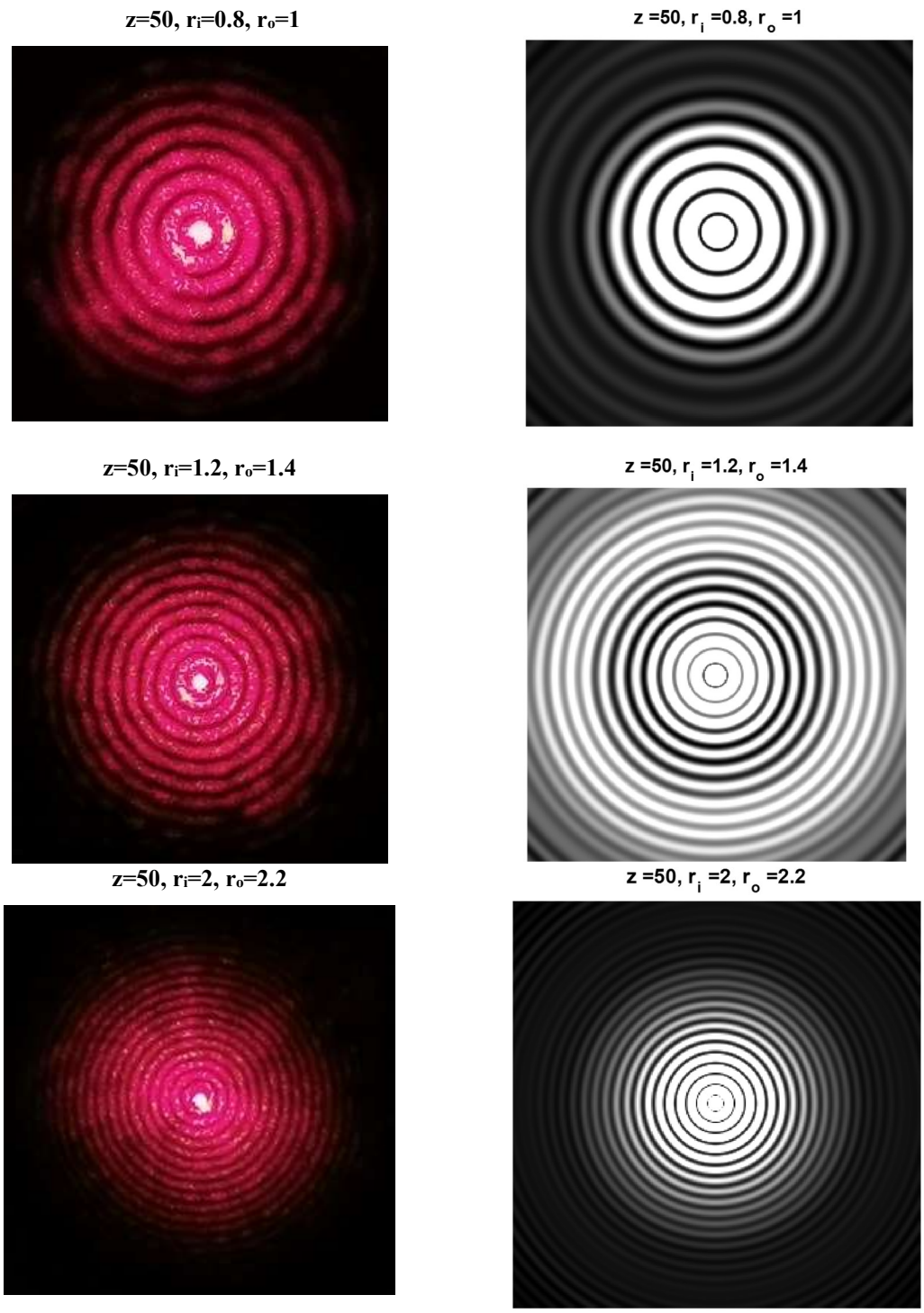

Figure 5.5 Transverse distribution obtained from Durnin's configuration with a lens of *F=50mm.* Left: CMOS image. Right: Numerical simulation. (Continued on next page).

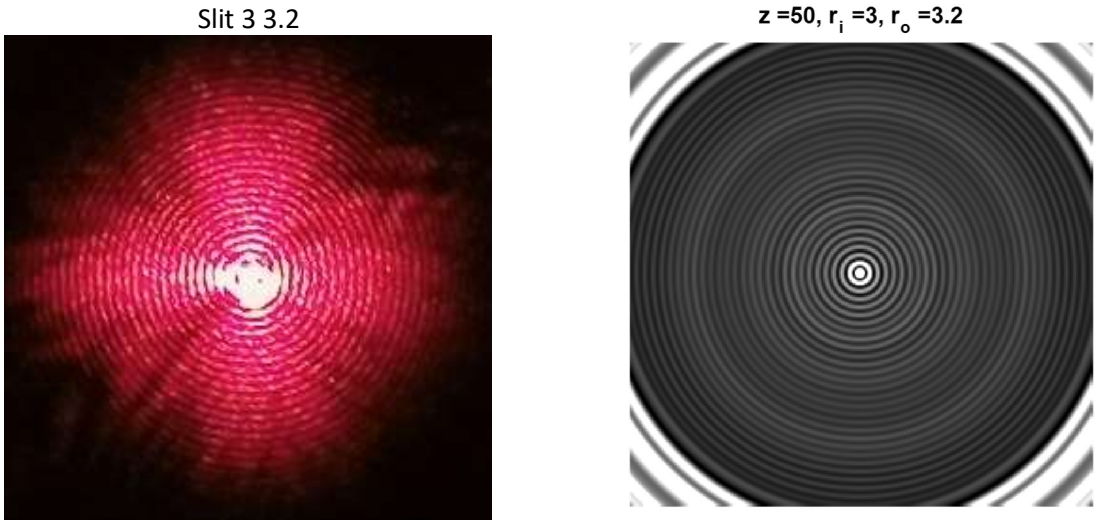

Figure 5.5 (Continued) Transverse distribution obtained from Durnin's configuration with a lens of *F=50mm.* Left: CMOS image. Right: Numerical simulation.

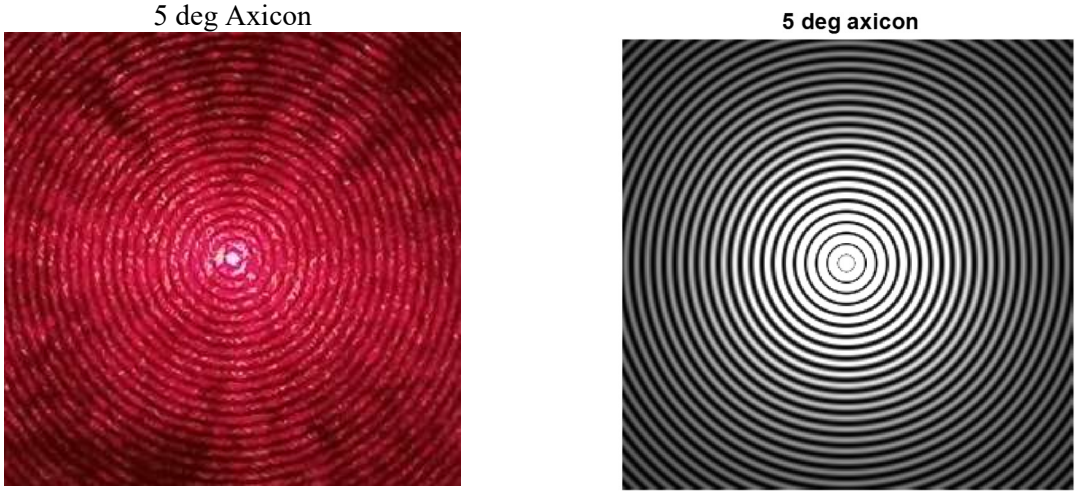

Figure 5.6 Transverse distribution obtained from an axicon with α=5°. Left: CMOS image. Right: Numerical simulation.

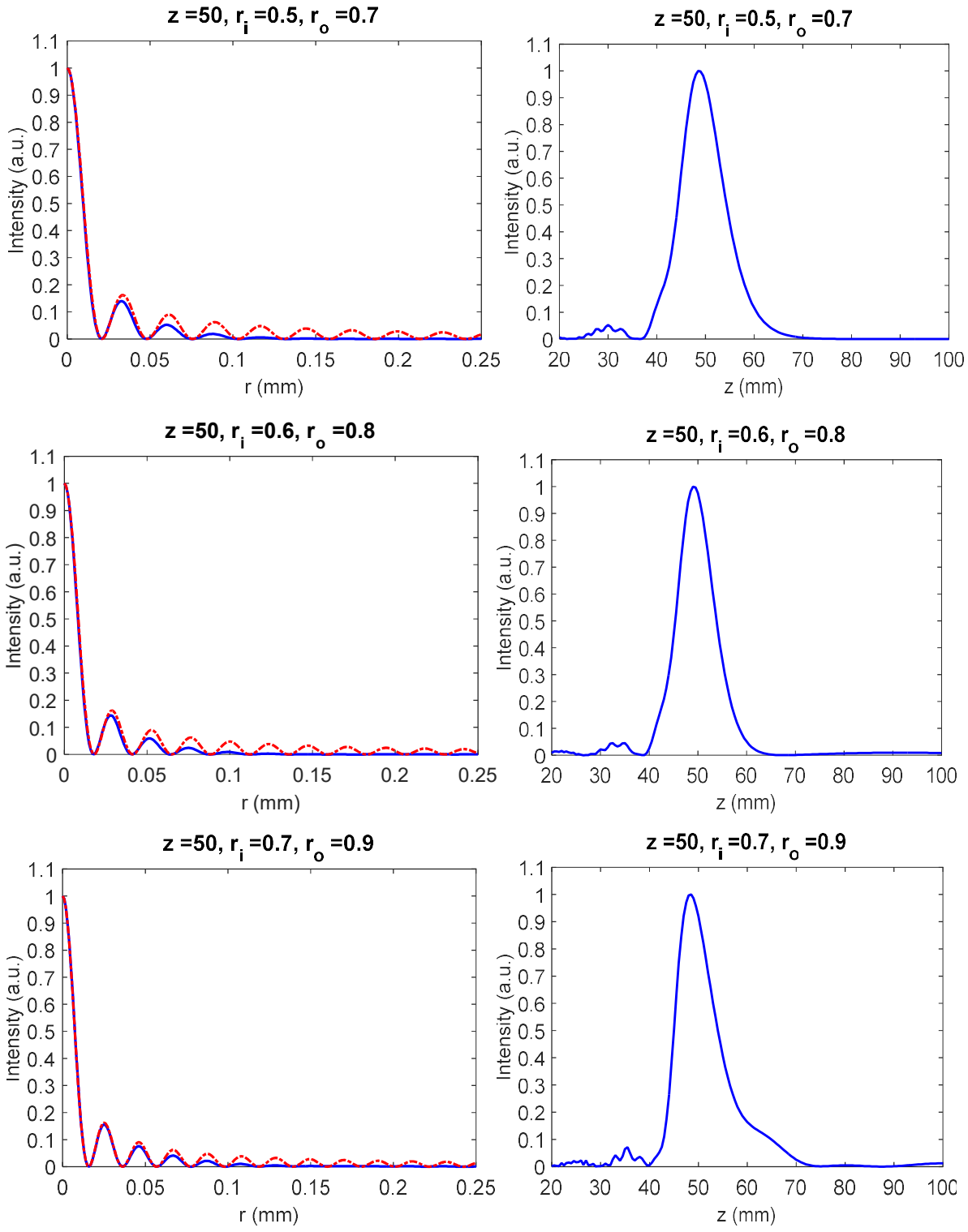

Figure 5.7 Transverse intensity distribution obtained from Durnin's configuration using a lens of *F=50mm* and different values of r_i and r_o. Red line: Bessel beam distribution with corresponding value of θ. Blue line: numerical simulation. (Continued on next page).

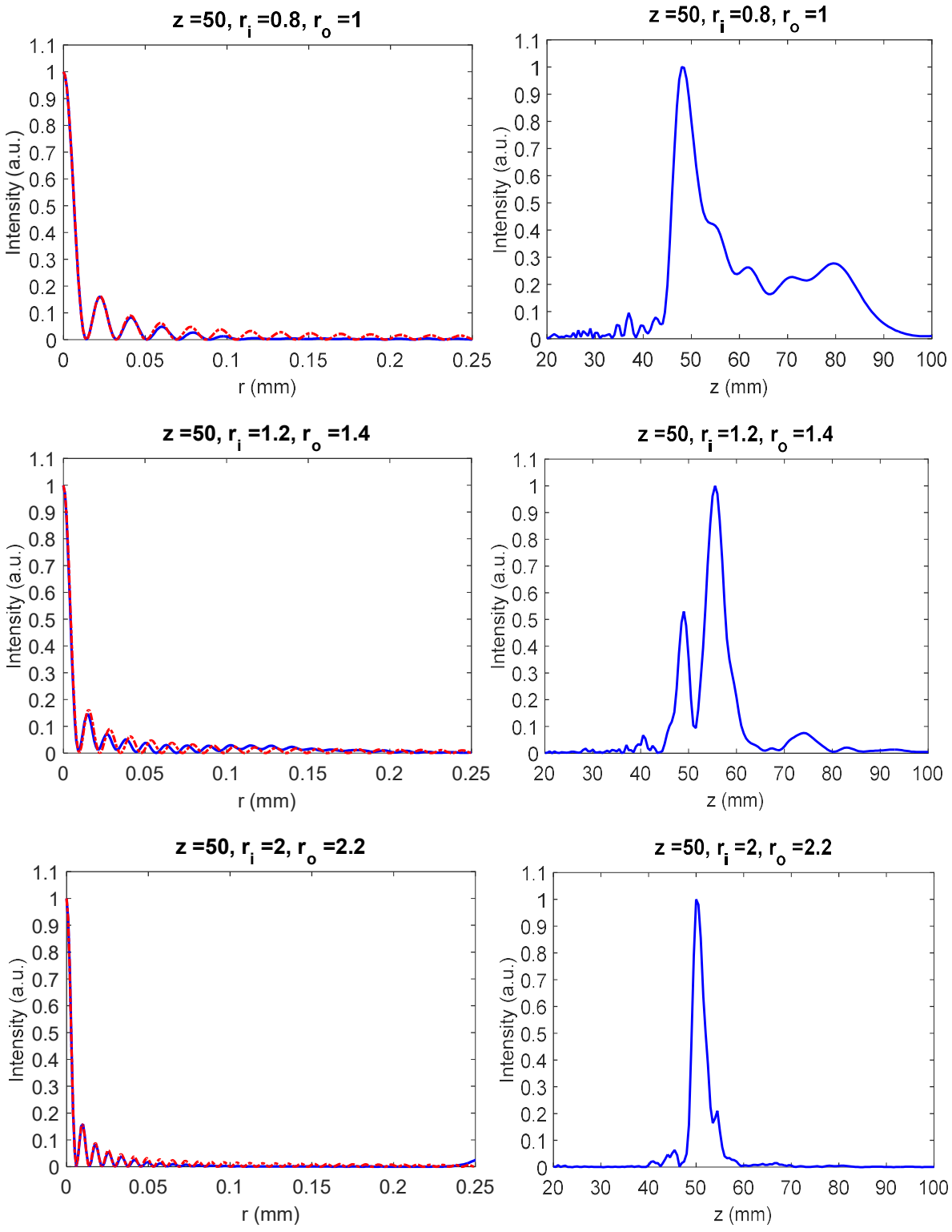

Figure 5.7 Transverse intensity distribution obtained from Durnin's configuration using a lens of *F=50mm* and different values of r_i and r_o. Red line: Bessel beam distribution with corresponding value of θ. Blue line: numerical simulation. (Continued on next page).

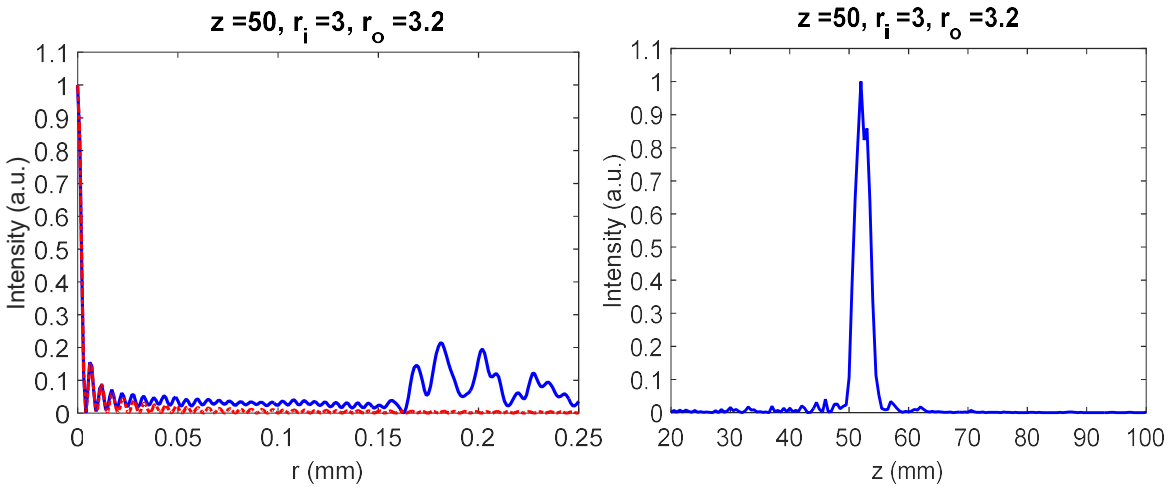

Figure 5.7 Transverse intensity distribution obtained from Durnin's configuration using a lens of *F=50mm* and different values of r_i and r_o. Red line: Bessel beam distribution with corresponding value of θ. Blue line: numerical simulation.

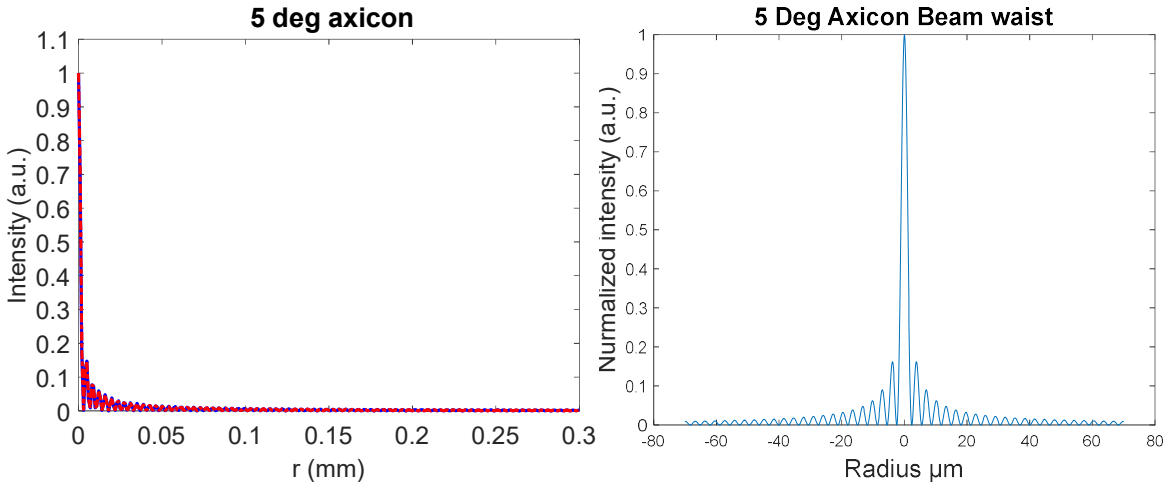

Figure 5.8 Intensity distribution of Bessel beam generated by an axicon with α=5°

Chapter 6

FLUID FLOW VELOCITY MEASUREMENTS AND ANALYSIS USING LBV

In this Chapter, we present fluid flow velocity measurements using the LBV systems described in Chapter 3. The measurements include the total two-dimensional velocities exiting a tank and the one dimensional, laminar and turbulent velocities in a pipe flow. Sample spectra of the photodetector signal, which were used to determine the velocities are presented. A commercial LDV system is used to validate the LBV measurements. We describe the procedures for mounting and adjusting the optical components of the instrumentation system. We present the parameters of the system defining the size of the measurement volume and the fringe spacing, and the procedure adopted to locate the measurement volume with respect to the axis of the test section.

6.1 Tank Discharge Experiments

One of the main advantages of the presented LBV technique is its ability to measure the total two dimensional velocity in an (x,y) coordinate system, with a single measurement and a simple system as opposed to LDV, which requires measurement of the two components separately. This is illustrated in Figure 6.1 with two examples. The total exit velocity from a tank and the velocity inside a thin tube with arbitrary orientation. It is assumed that in these applications the direction of the velocity is either known or not important.

Applying the Bernoulli and continuity equations to the tank discharge between points 1 and 2

$$p_1 + \frac{1}{2}\rho \mathrm{v}_1^2 + \rho g h_1 = p_2 + \frac{1}{2}\rho\, \mathrm{v}_2^2 + \rho g h_2 \quad (6.1)$$

$$A_1 \mathrm{v}_1 = A_2\, \mathrm{v}_2 \quad (6.2)$$

By assuming $A_1 \gg A_2$, we get the total velocity at exit from the tank

$$v_2 = \sqrt{2gh} \qquad (6.3)$$

Assuming symmetry and a uniform profile, this is usually the representative velocity at exit from the tank corresponding to the height h.

6.1.1 Adjustment of LBV Optics of Total Velocity Measurements

Referring to Figure 3.3 in chapter 3, the LBV system used comprises a laser light source of an output power of ~107mW, optical arrangements to transmit and collect the scattered light, a photodetector, and equipment for signal processing. Light from the laser is expanded by a telescope of two lenses (F=25mm, F=150mm) and transmitted through an axicon with base angle α=0.5° to form a fringe pattern in the local region of the fluid where velocity measurements are made. Using an adjustable stage, the laser beam height was adjusted and aligned such that it was parallel to the optical bench. The measurements were made directly into the fluid. Scattered light by seeding particles crossing the measurement volume is collected and the optical signal converted to an electronic signal for processing. The photodetector was mounted in the forward scatter mode for better signal detection close to the location of measurement to collect the scattered light.

6.1.2 Total Discharge Velocity Measurements

We perform velocity measurements at exit from a tank filled with water at different levels using the Axicon LBV system described in section 3.2.2. The tank was filled with domestic tap water to an initial height measured from the bottom of the tank of 350mm. The tank is filled from the top continuously at constant flowrate equal to the discharge rate, to maintain fluid level at constant height. It is observed from the experiment that the fluid disturbance has little effect on the adjusted

height. Aluminum oxide seeding particles of approximately 5μm size (Table 3.2), are blended into the tank. The drain is opened, and we observed and recorded the location of the free surface until it at the desired height, then measurements were made. Once the measurements were made, the experiment was repeated at height *h* levels of 10cm, 12cm, 15cm, 16cm, 17cm, 18cm and 20cm. All measurements were made using the same tank and with the initial height of liquid set to be the same for all measurements. The measurements and calculated values using equation 6.3 are plotted in Figure 6.3. The water density, ρ=998 kg/m^3, corresponding to a room temperature of 20ºC is used for the calculations. The spectra of sample measurements are shown in Figure 6.2 and the corresponding velocity values are calculated using:

$$v = \frac{\lambda f_B}{2\beta} \qquad (2.17)$$

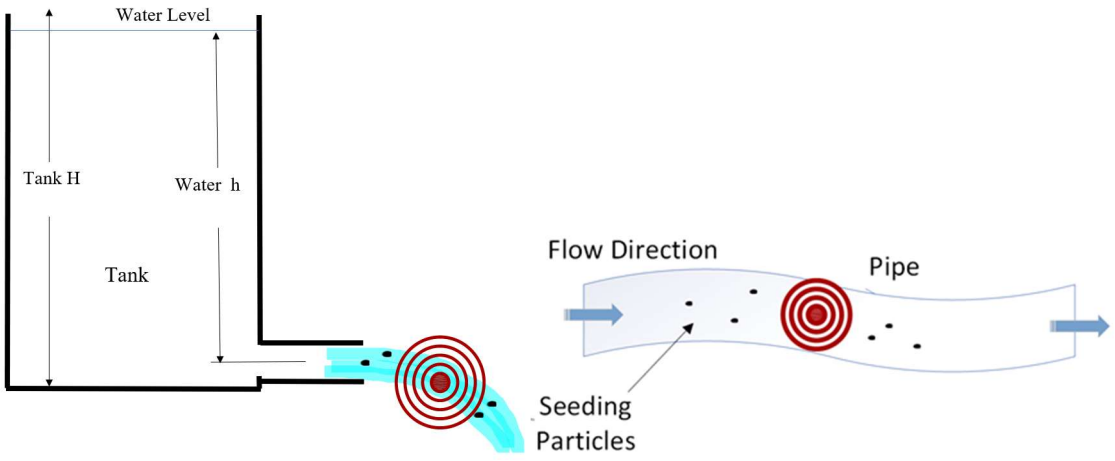

(a) (b)

Figure 6.1 Measurements of total 2D velocity (a) at exit from a tank (b) in a thin pipe with arbitrary orientation

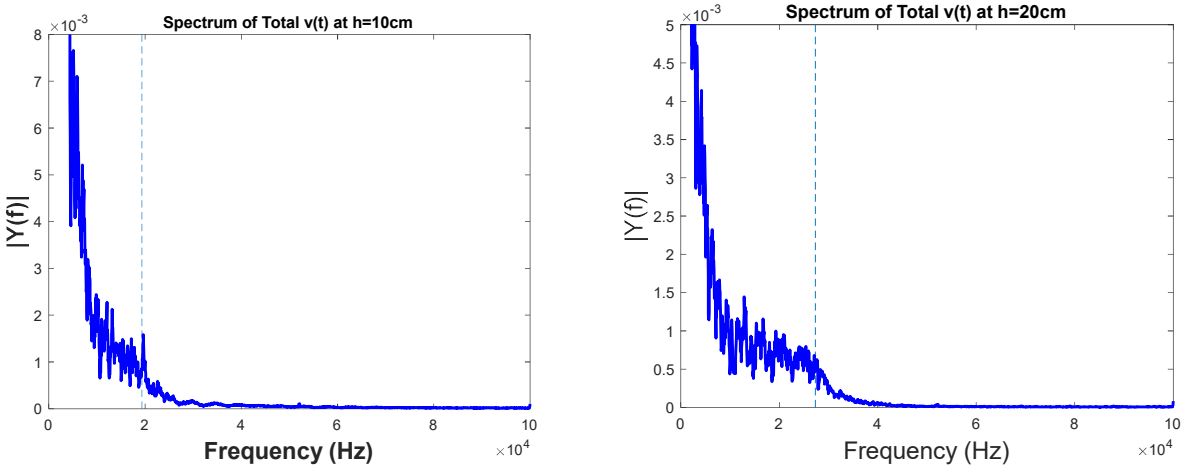

Figure 6.2 Spectra of scattered light intensity of total velocity measurements showing f_B at (a) h=10cm and (b) h=20cm

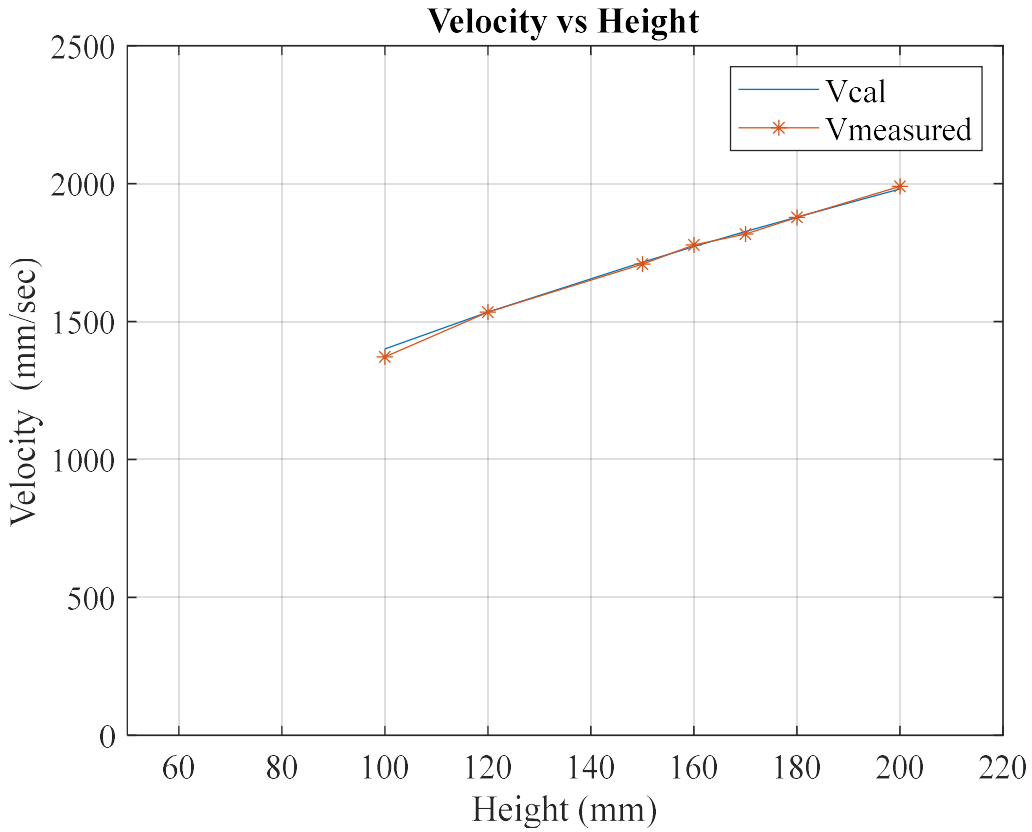

Figure 6.3 Plot of velocity vs height of water

6.2 Pipe Flow Experiments

6.2.1 Development of Flow

The flow regime development in a pipe depends on the Reynolds number, as defined in equation.

$$\mathrm{Re} = \frac{\rho\, U_{avg}\, D}{\mu_f} \qquad (6.4)$$

where U_{avg} is the average velocity, D is the inside pipe diameter, and μ_f is the dynamic viscosity of the fluid. For laminar and turbulent flow conditions, the flow is fully developed in a straight pipe, at locations beyond an entrance length (Le), which depends on the Reynolds number Re and pipe internal diameter D, [108]:

$$\frac{Le}{D} = 0.06 \times \mathrm{Re} \qquad \text{Laminar Flow (Re < 2300)} \qquad (6.5)$$

$$\frac{Le}{D} = 4.4 \times \mathrm{Re}^{\frac{1}{n}} \qquad \text{Turbulent Flow (Re > 4 000)} \qquad (6.6)$$

The flow is usually assumed transitional for 2300 ~< Re ~< 4000.

For fully developed steady laminar flow, the radial velocity profile is given by [109]

$$u(r) = 2U_{avg}\left(1 - \frac{r^2}{R^2}\right) \qquad (6.7)$$

$$u(r) = U_{max}\left(1 - \frac{r^2}{R^2}\right) \qquad (6.8)$$

Where *r* is the radial distance and *R* is the internal radius of the pipe, U_{ave} is the average velocity inside the pipe and U_{max} is the maximum velocity given by

$$U_{max} = 2U_{avg} \qquad (6.9)$$

The velocity profile for the steady laminar flow has a parabolic shape with a maximum velocity at the center of the pipe and zero velocity near the wall, *u(r) = 0*, due to the no-slip condition.

For turbulent flow, the velocity profile can be calculated from power law, given by the following equation [109]

$$u(r) = U_{max}\left(1 - \frac{r}{R}\right)^{\frac{1}{n}} \qquad (6.10)$$

Where *n* depends on the Reynolds number but many flows in practice are approximated with n=7. The average velocity is given by (Fundamentals of pipe flow) [110]

$$\frac{U_{avg}}{U_{max}} = \frac{2n^2}{(n+1)(2n+1)} \qquad (6.11)$$

To assess the flow development for the present experiments, we note that for the pipe flow water channel used and described in section 3.1.2, after the contraction, a PVC pipe of 3 m long was used, followed by glass pipe of equal inside diameter (38mm), and 1.5 m long, which constitutes the test section. The measurements were taken inside the test section, at a distance of 3.75m from the exit of the flow straightener. In the case of the laminar flow at Re ≈ 560 and Q=1 L/min, an approximate development length $Le = 0.16ReD = 34D$ *of 1.3m*, is required. For the turbulent flow, based on Re=8400 at Q=15 L/min an approximate development length of $Le = 25\ D\ Re^{\frac{1}{7}}$ *=16D=0.61m* is needed. This ensured that the flow was fully developed for both flows at the measurement location.

In some cases, the flow profile might deviate from the theoretical equation 6.8 for laminar and equation 6.10 turbulent flows respectively, even though the flow is allowed to fully develop. These deviations might be due imperfections in the geometry of the pipe, the presence of centerline curvature [111] or a partially filled pipe [112] [113]. For pipe curvature [111] , the centrifugal forces transport momentum towards the outside of the curved pipe causing the profile to be skewed with the maximum velocity away from the centerline. For horizontal partially filled pipes, it was

shown analytically [112] and theoretically [113], that the profile is skewed with the maximum velocity shifted above the centerline.

6.2.2 Measurements Procedure

By referring to the water channel presented in chapter 3 (Figure 3.2), the tank is filled with domestic tap water until the pump is completely submerged. The water temperature is at room conditions, T ≈22°C, and thus the corresponding kinematic viscosity of $\nu = 1.004\ mm^2\ s^{-1}$ is assumed. Aluminum Oxide tracer particles of approximately 5μm size (Table 3.2), are blended into the tank. Although the concentration of particles in the flow loop is not monitored, the tracers are added to the tank at approximately a concentration of 5 g/m3. As the pump is started, and the water is circulating in the water channel, valves B, C and A are opened, then valve B and C are closed to obtain maximum flow rate. Valve A is closed slowly to obtain the desired flow rate indicated by the flowmeter display and valve C is opened slowly to avoid pressure increase in the system. The water is allowed to run for few minutes until most of the air trapped inside the flow loop leaves the system, and the air bubbles that are initially visible in the flow disappear. The flow rate is varied in increments of 1L/min using valve A and valve C until the desired flowrate measured by the flowmeter stabilizes to its set value. When the flow rate is less than 5 L/min, the flow is laminar, and turbulent when the flow is 5 L/min and above. The distance from pipe entrance to the test section is set to 3.5m, since this ensured that the flow was fully developed. The optical bench is moved so that the center of the illuminated plane is located where the desired measurement would be performed. For adjustment of the system, the measurement point is set at the pipe center because the observation noise is smallest there. Using a program written in NI LabVIEW, the frequency is set according to the range of velocity to be measured and the maximum

number of samples is set to 10 records of 4096 points each. The velocity was determined from the flow rate Q which was controlled by the valves in the channel. The center of the test section is located by using the adjustable stage that moved the optical bench until flare is observed through the test section walls, and then moving half way in between to the test section center. A digital dial indicator in connection with the optical bench is used to accurately adjust the readings of the beam location in the test section. This is allowed the measurements to be normally made at equally spaced readings in increments of a half-turn of the stage knob at the desired location of measurement. The mounting setup allowed the scattering volume to be traversed over a known distance to any position in a cross-section of the test section. By fixing the stage and traversing the optical system in the vertical direction, the velocity measurement was conducted by changing the location of the measurement point. A velocity profile is taken by averaging 10 measurements for each point. The measurements are taken at steps of 2 mm away from the wall and 1mm close to it. An index matching glass box filled with water is used to decrease the aberration and light beam diffraction during measurements. At each desired location, the measurements were repeated several times for precision by checking the obtained spectra and fine tuning the optical adjustments. Measurements within 2 mm from the wall are not reliable due to reflection and refraction of the laser beam and are therefore discarded. The signal is obtained using the forward scatter mode since this method offers strong signal output due to higher scatter in the direction of the laser beam, approximately four times greater in intensity magnitude than for backward mode. To minimize the reflection of unwanted light on receiving optics, all ambient lights are turned off during measurements. The flow is assumed to be one dimensional. The optical bench and the development pipe and test section were adjusted and leveled so that the Bessel beam fringes measure the one-dimensional velocity in the pipe.

6.2.3 Adjustment of LBV Optics for Pipe Flow Measurements

The laser was mounted and aligned on an optical bench and turned on. Using an adjustable stage (jack), the laser beam height was adjusted such that it was parallel to the optical bench. A spherical lens (F=25mm) was mounted in front of the laser beam with a lens post and holder on the optical bench. The lens was fixed and aligned such that the laser beam passes through its center. A second spherical lens (F=75mm) was mounted with a lens holder and post at a distance 100mm from the first lens which is the summation of the focal length of both lenses (F1+F2) as shown in Figure 3.4 and aligned with the first lens such that the laser beam passes through its center. The laser beam diameter was expanded to three times its original diameter, $D_b = d_b \left(\frac{\mathrm{F2}}{\mathrm{F1}}\right)$, and collimated. Using the adjustable stage, the LBV optical system head was positioned in the horizontal direction until LBV signal is detected using the photodetector and corresponding optical components. Proper alignment of the laser beam with respect to the test section is necessary for reliable LBV measurements. Prior to each run and more often as required, the laser beam was operationally checked. The Bessel beam projection was checked with a microscope objective projecting its cross-section at a distance equal to the transmitting lens focal length. The adjusting stage carrying the LBV optical components was used, along with a caliper, to change the location of the measurement in the test section to allow obtaining velocity measurement profiles at various points of the transparent test section.

6.2.4 LBV Slits Adjustment

The annular slit was mounted with a post and holder in front of the second lens at its focal plane. The distance between the slit and the second lens was equal to 75mm. Fine adjustments were made

to the alignment to ensure that the beam passing through both lenses is collimated, passes symmetrically through the annular slit and is parallel to the optical bench. First, we used 50mm focal length lens after the slit, but because we installed a square box around the test section, an increase in the depth of field was needed to access the tube center. Therefore, a 57mm focal length lens was mounted after the slit to increase the focal length and location of measurement. The collimated laser beam passing through the slit (Durnin's ring) was passed through the center of the lens (F=57mm) projecting an annular laser ring. Fine tuning was made to ensure the beam passing through the projecting lens by observing the ring on a whiteboard at about 1m away from the optical system. The slit was not removed or replaced until all required measurements were made. For adjustment of Bessel beam and to ensure that the beam remained in focus, a 50X microscopic objective was used after the F=57mm lens to project the beam. The image of the Bessel beam cross-section was observed on a sheet placed at a distance away from the objective lens**.** A 20X microscopic objective was also used to project and observe an image of the Bessel beam. Each microscopic objective lens exhibited the Bessel beam rings in a different size depending on its magnification.

6.2.5 Adjustment of The Photodetector for LBV

The photodetector is mounted on the optical bench and positioned in front and facing the measurement volume to collect the scattered light in the forward scatter mode to ensure that a strong signal can be detected. The optimum position of the receiving lens and photodetector was determined based on the lens focal length and by maximizing the intensity of photodetector's signal measured using a voltmeter. After making the proper alignment and adjustment of the Bessel

beam, the measurement signal was checked by examining its spectra and comparing it the expected spectra of the LBV technique (Figure 2.7).

6.2.6 Pipe Velocity Measurements

Experimental measurements of velocity profiles across the cross-section of straight transparent circular tubes were made using Bessel beam (LBV) and LDV at different points in the test section to get a transverse velocity profile. The measurements were taken at flow rates corresponding to the laminar and turbulent regimes. A typical average variation of the Bessel beam spectra is shown in Figure 2.7. Based on the obtained spectra, we are to determine the experimental Bessel frequency, f_B, as the value at which the spectrum starts to decrease after presenting a nearly constant value, as indicated in [3]. All equation for estimating the uncertainty were used from (Theory and Design for Mechanical Measurements fifth edition, by Richard S. Figliola and Donald E. Beasley).

6.2.6.a Laminar Flow Measurements

In this section, experimental measurements of the laminar flow velocity profiles in the water channel at the cross-section of straight circular tubes using LDV and LBV are presented. In order to achieve laminar flow, the flowrate was set to around 1 liter per minute. First, we describe the measurements made using the commercial LDV, and compare them to the theoretical profiles for fully developed laminar pipe flow described by Eq. 6.8. The results are presented in Figure 6.4. From this figure, it can be seen that the profile is parabolic, resembling that of a laminar flow, but skewed away from the central axis of the tube with the maximum velocity shifted above the center. At first this behavior seemed confusing since the location of measurements is fully developed flow region. Hence, more adjustments to the system and leveling of the optical bench and water channel

were made. The measurements were repeated for different flow rates at the laminar flow regime, and the skewness persisted which confirmed that this was indeed the actual flow profile and not an error in the measurement. To overcome the skewed velocity profile effect, a flow contraction was added to the water channel and a flow straightener was placed upstream of the pipe as shown in Figure 3.2. Even though with these measures the asymmetry was reduced, it was not completely removed as shown in Figure 6.4. As mentioned earlier the possible reasons for asymmetry in the velocity profile and maximum velocity occurring off the centerline, include: an imperfection in the pipe geometry, longitudinal curvature of the pipe and a partially filled pipe. The longitudinal curvature was excluded since the flow was straightened after the contraction and allowed to develop in a straight pipe for an extended length. The pipes were also rotated too but the skewness remained in the same direction with a maximum velocity above the centerline. This leaves the possibility of a partially filled pipe, even though this was not visible to the naked eye at the cross section, it may be that the fluid was not in complete contact to the upper surface of the pipe. To exclude this possibility, we tried to pressurize the water channel, this resulted in some leaks at different places, and to avoid damage we abandoned this measure. Since the main objective of the present work is to validate a new measurement technique it was decided to proceed with these LDV measurements and to use them to validate the new technique.

LBV measurements were carried out for the same flow conditions as the LDV measurements with two different annular slits (r_1=0.7mm, r_2=0.9mm and r_1=2mm, r_2=2.2mm). Some sample spectra are presented in Figure 6.7 and Figure 6.8. By examining the spectra, the trend of measured Bessel frequency is identified from the average curve of the spectra, as the intensity of the spectra starts to drop significantly towards the x-axis to reach a near-zero value. The corresponding velocity values using equation:

$$v = \frac{\lambda f_B}{2\beta} \qquad (2.17)$$

were calculated. Velocity profiles were obtained using the LBV system with annular slits (r_1=0.7mm, r_2=0.9mm and r_1=2mm, r_2=2.2mm), herein referred to as 0.7/0.9 and 2/2.2, respectively. Other slits were tried but did not yield good results probably because for most of them the opening area allowing laser to pass through was smaller resulting in a reduced light intensity. It should be mentioned that several slits were used for measurements, and their results were less accurate because of lower laser intensity passing through or irregular DOF.

These results are not included here. The results for the 0.7/0.9 and 2/2.3 slits are presented in Figure 6.5 and Figure 6.6 respectively along with the LDV measurements. From these plots it can be seen that the velocity profile is parabolic and skewed away from the center axis of the pipe similar to the profile obtained from the LDV measurements. In addition, these measurements agree reasonably well with LDV measurements. By referring to Chapter 5, the 0.7/0.9 slit generates a nearly Bessel beam with a DOF= 5.972mm, fringe spacing=0.0235mm and an effective diameter of d_{eff} =0.22mm. The 2/2.2 slit generates a nearly Bessel beam with DOF= 2.275mm fringe spacing= 0.0090mm and an effective diameter of d_{eff} =0.16mm Both annular slits showed comparable measurements and the deviation with the LDV measurements for both was comparable.

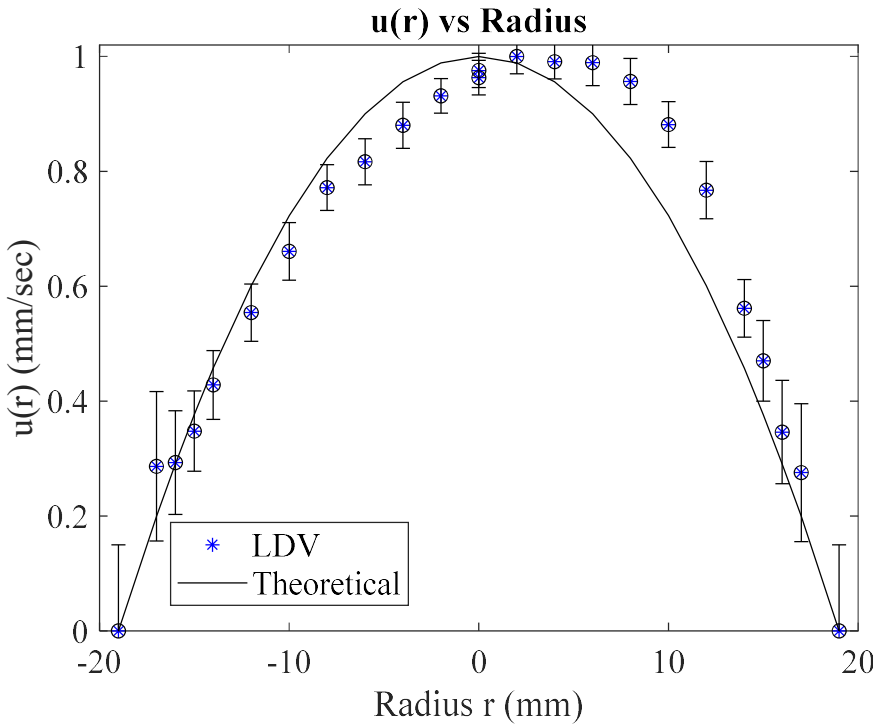

Figure 6.4 Experimental velocity profile in laminar flow of LDV compared to theoretical profile (Flow Rate ≈1 L/min, Re= 556)

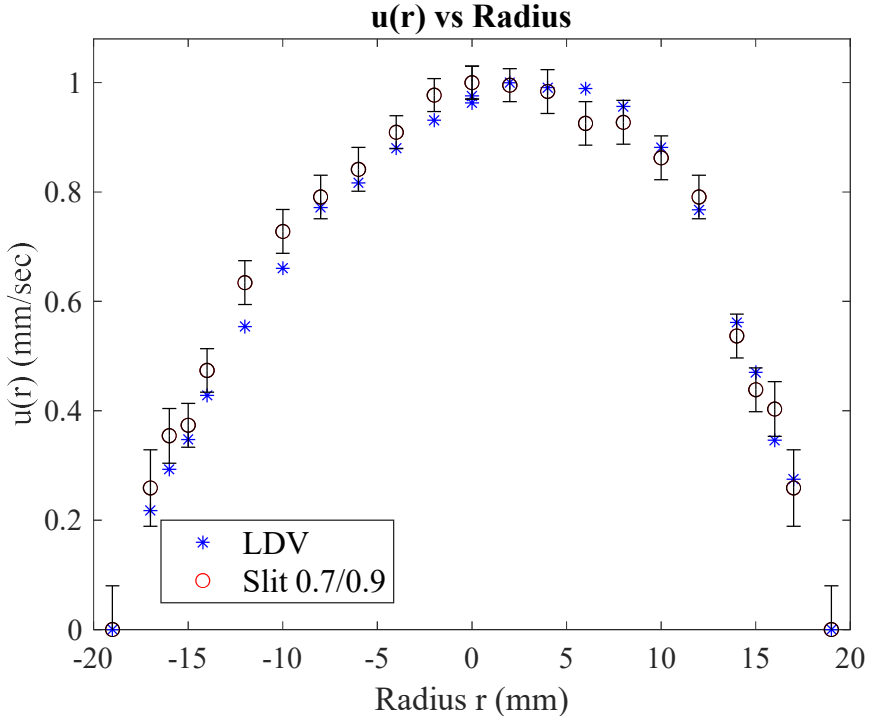

Figure 6.5 Experimental velocity profile in laminar flow comparison of LBV using Slit 0.7/0.9 and LDV (Flow Rate ≈1 L/min, Re= 556)

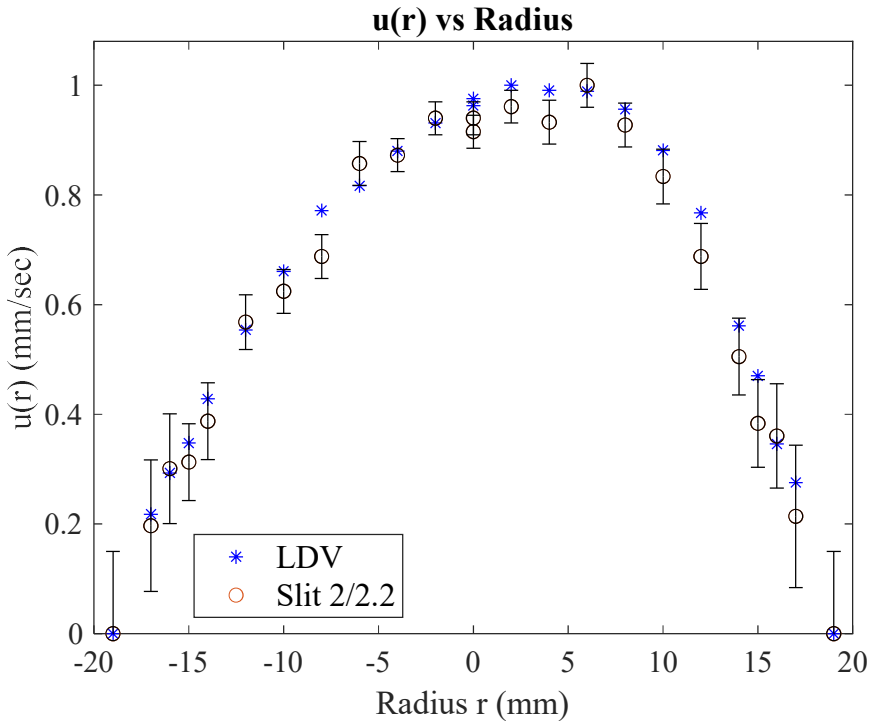

Figure 6.6 Experimental velocity profile in laminar flow comparison of LBV using Slit 2/2.2 and LDV (Flow Rate ≈1 L/min, Re= 556)

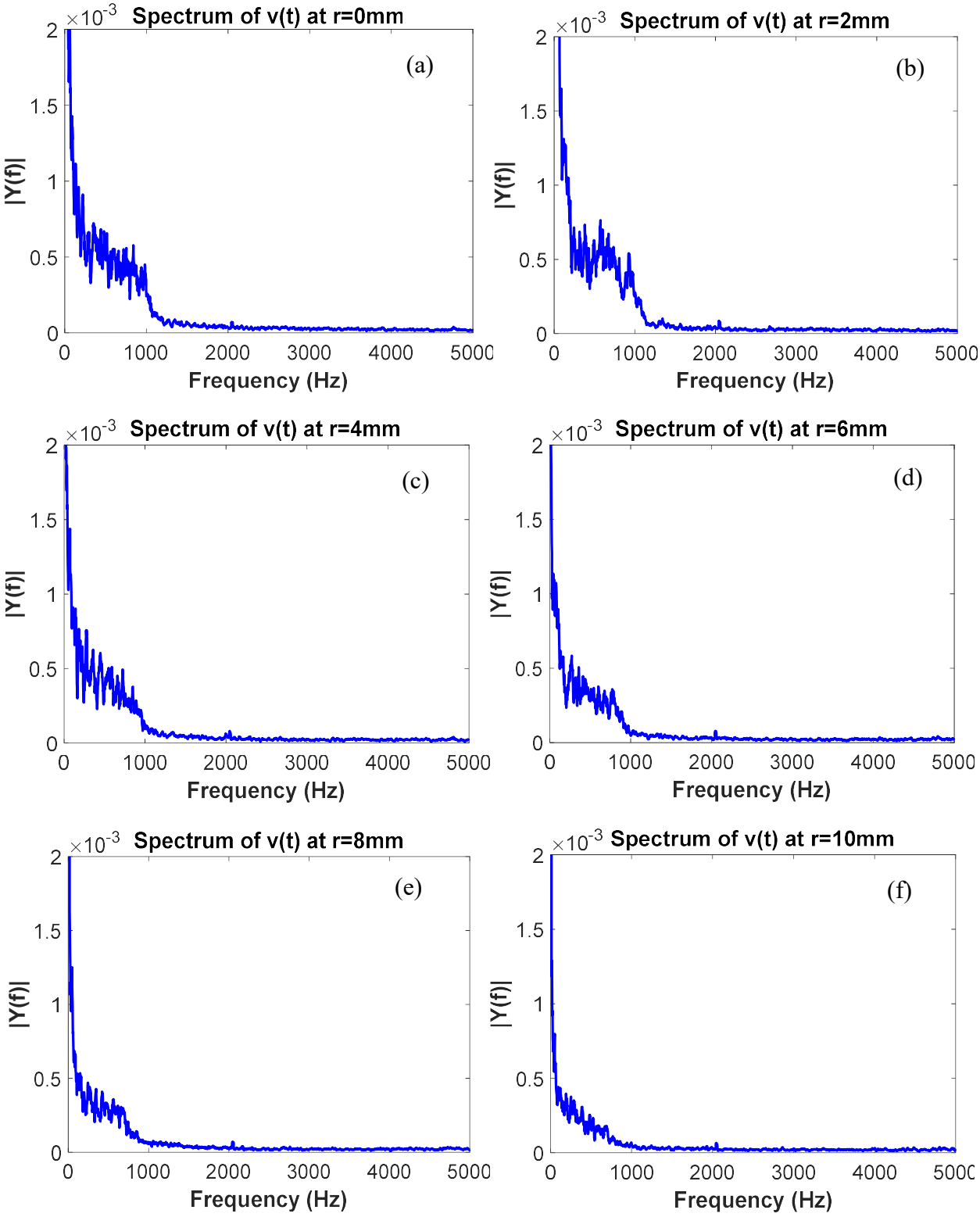

Figure 6.7 Spectra of scattered light intensity of laminar flow of LBV using slit 0.7/0.9 (Flow Rate≈1L/min, Re= 556) showing f_B at different positions along the pipe diameter: (a) r=0mm, (b) r=2mm. (c) r=4mm, (d) r=6mm (e) r=8mm, (f) 10mm

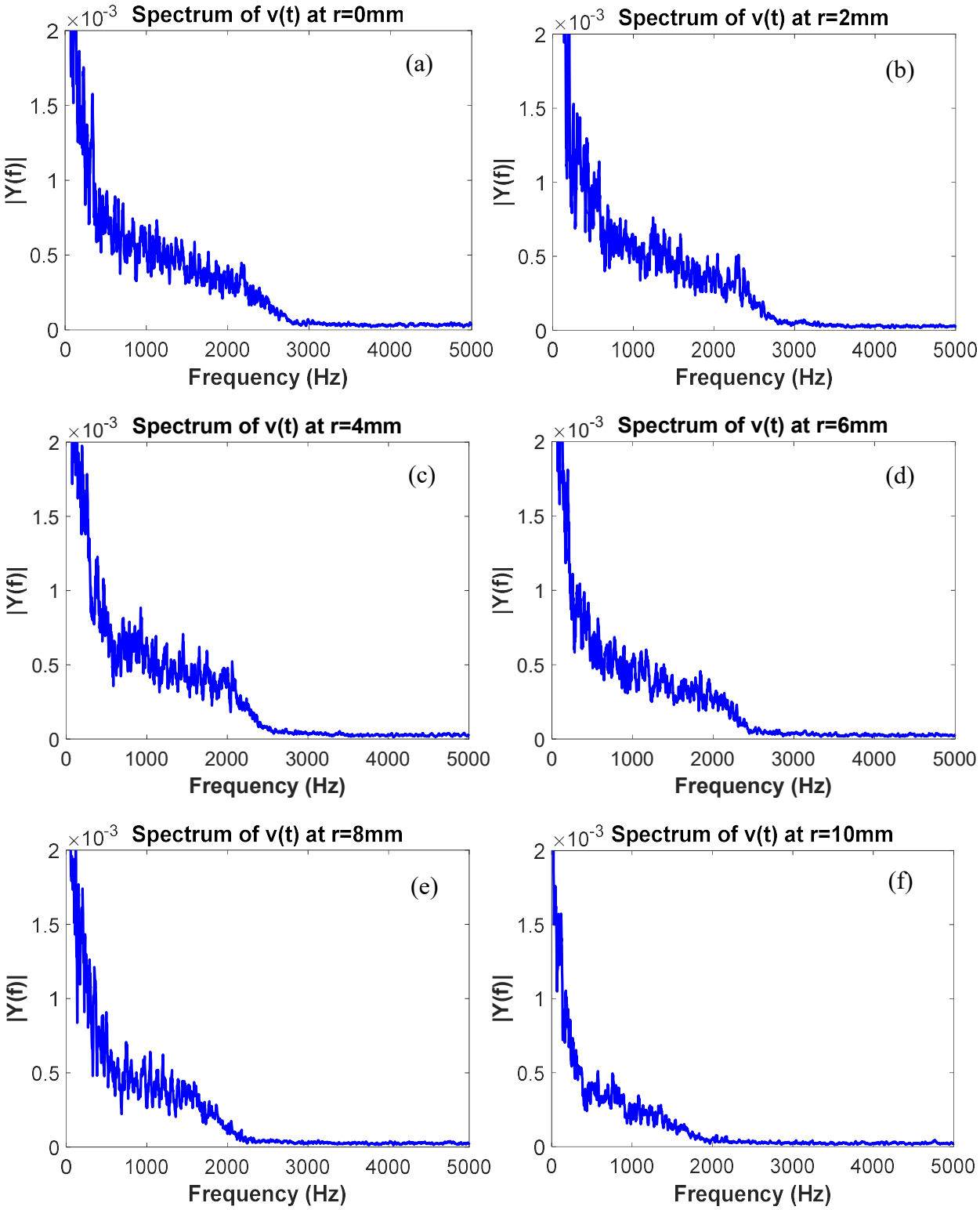

Figure 6.8 Spectra of scattered light intensity of laminar flow of LBV using slit 2/2.2 (Flow Rate≈1L/min, Re= 556) showing f_B at different positions along the pipe diameter: (a) r=0mm, (b) r=2mm. (c) r=4mm, (d) r=6mm (e) r=8mm, (f) 10mm

6.2.6.b Turbulent Flow Measurements

First, the experimental measurements for the turbulent flow were performed using the commercial LDV system and the results are compared to the theoretical profile as shown in Figure 6.9. From the plot, it can be seen that the profile is not always smooth probably due unsteadiness in the pump. As expected, the turbulent velocity profile is flatter than the laminar one. However, as shown in Figure 6.9, the peak of the turbulent velocity profile is almost in the center of the pipe. It is observed from this profile that the skewness is significantly reduced in comparison to laminar flow results. The profile shows better symmetric behaviour. The reason for this is possibly that for turbulence flow, the fluid is rapidly mixing in all directions resulting in the velocity being more uniform across the pipe and there is more momentum transfer toward the boundary layers and the walls of the pipe. It should also be mentioned that measurements were performed both at the beginning and end of the test section and provided similar results confirming that the flow is fully developed at the location of the measurement. The LBV turbulent profile measurements were performed using annular slits (0.5/0.7 and 1.2/1.4). The corresponding spectra are presented in Figure 6.12 and Figure 6.13 respectively. The Bessel frequency f_B is identified from the average curve of the spectra, as the intensity of the spectra starts to drop significantly towards the x-axis to reach a near-zero value. The spectra are much clear at locations away from the wall and starts to degrade as the measurements approaches the tube wall. The velocities are calculated using equation 2.17 and the results are plotted and presented in Figure 6.10 and Figure 6.11, for slits 0.5/0.7 and 1.2/1.4 respectively. By referring to Chapter 5, the 0.5/0.7 slit generates a nearly Bessel beam with the following characteristic: DOF=7.963mm, fringe spacing d_f=0.0314mm and an effective diameter of d_{eff} =0.3mm. The 1.2/1.4 slit generates a nearly Bessel beam with DOF=3.675mm, fringe spacing d_f= 0.0145 mm and an effective diameter of d_{eff} =0.18mm. From

Figures 6.10 and 6.11 it can be seen that the annular slit 0.5/0.7 produced better measurements compared to the annular slit 1.2/1.4, even though the measurement volume of the latter is smaller. Since the quality of measurement results also depends on the intensity, the annular slit (0.5/0.7) has higher intensity that gave better results with stronger signal to noise ratio (SNR) even though it has longer DOF. In addition, it should be mentioned that the DOF values are obtained from approximate relations reported in [11]. By examining the longitudinal intensity distribution calculated from scalar diffraction theory and produced by slit 1.2/1.4 (Figure 5.7), we notice two peaks at the center and an irregular distribution which produced results with less quality than slit 0.5/0.7 and with more uncertainty. Despite that care was taken in constructing the test section, and performing measurements, it turned out that significant sources of measurement error were still present close to the wall in turbulent and laminar flows. These error sources caused the quality degradation of spectra and showed up as noise or scatter in the plot, in particular at measurement positions approximately 1mm away from the wall. They are mostly due to low velocities and flare and reflections of the laser light from the pipe wall that were picked up by the receiving optics have been the cause of the inaccuracies in the wall region. This location is extremely sensitive to measurement noise. As the beam approaches the wall, the measuring volume is truncated at the wall that loses some of its dimensions which greatly affected the measurements producing noisy signal. The laser beam measuring the velocity component, is most sensitive to such disturbances. The measurements away from the wall do not suffer from large error sources and have relatively good accuracy compared to those near the wall. These factors may have affected the velocity distribution as a result, the error possibly increased.

Another major difficulty which affected both laminar and turbulent pipe flow measurements accuracy is the difficulty in focusing the photodetector optical components on the measurement

volume. Contrary to the LDV where the measurement volume is clearly indicated by the intersection of two beams, the measurement volume for LBV cannot be easily identified by the naked eye.

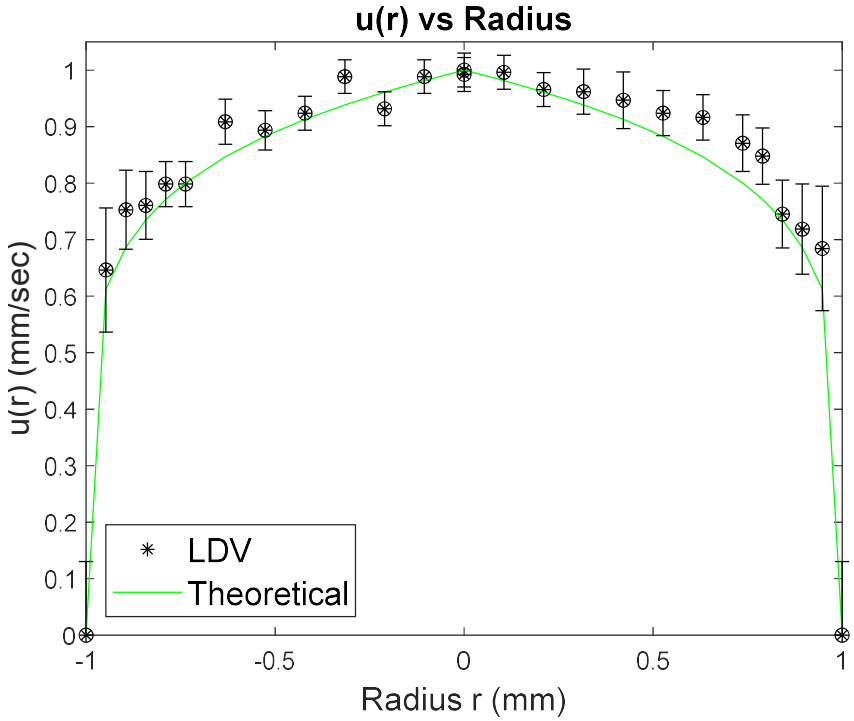

Figure 6.9 Experimental velocity profile in turbulent flow comparison of LDV measurements to theoretical profile (Flow Rate ≈15 L/min, Re= 8340)

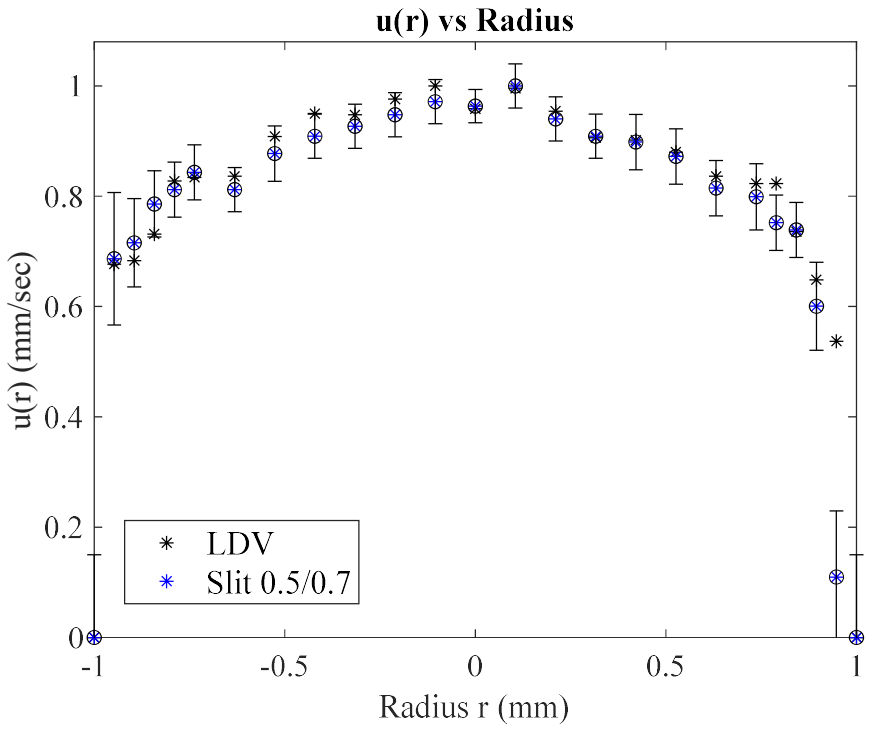

Figure 6.10 Experimental velocity profile in turbulent flow comparison of LBV using Slit 0.5/0.7 to LDV measurements (Flow Rate ≈15 L/min, Re= 8340)

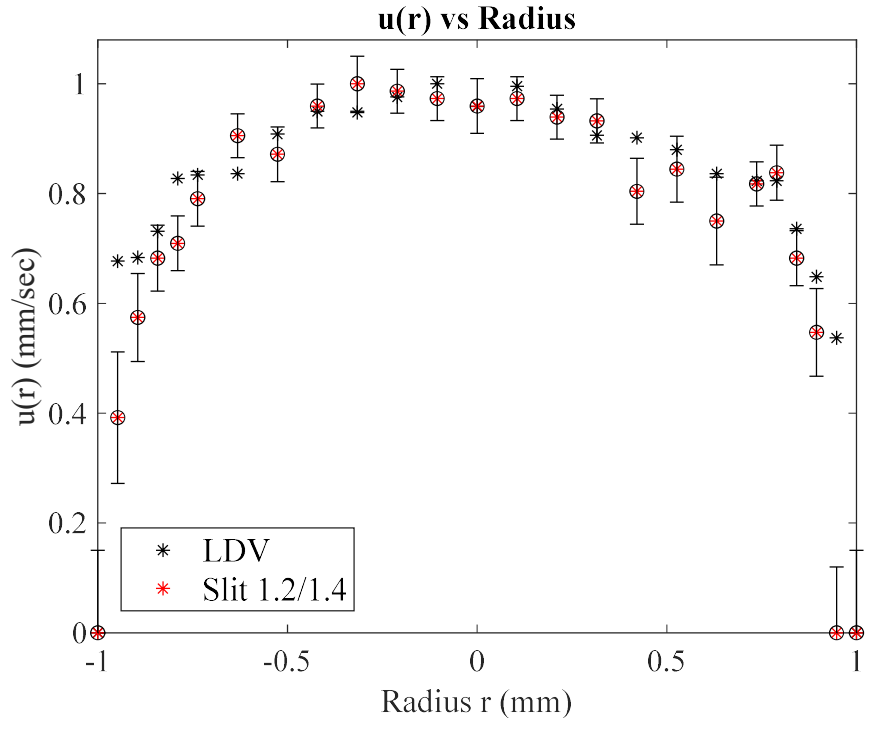

Figure 6.11 Experimental velocity profile in turbulent flow comparison of LBV using Slit 1.2/1.4 to LDV measurements (Flow Rate ≈15 L/min, Re =8340)

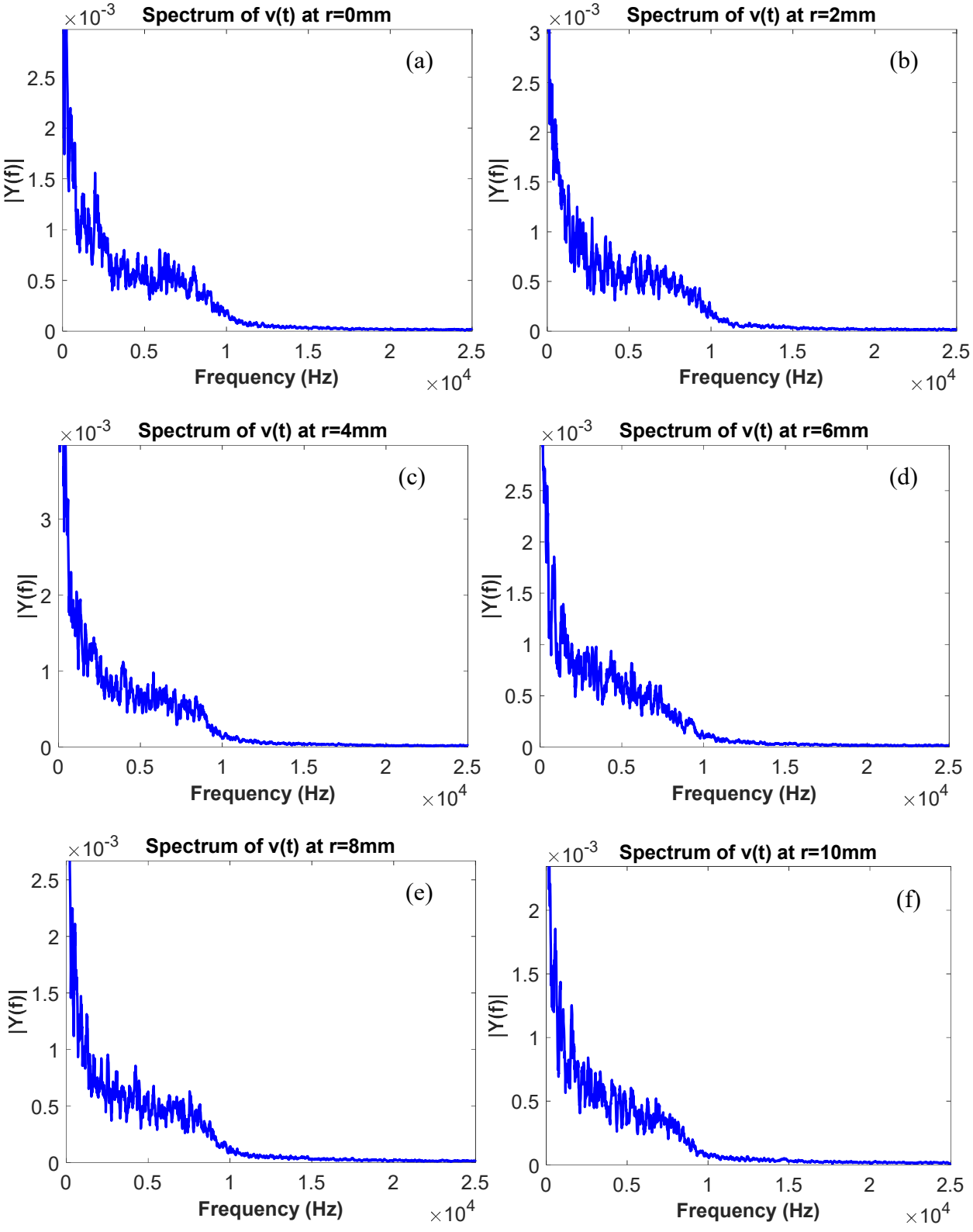

Figure 6.12 Spectra of scattered light intensity of turbulent flow of LBV using Slit 0.5/0.7 (Flow Rate≈15 LPM, Re=8340) showing f_B at different positions along the pipe diameter: (a), r=0mm, (b) r=2mm (c) r=4mm, (d) r=6mm, (e) r=8mm, (f) r=10mm

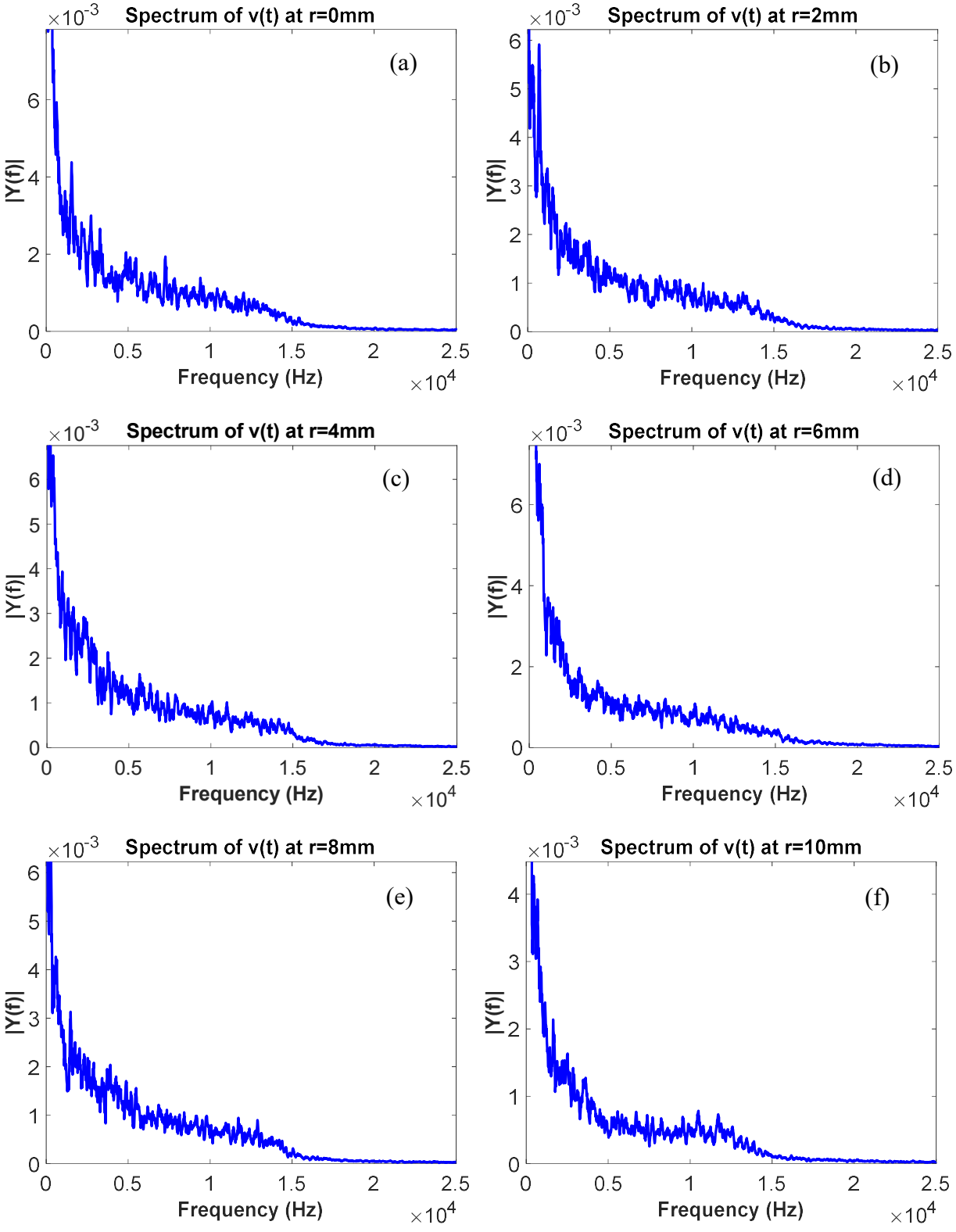

Figure 6.13 Spectra of scattered light intensity of turbulent flow of LBV using Slit 1.2/1.4 (Flow Rate≈15 LPM, Re=8340) showing f_B at different positions along the pipe diameter: (a), r=0mm, (b) r=2mm (c) r=4mm, (d) r=6mm, (e) r=8mm, (f) r=10mm

6.2.7. Measurements Uncertainty Analysis

In estimating the accuracy of my velocity measurements, the sources of uncertainty are presented and how these sources combine to add to the overall uncertainty in velocity is explained. The overall uncertainty estimation follows the theory of uncertainties approach [1]. The measured velocity can be calculated from equation 2.17

$$\mathrm{v} = \frac{\lambda \mathrm{f_B}}{2\beta} \qquad (2.17)$$

Based on equation 2.17, the uncertainty in the velocity variation could be expressed as a function of: u_λ, the uncertainty in the wavelength λ, u_f, the uncertainty in Bessel frequency f_B and u_β, the uncertainty in the angle of refraction β.

$$v = f(\lambda, f_\beta, \beta) \qquad (6.12)$$

$$u_v = g(u_\lambda, u_f, u_\beta) \qquad (6.13)$$

From the theory of uncertainties [1]

$$u_v = \pm\sqrt{\left[\left(\frac{\partial v}{\partial \lambda}u_\lambda\right)^2 + \left(\frac{\partial v}{\partial f_B}u_f\right)^2 + \left(\frac{\partial v}{\partial \beta}u_\beta\right)^2\right]} \qquad (6.14)$$

By substituting for the partial derivatives

$$u_v = \pm\sqrt{\left(\frac{f_B}{2\beta}u_\lambda\right)^2 + \left(\frac{\lambda}{2\beta}u_f\right)^2 + \left(\frac{-\lambda f_B}{4\beta^2}u_\beta\right)^2} \qquad (6.15)$$

based on the manufacturer's specifications, the laser beam wavelength (λ=660 nm) has an uncertainty of ±5% leading to $u_\lambda = 3.3\text{x}10^{-5}$ mm

In order to estimate u_β, we use the expression of the angle β is given by:

$$\beta = tan^{-1}\left(\frac{R}{F}\right)$$

From the Thorlabs manufacturer, the lens used with focal length F=57mm has the following uncertainties [2]:

Lens radius uncertainty u_R =±0.05mm

Focal length is ±1%, then u_F = ±0.57mm

The uncertainty u_β in the refraction angle β can be found using

$$u_\beta = \pm\sqrt{\left(\frac{\partial\beta}{\partial R}u_R\right)^2 + \left(\frac{\partial\beta}{\partial F}u_F\right)^2} \qquad (6.16)$$

The derivatives $\frac{\partial\beta}{\partial R}$ and $\frac{\partial\beta}{\partial F}$ are found using the following equations:

$$\frac{\partial\beta}{\partial R} = \frac{\partial}{\partial R}\left(\tan^{-1}\left(\frac{R}{F}\right)\right) = \frac{F}{R^2+F^2}$$

$$\frac{\partial\beta}{\partial F} = \frac{\partial}{\partial F}\left(\tan^{-1}\left(\frac{R}{F}\right)\right) = -\frac{R}{R^2+F^2}$$

Based on the above equations,

$$u_\beta \approx 0.0023\, rad$$

The mean value of the frequency was obtained from the spectra plot, by taking the average of the minimum and maximum possible values of f_B. The difference in these frequency values was used as the frequency uncertainty u_f. With these uncertainties it is now possible to evaluate the uncertainties in the velocity.

The inferential error bars on velocity plots represent the uncertainty on each measurement point. Since the spectra away from the wall show much better trend and have relatively good accuracy compared to those near the wall, the frequency can be identified from the average curve easily which have smaller error bars. Measurements closer to the pipe wall were not very clear which show large error bar compared to the measurements in the center.

Chapter 7

CONCLUSIONS AND CONTRIBUTIONS

In this chapter I summarize the main contributions of this thesis, their potential and shortcomings. I conclude by proposing areas of improvements and future research. A novel method for 2D velocity components measurement using Bessel beams was presented. The Bessel frequency and Doppler frequency were used to resolve the two velocity components in a simple Bessel beam-based fringe type LDV system. This system was demonstrated by making two velocity components measurements on solid surface velocities but can be extended to fluid flow velocity measurements. A better understanding of the intersection was achieved by experimental and numerical characterization. One of the objectives of the present thesis was to use the LBV technique, previously used for solid surface velocity measurements, to perform fluid flow velocity measurements. In order to have an acceptable spatial resolution using this technique it was necessary to create near Bessel beams with limited DOF and transverse propagation. Several masks containing annular slits with finite width were fabricated on thin glass plates for use in this work. We have demonstrated experimentally and numerically that it is possible to control the DOF and transverse extent of the nearly Bessel beam generated by these masks. Using annular slits, the transverse intensity was controlled but the longitudinal (DOF) was still too long to significantly improve the longitudinal spatial resolution. To reduce the DOF further, a lens with shorter focal length could be used but this would cause the generated Bessel beam to be located at shorter distance from the lens and not attaining the center of the pipe where measurements have to be performed. Another challenge was the significant attenuations of the power of the laser beam used for measurements due to the blockage by these masks, allowing only a fraction of the beam to pass through the annular rings. Even with these limitations, this thesis presented what is believed to be

the first experimental demonstration of the use of Bessel beams to measure fluid flow velocities. Based on the results described in Chapter 6, the Bessel beam velocimetry technique offered measurements reasonably comparable to those obtained from LDV measurements in laminar and turbulent pipe flow measurements. The use of square box with flat thin glass walls was found to be adequate to reduce refraction and helped making LDV and LBV measurements in this particular arrangement. The LBV differs from the well-established technique of LDV by the simplicity of implementation and the low cost of its technology but with non-uniform fringe spacing and larger depth of field. However, LDV remains so far, the most powerful optical tool to accurately measure fluid flow velocity and to provide velocity direction and components. It has the advantage that small measuring volume with uniform fringe spacing and the capability to resolve velocity components and flow direction. The research has been conducted with the ambition of improving the LBV tools experimentally. However, there are still factors which can be further explored to develop this technique into a viable measurement alternative. One of the main advantages is to produce acceptable spatial resolution, but the LBV technique presented still cannot resolve velocity direction or its components. Performing accurate measurements of velocity directions and components proved to be difficult with the current configurations in the fluid flow channel. Due to the simplicity of the system, there is a potential that the LBV system can be developed into a probe of lightweight and compact that would be embedded inside models and machinery for measurements where larger probes are unusable and improvements in capabilities can be expected. It might be vital to make the system compact by using a small but powerful laser diode, small collimating lenses, backscattering for light collection, and fiber optics for light transmission. A significant advantage of LBV, even with its current configuration, was demonstrated by conducting experiment to measure the total velocity draining from the test tank using Bessel beam.

Due to the Bessel beam fringe configuration, by observing the scattered light from different directions, or by taking the measurements with different direction of the laser illumination, the total velocity measurements was obtained in (x,y) plane. Using LDV would require the use of a very expensive two-dimensional system and performing separate measurements for each component.

7.1 Future Work

In this work, a proof of concept of using Bessel beams to measure velocity was achieved. There is more work yet to be done. Detailed velocity measurements including direction and components are still to be taken. The simple LBV single beam configuration cannot resolve velocity components and direction because the Bessel beam fringes are axisymmetric.

To summarize, the following topics will improve the LBV technique for fluid flow velocity measurement and extend its applicability:

1) Improving its spatial resolution.
2) Resolving the velocity directions.
3) Using LBV to measure three velocity components.
4) Improving SNR for measurements would be very important to enhance the system to become an alternative technique in optical flow measurements.

REFERENCES

[1] H. Albrecht, M. Borys, N. Damaschke and C. Tropea, Laser Doppler and phase Doppler measurement techniques, Springer, 2003.

[2] J. Durnin., "Exact solutions for non-diffracting beams.I. The scalar theory," *JOSA,* vol. 4, no. 4, pp. 651-654, 1987.

[3] M. Sakah, B. Chebbi and I. Golub, "Measuring velocity with Bessel beam fringes," *Optical Engineering,* vol. 54, no. 8, pp. 084106-084106., 2015.

[4] M. Sakah and C. Brahim, "Measuring solid surface velocity and detection of particle movement by laser Bessel beams," *Optical Engineering,* vol. 55, no. 9, p. 091411, 2016.

[5] Greenleaf, J. F and J. Y. Lu, "Ultrasonic nondiffracting transducer for medical imaging," *Ultrason., Ferroelec., Freq. Cont.,* vol. 37, no. 5, p. 438–447, Sept. 1990.

[6] L. Paterson, E. Papagiakoumou, G. Milne, V. Garcés-Chávez, S. Tatarkova, W. Sibbett, F. Gunn-Moore, P. Bryant, A. Riches and K. Dholakia, "Light-induced cell separation in a tailored optical landscape," *Applied Physics Letters,* vol. 87, no. 12, p. 123901, 2005.

[7] J. Durnin, J. Miceli Jr and J. H. Eberly, "Diffraction-free beams," *Physical review letters,* vol. 58, no. 15, pp. 1499-501, 1987.

[8] A. Zannotti, C. Denz, M. A. Alonso and M. R. Dennis, "Shaping caustics into propagation-invariant light," *Nature communications,* vol. 11, no. 1, pp. 1--7, 2020.

[9] S. Monk, J. Arlt, D. A. Robertson, J. Courtial and M. J. Padgett, "The generation of Bessel beams at millimetre-wave frequencies by use of an axicon," *Opt. commun.,* vol. 170, no. 4, pp. 213-215, 1999.

[10] M. Sakah and B. Chebbi, " Interference of two intersecting Bessel beams and application to laser Doppler velocimetry.," *Applied Optics,* vol. 59, no. 27, pp. 8235-8241, 2020.

[11] M. A. Mahmoud, M. Y. Shalaby and D. Khalil, "Propagation of Bessel beams generated using finite-width Durnin ring," *Applied optics,* vol. 52, no. 2, pp. 256--263, 2013.

[12] J. Hecht, "Beam: The Race to make the laser," *Optics and photonics news,* vol. 16, no. 7, pp. 24-29, 2005.

[13] J. H. McLeod, "Axicons and their uses," *The Journal of the Optical Society of America,* vol. 50, p. 166–169, 1960.

[14] H. Albrecht, N. Damaschke, M. Borys and C. Tropea, "Laser Doppler and Phase Doppler Measurement Techniques," *Springer,* 2002.

[15] Ichikawa, Tadashi, Hiroshi Ito, Manabu Kagami, and Satoru Kato, "Laser doppler velocimeter," *U.S. Patent 5,587,785,* December 24, 1996.

[16] F. Durst, A. Melling and J. H. Whitelaw, Principles and practice of laser Doppler anemometry, 1981.

[17] J. Durnin, J. Miceli Jr and J. Eberly, " Diffraction-free beams," *Physical Review Letters,* vol. 58, no. 15, p. 1499, 1987.

[18] L. Staroński, J. Sochacki, Z. Jaroszewicz and A. Kołodziejczyk, " Lateral distribution and flow of energy in uniform-intensity axicons," *J. Opt. Soc. Am. ,* vol. 9, no. 11, pp. 2091-2094, 1992.

[19] T. Čižmár and K. Dholakia, "Tunable Bessel light modes: engineering the axial propagation," *Opt. exp.,* vol. 17, no. 18, pp. 15558-15570, 2009.

[20] P. L. Overfelt and C. S. Kenney, "Comparison of the propagation characteristics of Bessel, Bessel-Gauss, and Gaussian beams diffracted by a circular aperture," *JOSA A,* vol. 8, no. 5, pp. 732-745, 1991.

[21] C. A. McQueen, J. J. Arlt and K. Dholakia, "An experiment to study a “nondiffracting” light beam.," *American Journal of Physics,* vol. 67, no. 10, pp. 912-915, 1999.

[22] D. McGloin and K. Dholakia, "Bessel beams: diffraction in a new light," *Contemporary Physics,* vol. 46, no. 1, pp. 15-28, 2005.

[23] D. J. Fischer, C. J. Harkride and D. T. Moore, "Design and manufacture of a gradient-index axicon," *Appl. Opt.,* vol. 39, p. 2687–2694, 2000.

[24] D. M. a. K. Dholakia, "Bessel beams: diffraction in a new light," *Contemporary Physics,* vol. 46, no. 1, pp. 15-28, 2005.

[25] J. Arlt, V. Garces-Chavez, W. Sibbett and K. Dholakia, " Optical micromanipulation using a Bessel light beam," *Optics Communications,* vol. 197, no. 4, pp. 239-245, 2001.

[26] J. Durnin, "Exact solutions for nondiffracting beams. I. The scalar theory," *JOSA A,* vol. 4, no. 4, pp. 651--654, 1987.

[27] I. Abdo, N. Ashry, M. Sadek, M. A. Hakim and D. Khalil, Effect of ring width on ring generated Bessel beam, vol. 8236, 2012.

[28] G. Scott and N. McArdle, "Efficient generation of nearly diffraction-free beams using an axicon," *Opt. Eng.,* vol. 31, no. 12, pp. 2640-2643, 1992.

[29] W.-X. Cong, N.-X. Chen and G. Ben-Yuan, "Generation of nondiffracting beams by diffractive phase elements," *JOSA A,* vol. 15, no. 9, pp. 2362-2364, 1998.

[30] J. Turunen, A. Vasara and A. T. Friberg, "Holographic generation of diffraction-free beams," *Appl. opt.,* vol. 27, no. 19, pp. 3959-3962, 1988.

[31] K. Thewes, M. A. Karim and A. A. S. Awwal, " Diffraction free beam generation using refracting systems," *Opt. Laser Technol.,* vol. 23, no. 2, p. 105–108, 1991.

[32] A. J. Cox and D. C. Dibble., "Nondiffracting beam from a spatially filtered Fabry-Perot resonator," *JOSA A,* vol. 9, no. 2, pp. 282-286, 1992.

[33] M. Couture and M. Piché, ""Focusing properties of an axicon pair," *Canadian journal of physics,* vol. 71, no. 1-2, pp. 70-78, 1993.

[34] N. Davidson, A. A. Friesem and E. Hasman, "Holographic axilens: high resolution and long focal depth," *Opt. lett.,* vol. 16, no. 7, pp. 523-525, 1991.

[35] J. Durnin, J. Miceli and J. Eberly, *Opt. Lett.,* vol. 13, pp. 79-80, 1998.

[36] Y. Lin, W. Seka, J. H. Eberly, H. Huang and D. L. Brown, "Experimental investigation of Bessel beam characteristics," *Applied optics,* vol. 31, no. 15, pp. 2708-2713, 1992.

[37] Belanger and M. P.A. Rioux, "Ring pattern of a lens-axicon doublet illuminated by a gaussian beam," *Applied Optics ,* vol. 17, no. 7, p. 1080–1086, 1978.

[38] Z. Jaroszewicz, "Axicons Design and Propagation Properties," Res. Dev. Treatises, v. 5, SPIE Polish Chapter, 1997.

[39] Z. Jaroszewicz, A. Burvall and T. Friberg, "Axicon – The Most Important Optical Element," *Optics and Photonics News,* vol. 16, no. 4, p. 34–39, April 2005.

[40] B. Chebbi, S. Minko, N. Al-Akwaa and I. Golub, " Remote control of extended depth of field focusing," *Opt. Commun.,* vol. 283, no. 9, p. 1678–1683, 2009.

[41] Z. Zhai, S. Ding, Q. Lv, X. Wang and Y. Zhong, "Extended depth of field through an axicon," *Journal of modern Optics,* vol. 56, no. 11, pp. 1304-1308, 2009.

[42] G. Milne, L. Paterson, D. McGloin, A. Riches and K. Dholakia, " "Light-induced separation and flow of microscopic and biological particles." In Nanomanipulation with Light," *International Society for Optics and Photonics,* vol. 5736, pp. 46-53, 2005.

[43] L. Paterson, E. Papagiakoumou, G. Milne, V. Garcvez, S. Tatarkova, W. Sibbett, F. J. Gunn-Moore, P. Bryant, A. C. Riches and K. Dholakia, "Light-induced cell separation in a tailored optical landscape," *Applied Physics Letters,* vol. 87, no. 12, p. 123901, 2005.

[44] X. Tsampoula, V. Garces-Chavez, M. Comrie, D. Stevenson, B. Agate, C. Brown, F. Gunn-Moore and K. Dholakia, "Femtosecond cellular transfection using a nondiffracting light beam," *Applied Physics Letters,* vol. 9, no. 15, p. p.053902.

[45] J. Arlt, V. Garcés-Chávez, W. Sibbett and K. Dholakia., "Optical micromanipulation using a Bessel light beam," *Optics communications,* vol. 197, no. 4-6, pp. 239-245, 2001.

[46] V. Garcés-Chávez, D. McGloin, H. Melville, W. Sibbett and K. Dholakia, "Simultaneous micromanipulation in multiple planes using a self-reconstructing light beam," *Nature ,* vol. 419, no. 6903, pp. 145-147, 2002.

[47] T. Aruga and S. W. Li, "Super high resolution for long-range imaging," *Appl. opt.,* vol. 38, no. 13, pp. 2795-2799., 1999.

[48] K. Wang, L. Zeng and C. Yin, "Influence of the incident wave-front on intensity distribution of the nondiffracting beam used in large-scale measurement," *Opt. Commun.,* vol. 216, no. 1-3, p. 99–103, 200.

[49] S. C. Tidwell, D. H. Ford and W. D. Kimura, "Transporting and focusing radially polarized laser beams," *Opt. commun.,* vol. 31, no. 7, pp. 1527-1531, 1992.

[50] N. Xu, G. Liu, Z. Kong and Q. Tan, "Creation of super-resolution hollow beams with long depth of focus using binary optics," *Applied Physics Express,* vol. 13, no. 1, p. 012003, 2019.

[51] R. A. Suarez, L. A. Ambrosio, A. A. Neves, M. Zamboni-Rached and M. R. Gesualdi, "Experimental optical trapping with frozen waves," *Optics letters,* vol. 45, no. 9, pp. 2514--2517, 2020.

[52] A. Porfirev, "Realisation of active pulling/pushing laser beams for light-absorbing particles in the air with a pair of diffractive optical elements," *Optics \& Laser Technology,* vol. 133, p. 106584, 2021.

[53] Z. Liu, X. Tang, Y. Zhang, Y. Zhang, L. Ma, M. Zhang, X. Yang, J. Zhang, J. Yang and L. Yuan, "Simultaneous trapping of low-index and high-index microparticles using a single optical fiber Bessel beam," *Optics and Lasers in Engineering,* vol. 131, p. 106119, 2020.

[54] R. Ali, F. Pinheiro, R. Dutra and P. M. Neto, "Tailoring optical pulling forces with composite microspheres," *Physical Review A,* vol. 102, no. 2, p. 023514, 2020.

[55] A. Riaud, M. Baudoin, J.-L. Thomas and O. B. Matar, "Cyclones and attractive streaming generated by acoustical vortices," *Physical Review E,* vol. 90, no. 1, p. 013008, 2014.

[56] Y. Arita, J. Lee, H. Kawaguchi, R. Matsuo, K. Miyamoto, K. Dholakia and T. Omatsu, "Photopolymerization with high-order Bessel light beams}," *Optics Letters,* vol. 45, no. 14, pp. 4080--4083, 2020.

[57] D. Li, K. Imasaki, S. Miyamoto, S. Amano and T. Mochizuki, "Conceptual design of Bessel beam cavity for free-electron laser," *International journal of infrared and millimeter waves,* vol. 27, no. 2, pp. 165-171, 2006.

[58] S. P. Tewari, H. Huang and R. W. Boyd, "Theory of third-harmonic generation using Bessel beams, and self-phase-matching," *Physical Review A,* vol. 54, no. 3, p. 2314, 1996.

[59] S. Hughes and J. M. Burzler, "Theory of Z-scan measurements using Gaussian-Bessel beams," *Physical Review ,* vol. 56, no. 2, pp. R1103-R1106, 1997.

[60] C. Shi, M. Dubois, Y. and Wang and X. Zhang, "High-speed acoustic communication by multiplexing orbital angular momentum," *Proceedings of the National Academy of Sciences,* vol. 114, no. 28, pp. 7250--7253, 2017.

[61] D. Hsu, F. Margetan and D. Thompson, "Bessel beam ultrasonic transducer: Fabrication method and experimental results," *Applied physics letters,* vol. 55, no. 20, pp. 2066--2068, 1989.

[62] J. F. Greenleaf, H. Zou, J.-y. Lu and X.-L. Xu, "Application of Bessel beam for Doppler velocity estimation," *IEEE transactions on ultrasonics, ferroelectrics, and frequency control,* vol. 42, no. 4, pp. 649--662, 1995.

[63] Y. A. Ayala, A. V. Arzola and K. Volke-Sep{\'u}lveda, "Comparative study of optical levitation traps: focused Bessel beam versus Gaussian beams," *JOSA B,* vol. 33, no. 6, pp. 1060--1067, 2016.

[64] S. N. Khonina, N. L. Kazanskiy, S. V. Karpeev and M. A. Butt, "Bessel beam: Significance and applications—A progressive review," *Micromachines,* vol. 11, no. 11, p. 997, 2020.

[65] F. Saadati-Sharafeh, A. Borhanifar, A. P. Porfirev, P. Amiri, E. A. Akhlaghi, S. N. Khonina and Y. Azizian-Kalandaragh, "The superposition of the Bessel and mirrored Bessel beams and investigation of their self-healing characteristic," *Optik,* vol. 208, p. 164057, 2020.

[66] V. S. Vasilev, A. I. Kapustin, R. V. Skidanov, N. A. Ivliev, V. V. Podlipnov and S. V. Ganchevskaya, "Experimental investigation of the stability of Bessel beams in the atmosphere," *Computer Optics,* vol. 43, no. 3, pp. 376--384, 2019.

[67] A. Kuchmizhak, A. Porfirev, S. Syubaev, P. Danilov, A. Ionin, O. Vitrik, Y. N. Kulchin, S. Khonina and S. Kudryashov, "Multi-beam pulsed-laser patterning of plasmonic films

using broadband diffractive optical elements," *Optics letters,* vol. 42, no. 14, pp. 2838--2841, 2017.

[68] S. Syubaev, A. Zhizhchenko, O. Vitrik, A. Porfirev, S. Fomchenkov, S. Khonina, S. Kudryashov and A. Kuchmizhak, "Chirality of laser-printed plasmonic nanoneedles tunable by tailoring spiral-shape pulses," *Applied Surface Science,* vol. 470, pp. 526--534, 2019.

[69] R. Skidanov, D. Kachalov, S. Khonina, A. Porfirev and V. Pavelyev, "Three-dimensional laser trapping on the base of binary radial diffractive optical element," *Journal of Modern Optics,* vol. 62, no. 14, pp. 1183--1186, 2015.

[70] S. Khonina, S. Karpeev and V. Paranin, "Birefringence detection of a gradient-index lens based on astigmatic transformation of a Bessel beam," *Optik,* vol. 164, pp. 679--685, 2018.

[71] S. N. Khonina, V. D. Paranin, A. V. Ustinov and A. P. Krasnov, "Astigmatic transformation of Bessel beams in a uniaxial crystal," *Optica Applicata,* vol. 46, no. 1, 2016.

[72] S. Khonina, "Experimental generation various nondiffractive laser beams by masking the vortical ring spatial spectrum," *Izvest. SNC RAS,* vol. 11, no. 3, pp. 103--110, 2009.

[73] S. N. Khonina, A. V. Ustinov and A. P. Porfirev, "Fractional two-parameter parabolic diffraction-free beams," *Optics Communications,* vol. 450, pp. 103--111, 2019.

[74] S. Khonina and S. Degtyarev, "Analysis of the formation of a longitudinally polarized optical needle by a lens and axicon under tightly focused conditions," *Journal of Optical Technology,* vol. 83, no. 4, pp. 197--205, 2016.

[75] S. N. Khonina and A. V. Ustinov, "Sharper focal spot for a radially polarized beam using ring aperture with phase jump," *Journal of Engineering,* vol. 2013, 2013.

[76] M. A. Sakah, "Development of a new velocity measurement technique: the laser bessel velocimetry," Laurentian University , Sudbury, Ont, 2015.

[77] S. Tavoularis, Measurement in Fluid Mechanics Paperback, 2009.

[78] S. Andrews, D. Nover, K. Reardon, J. Reuter and S. Schladow, "The influence of ambient light intensity on in situ laser diffractometers," *Water Resources Research,* vol. 47, no. 6, 2011.

[79] MSE, "http://measurementsci.com/wp-content/uploads/2014/10/miniLDV_brochure.pdf," Measurement Science Enterprise. [Online].

[80] F. Durst, J. Jovanović and J. Sender, "LDA measurements in the near-wall region of a turbulent pipe flow.," *Journal of Fluid Mechanics,* vol. 295, pp. 305--335, 1995.

[81] J. Den Toonder and F. Nieuwstadt, "Reynolds number effects in a turbulent pipe flow for low to moderate Re," *Physics of Fluids,* vol. 9, no. 11, pp. 3398--3409, 1997.

[82] U. Lei, M. Lin, H. Sheen and C. Lin, "Velocity measurements of the laminar flow through a rotating straight pipe," *Physics of Fluids,* vol. 6, no. 6, pp. 1972--1982, 1994.

[83] A. Bicen and J. Whitelaw, "Refraction correction for LDA measurements in flows with curved optical boundaries," in *bicen1981refraction*, Imperial College of Science and Technology, Department of Mechanical Engineering, Fluids Sect, 1981.

[84] S. Chávez-Cerda, M. A. M.-N. and J. M. Hickmann, "Interference of traveling nondiffracting beams.," *Optics letters,* vol. 23, no. 24, pp. 1871-1873, 1998.

[85] Z. Jaroszewicz, A. Kolodziejczyk, A. Kujawski and C. Gomez-Reino., "Diffractive patterns of small cores generated by interference of Bessel beams.," *Optics letters,* vol. 21, no. 20, pp. 839-841, 1996.

[86] S. Chavez-Cerda, E. Tepichin, M. A. Meneses-Nava, G. Ramirez and J. M. Hickmann, "Experimental observation of interfering Bessel beams," *Optics express ,* vol. 3, no. 13, pp. 524-529., 1998.

[87] Z. Jaroszewicz, A. Nowakowski, A. T. F. A. Thaning and J. I., "Focal segments obtained by interference of multiple Bessel beams," *In 13th Polish-Czech-Slovak Conference on Wave and Quantum Aspects of Contemporary Optics,* vol. vol. 5259, no. International Society for Optics and Photonics, pp. 121-125, 2003.

[88] D. McGloin, V. Garcés-Chávez and K. Dholakia, "Interfering Bessel beams for optical micromanipulation.," *Optics letters,* vol. 28, no. 8, pp. 657-659., 2003.

[89] M. Fortin, M. Piché and F. B. Ermanno, "Optical tests with Bessel beam interferometry," *Optics Express ,* vol. 12, no. 24, pp. 5887-5895, 2004.

[90] A. e. Boutier, Laser velocimetry in fluid mechanics, John Wiley & Sons, 2013.

[91] H.-E. Albrecht, N. Damaschke, M. Borys and C. Tropea, Laser Doppler and phase Doppler measurement techniques., Springer Science & Business Media, 2013.

[92] C. Resagk, U. Schellenberger, J. Grabow, C. Tropea and M. Stieglmeier., "Two-component LDA using optical multiplexing," *Measurement Science and Technology,* vol. 6, no. 6, p. 674., 1995.

[93] H. Wang, V. Strunck, H. Müller and D. Dopheide, "New technique for multi-component flow velocity measurements using a single HF-pulsed diode laser and a single photodetector.," *Experiments in fluids,* vol. 18, no. 1-2, pp. 36-40, 1994.

[94] A. Voigt, S. Heitkam, L. Büttner and J. Czarske, "A Bessel beam laser Doppler velocimeter," *Opt. Commun.,* vol. 282, no. 9, pp. 1874-1878, 2009.

[95] J. Durnin, J. J. Miceli and J. Eberly, "Diffraction-free beams," *Rev. Lett.,* vol. 58, p. 1499–1501, 1987.

[96] A. Piccato, C. Francese and R. Malvano., "A portable rotating disk prototype for LDA calibration," *Flow Measurement and Instrumentation,* vol. 38, no. 5, pp. 54-61, 2014.

[97] F. Gori, G. Guattari and C. Padovani., " Bessel-gauss beams," *Optics communications,* vol. 64, no. 6, pp. 491-495, 1987.

[98] S. V. K. Mekid, "Differential laser doppler based non-contact sensor for dimensional inspection with error propagation evaluation," *Sensors,* vol. 6, no. 6, pp. 546--556, 2006.

[99] F. Mayinger, Optical measurements: techniques and applications, Springer Science & Business Media, 2013.

[100] D. A. Compton and J. K. Eaton, " A high-resolution laser Doppler anemometer for three-dimensional turbulent boundary layers," *Experiments in fluids ,* vol. 22, no. 2, pp. 111-117, 1996.

[101] A. S. Rao and G. Samanta, "Generation of high peak power, segmented and Bessel beams of tunable range without on-axis intensity modulation," *arXiv preprint arXiv,* p. 1803.10419, 2018.

[102] A. Müller, M. C. Wapler and U. Wallrabe, " Segmented Bessel beams," *Optics Express,* vol. 25, no. 19, pp. 22640-22647, 2017.

[103] Y. Lin, W. Seka, J. H. Eberly, H. Huang and D. L. Brown, " Experimental investigation of Bessel beam characteristics.," *Applied optics,* vol. 31, no. 15, pp. 2708-2713, 1992.

[104] M. Lapointe, "Review of non-diffracting Bessel beam experiments," *Optics & Laser Technology,* vol. 24, no. 6, pp. 315--321, 1992.

[105] J. Goodman, Introduction to Fourier optics, Englewood, Colorado, USA: Roberts and Company, 2005.

[106] B. Chebbi, S. Minko, N. Al-Akwaa and I. Golub, " Remote control of extended depth of field focusing.," *Optics communications,,* vol. 283, no. 9, pp. 1678-1683, 2010.

[107] F. Gori, G. Guattari and C. Padovani, " Bessel-gauss beams," *Optics communications,* vol. 64, no. 6 , pp. 491-495., 1987.

[108] Y. A. Cencgel and J. M. Cimbala, Fluid Mechanics fundamentals and applications, Fourth Edition, 2 Penn Plazza New York, NY: McGraw-Hill Education, 2014.

[109] Y. A. Cengel and J. M. Cimbala, Fluid Mechanics Fundementals and Applications, New York: McGraw Hill Education, 2018.

[110] R. P. Benedict, Fundamentals of pipe flow "Text Book", New York: Wiley, 1980.

[111] F. T. Smith, "Fluid flow into a curved pipe," *Proceedings of the Royal Society of London. A. Mathematical and Physical Sciences,* vol. 351, no. 1664, pp. 71--87, 1976.

[112] H. C.-H. Ng, H. L. Cregan, J. M. Dodds, R. J. Poole and D. J. Dennis, "Partially filled pipes: experiments in laminar and turbulent flow," *Journal of Fluid Mechanics,* vol. 848, pp. 467--507, 2018.

[113] L. A. Fullard and G. C. Wake, "An analytical series solution to the steady laminar flow of a Newtonian fluid in a partially filled pipe, including the velocity distribution and the dip phenomenon," *IMA Journal of Applied Mathematics,* vol. 80, no. 6, pp. 1890--1901, 2015.

[114] R. S. Figliola and D. E. Beasley, Theory and Design for Mechanical Measurements fifth edition, Printed in the United States of America: John Wiley & Sons, Inc., 2011.

[115] Thorlabs, "https://www.thorlabs.com/NewGroupPage9.cfm?ObjectGroup_ID=4850".

[116] J. Y. Lu, X. L. Xu, H. Zou and J. F. Greenleaf, "Application of Bessel beam for Doppler velocity estimation,Ultrasonics, Ferroelectrics, and Frequency Contro," *IEEE Transactions on ,* vol. 42, no. 4, pp. 649-662, 1995.

[117] V. V. Kotlyar, A. A. Kovalev, R. V. Skidanov and V. A. Soifer, " Asymmetric Bessel–Gauss beams," *JOSA,* vol. 31, no. 9, pp. 1977-1983, 2014.

[118] E. a. M. F. Huber, "Light scattering by small particles," *Aqua 47,* pp. 87-94, 1998.

[119] C. F. Bohren and D. R. Huffman, Absorption and scattering of light by small particles, John Wiley & Sons, 2008.

[120] Hulst, Hendrik Christoffel, and H. C. Van De Hulst, " Light scattering by small particles," *Courier Dover Publications,* 1957.

[121] "www.thorlabs.com/thorproduct.cfm?partnumber=PDA36A2," Thorlabs, 21 4 2020. [Online].

[122] Y. Agrawal, L. Talbot and K. Gong, " Laser anemometer study of flow development in curved circular pipes," *Journal of Fluid Mechanics,* vol. 85, no. 3, pp. 497-518., 1978.

[123] K. Thole, M. Gritsch, A. Schulz and S. Wittig, "TFlowfield measurements for film-cooling holes with expanded exits," *In ASME 1996 International Gas Turbine and Aeroengine Congress and Exhibition American Society of Mechanical Engineers,* pp. V004T09A010-V004T09A010, 1996.

[124] Rogers, Philip L., and Kerry J. Vahala. , "Laser doppler velocimeter," *U.S. Patent 6,141,086,* October 31, 2000.

[125] D. Y. Goswami, "Velocity profiles of Liquid Flow through Circular Tubes and how they affect Flow measurement," *goswami1991velocity,* pp. 206-210, 1991.

[126] S. Tavoularis, "Measurement in Fluid Mechanics Paperback", 2009.